PhD Thesis
Machine Induced Experimental Background Conditions in the LHC

Yngve Inntjore Levinsen
University of Oslo & CERN

19. of September, 2012

Abstract

The Large Hadron Collider set a new energy record for particle accelerators in late 2009, breaking the previous record held by Tevatron of 2 TeV collision energy. The LHC today operates at a collision energy of 7 TeV. With higher beam energy and intensity, measures have to be taken to ensure optimal experimental conditions and safety of the machine and detectors. Machine induced experimental background can severely reduce the quality of experimental triggers and track reconstruction. In a worst case, the radiation levels can be damaging for some of the subdetectors.

The LHC is a particular challenge in this regard due to the vastly different operating conditions of the different experiments. The nominal luminosity varies by four orders of magnitude. The unprecedented stored beam energy and the amount of superconducting elements can make it challenging to protect the accelerator itself as well.

In this work we have simulated and measured the machine induced background originating from various sources: the beam colliding with rest-gas, collision residues that are transported between the experiments, and from beam halo impacting on aperture restrictions. The aim of the work has been to get a first complete overview of all background sources, in order to better understand how we can optimise the running conditions for the LHC experiments.

We have found that the most important background source is beam-gas background, with an expected background rate towards the experiments for the nominal machine on the order of MHz. Other sources of background have been carefully considered and are found to pose less of a challenge under normal running conditions.

Contents

1 Acknowledgements **1**

2 Introduction **3**
2.1 Norwegian Accelerator Physics Heritage 3
2.2 Hadron Colliders 4
2.3 CERN and the Large Hadron Collider 6
2.4 Motivation for This Work 8
2.5 Work Presented in This Thesis 9
2.6 Thesis Outline 11
2.6.1 Publications 11

3 Accelerator Physics and Optics **13**
3.1 Magnets 13
3.2 Coordinate System 15
3.3 Matrix Elements 16
3.3.1 Betatron Motion 18
3.4 Machine Imperfections 20
3.4.1 Dispersion 20
3.4.2 Coupling 22
3.4.3 Chromaticity 22
3.5 Diffusion Processes 22
3.5.1 Beam-Gas Scattering 23
3.5.2 Electron Cloud 23
3.5.3 Intrabeam Scattering 24
3.5.4 Burnout from Collisions 25
3.5.5 Beam-Beam Interaction 25
3.6 Machine Aperture 26

3.7 Particle Tracking 29
3.7.1 Symplecticity 29
3.7.2 Off-Momentum Tracking 30

4 LHC Layout **31**
4.1 General Parameters 31
4.1.1 Nominal Optics 37
4.1.2 Interface Plane 37
4.2 The Interaction Regions and Experiments 37
4.3 Low Luminosity Interaction Regions 38
4.3.1 ALICE 38
4.3.2 LHCb 40
4.4 High Luminosity Experiments 42
4.4.1 ATLAS 43
4.4.2 CMS 44
4.5 Machine Aperture 45
4.5.1 Collimator Settings 49

5 Studies of Beam–Gas Scattering **51**
5.1 Rates and Lifetime 51
5.2 Pressure Distribution 53
5.3 Physics Processes 56
5.4 Local, LSS and Distant Beam-Gas 59
5.5 Earlier Studies 61
5.6 Simulations 62
5.6.1 Nominal Machine 66
5.6.2 Loss Origins 72
5.6.3 Impact Parameter 80
5.6.4 Summary for the Nominal Machine 81
5.7 3.5 TeV 83

6 Studies of Other Background Sources **85**
6.1 Interaction Region Cross-Talk 85
6.1.1 Lorentz Boost 86
6.1.2 Phase Advances 89
6.1.3 Simulations 90
6.1.4 Loss Rates During Van der Meer Scans 91
6.2 Tertiary Halo Background 95
6.3 Studies of Particle Showers 97

6.4 Summary 97

7 Fill Analysis and Background Observations 99
7.1 Motivation 99
7.2 Machine Performance 101
7.3 Background Observations 103
7.3.1 ALICE Background Challenges 103
7.3.2 ATLAS, CMS, and LHCb Background 104
7.4 Vacuum in the LSS 105
7.5 Beam Lifetime 106
7.5.1 Burnout 107
7.5.2 Beam-Gas 107
7.5.3 Total Beam Lifetime 108
7.5.4 Luminosity Lifetime 109
7.5.5 Specific Luminosity 111
7.6 Outlook 111

8 Summary and Outlook 113

A Linear Equations of Motion 125

B Courant–Snyder Parametrization 131

C BeamGas Module in Sixtrack 135
C.1 Compiling SixTrack with BeamGas Module 135
C.2 Running Beam-Gas Simulations 136
C.2.1 Input Files 137
C.3 Output 138
C.4 Implementation Details 139

D Articles 143
D.1 Simulation of Beam-Gas Scattering in the LHC 144
D.2 Beam-Gas Loss rates in the LHC 148
D.3 IR Crosstalk in the LHC 152
D.4 Methodology of MIB Simulations 156
D.5 Fill Analysis and Background Observations 167
D.6 Summary of Notes 171
D.6.1 Beam-Gas Simulations for the 2009 run 171
D.6.2 ALICE MIB at Nominal Energy 172

Chapter 1

Acknowledgements

I would like to express my gratitude for my two supervisors that made this thesis possible. It has been great to experience the effectiveness and sheer knowledge wealth that is Steinar Stapnes. He has made the administrative part of this thesis work surprisingly pleasant, and served as an excellent bridge to the University and the scientific community in Norway. Helmut Burkhardt has served as my scientific supervisor, an endless well of knowledge and love for the field that is accelerator physics. Nearly every day, and sometimes several times a day I have been knocking on his door. Not once has he turned down my request no matter how ignorant it might have been. It goes without saying that this thesis work would not have been possible without their continuous support.

This work has not all been done alone. My colleagues who I have been working more closely with during these years include Robert Barrie Appleby, Vadim Talanov, Alick Macpherson, Gloria Corti, Kajetan Fuchsberger, and Giuseppe Bregliozzi. Thank you all for your making work become so interesting and fun. All members of the LHC Background Study Group deserves thanks as well for countless interesting discussions.

I would like to give thanks as well to my good friend Paul Anton Letnes, for many interesting off- and on-topic discussions, and for reading English grammar in this thesis. I wish you the best of luck with the finalization of your PhD!

During my stay in 9-R-016, several office companions have been around. Thank you Simon Mathieu White, Eirini Koukovini Platia, Sophie Cavalier, and Yipeng Sun for making the atmosphere in the office so enjoyable. To all the coffee mates and lunch buddies, Jochem Snuverink, Javier Barranco, Alexander Gerbershagen, Seyd Hamed Shaker, Glenn Vanbavinckove, Alan Belle, Nikolaki Charitonidis, Bartoloměj Biskup,

Andrea Tsinganis, Lawrence Deacon, David Mcfarland, Marion Picard, Erwan Harrouch, Theo Rutter, Tobias Hakan Björn Persson, Jürgen Pfingstner, Hannes Bartosik, Miriam Fitterer, Benoit Salvant, Rogelio Tomas, Giovanni Rumolo, Tatiana Pieloni, Rama Calaga, and Giulia Bellodi, thank you for the great physics discussions, political discussions, and the important nonsense discussions that have made this time so enjoyable. Having friends from all corners of Europe and even many corners of the world is a very important part of what makes CERN the awesome place that it is.

For letting there be "et lite stykke Norge" left in Switzerland, I would like to extend my appreciation to some of my Norwegian colleagues at CERN: Erik Adli, Øystein Midtun and Elisabeth Garmann Johnsen, Reidun Anette Hagen, Øystein Alvestad, Vegar Lein Ausrød, Børge Antonsen, Ole Martin Hansen, Reidar Lunde Lillestøl, Kyrre Ness Sjøbæk, Lene Norderhaug Drøsdal, and last but not least, the almost-Norwegian mountain goat Christian Hansen. Having you guys and girls around makes being away from Norway for so long more manageable, thank you!

Last but surely not least, I would like to give my gratitude to my dear family. Kjære mamma og pappa, Sindre og Nora-Juline. Hjærtelig takk for all den støtten dere har vist meg. Det å ha en familie rundt seg som holder sammen gjennom tykt og tynt betyr veldig mye, og er noe jeg alltid vil være takknemlig for.

Chapter 2

Introduction

Particle accelerators have been an essential part of fundamental physics research since Rutherford discovered the nucleus in 1911. As technology advancement allowed for more and more energetic beams, smaller and smaller constituents of our world have been explored. The latest instalment in this energetic race is the Large Hadron Collider situated outside Geneva, Switzerland.

Accelerator physics is a term used for the science of studying the motion and stability of these energetic beams. It includes the physical knowledge and technology needed to get the particles to the collision point. In this chapter we will present CERN and the LHC. Finally, we give a description of this thesis work and an outline. First, we will briefly present some of the Norwegian scientists that have made significant contributions to the field.

2.1 Norwegian Accelerator Physics Heritage

In the 1920s, a young Norwegian electrical engineer named Rolf Widerøe went to Germany to study physics. As a PhD work he attempted to demonstrate the betatron concept[1] without success. However, he made a successful attempt at demonstrating another type of acceleration — the acceleration of charged particles by "surfing" on a synchronous radio-frequency electric field. This work paved the way for modern high energy physics, and Widerøe is now known by many as the "grandfather of particle accelerators".

[1] Betatron acceleration is the acceleration by an alternating magnetic field.

Widerøe is not the only Norwegian in the history of accelerator physics, even though particle accelerator physics is not a major research field in Norway today. In the beginning of the 1950s, 11 countries in Western Europe including Norway began the planning of a new European collaboration for nuclear research. The temporary name was "Conseil Européen pour la Recherche Nucléaire", with the acronym CERN. In 1954 they founded "Organisation Européenne pour la Recherche Nucléaire" together with one more country, but kept the old acronym. The first larger project, the construction of the Proton Synchrotron (PS), was led by a Norwegian named Odd Dahl. Dahl was a practical man with no formal training in science. He had read physics while on the Maud expedition to the Arctic, with help from H. U. Sverdrup. The PS was put into operation in 1959, and is still a vital part of the injector chain at CERN.

Following a recommendation from Odd Dahl and one of the founders of CERN, Kjell Johnsen was hired as one of the first CERN staff members in 1952. He had a degree in electrical engineering from NTH in Trondheim, Norway. After working on the PS for several years, he went on to promote his new pet project, a proton–proton collider. The project named the Intersecting Storage Rings (ISR) was finally approved in 1966 by the CERN Council. Kjell Johnsen lead the project, and in 1971 they collided two proton beams for the very first time in history. This opened up for an entirely new energy frontier in high energy physics. Because the charge/mass ratio is a factor 2000 lower for the protons compared to electrons, they suffer less from synchrotron radiation. As a result higher energies can be achieved in a circular machine.

2.2 Hadron Colliders

In accelerator physics we generally divide in two main categories of synchrotron accelerators, hadron and lepton colliders. The reason for this is that in particular the synchrotron radiation produced from bending the particle trajectory is highly dependent on the mass/charge ratio,

$$P \propto \frac{(\beta E)^4}{\rho^2 m^4}. \tag{2.1}$$

Here, P is the power radiated from the particle, β is the ratio of the velocity of the particle to the speed of light (equal to 1 for relativistic energies), E is the energy of the particle, ρ is the radius of curvature of the trajectory, and m is the mass of the particle. The proton is about 2000 times heavier than the electron, which means that the radiation is eight orders of magnitude lower for the same energy and accelerator size. We can also note that the increase in energy follows the length of the machine squared, if we want to keep the radiated power constant. If we then assume that the cost of an accelerator is approximately proportional to the length of the machine, we

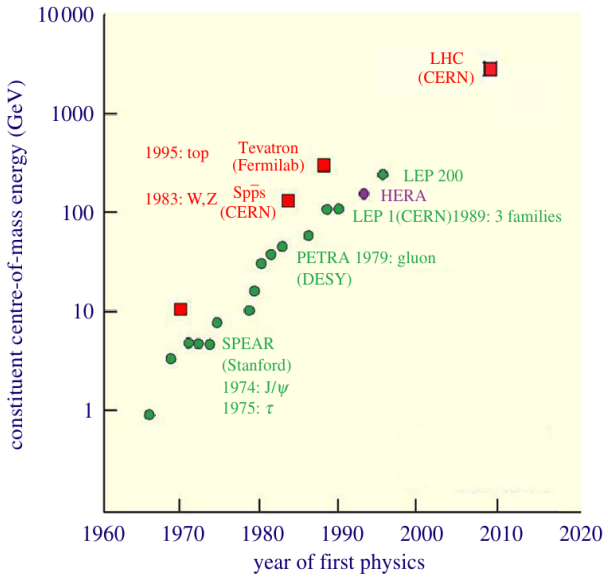

Figure 2.1: The collision energy of particle accelerators, with a logarithmic vertical scale. In red squares hadron colliders, in green circles lepton colliders. HERA as electron-proton collider in purple. Figure from [1].

understand that there is little gain from increasing the size of an accelerator once the maximum sustainable power loss of the particles is reached.

In a synchrotron accelerator the particles are accelerated by RF cavities, and steered and focused by magnets. LEP was the previous large project at CERN, an electron–positron collider with a ring circumference of almost 27 km. The energy loss due to synchrotron radiation was 3 % per turn. That means that if the RF cavities were turned off, the beam would be lost in a fraction of a turn. In order to counteract the energy loss, RF cavities were installed everywhere possible. It is likely that LEP will go down in history as the largest circular lepton collider ever built.

In Figure 2.1 we see the evolution of collision energy of particle accelerators. The energy as a function of time follows a fairly clear logarithmic trend. Hadron machines can reach higher energies than their lepton counterparts. For that reason, they are highly suitable to explore new energy regimes. On the other hand, the collisions are intrinsically more complex. A hadronic collision is a mixture of gluons and quarks

colliding, while leptons are fundamental particles. The first red dot from around 1970 is the ISR which project leader was Kjell Johnsen as mentioned earlier.

Tevatron held the previous world record in collision energy of approximately 2 TeV. In spring of 2008, a few months before this thesis work started, representatives from Tevatron, RHIC, and HERA were invited to describe their experience with background related issues in their machines [2]. Some general observations from this workshop were that any machine have some surprises, and that one should be well prepared with simulations and measurement devices in order to understand the machine properly.

Tevatron experienced reduced data quality and radiation damage to some of the subdetectors due to machine induced background [3]. Mitigations included shielding in front of the experimental caverns [4, 5], and a two-stage collimation system [6].

HERA experienced serious challenges after the luminosity upgrade in 2000-2001 [7, 8]. Synchrotron radiation from focusing of the electron beam, in combination with proton-gas background were found to be particularly problematic. Comprehensive simulations and specialised measurements were needed. Amongst others, installation of additional collimators and vacuum pumps was needed in order to improve the background conditions.

2.3 CERN and the Large Hadron Collider

After LEP was shut down the construction of a hadron collider in the same tunnel started in 2001. The Large Hadron Collider (LHC) is a 26.6 km long hadron accelerator. It is primarily designed for proton-proton collisions, with one experiment, ALICE, optimised for ion collisions. The LHC will run at a nominal collision energy of 14 TeV, approximately 7 times that of Tevatron [9]. Tevatron had the highest collision energy in the world before LHC, approximately 2 TeV centre of mass energy. At nominal operation, the LHC will have 2808 bunches per beam, each consisting of 10^{11} protons. That will result in a maximum inelastic collision rate of protons of around 700 MHz per collision point.

A complex injector chain is providing the protons for the LHC. The proton source is placed at the beginning of a linear accelerator known as LINAC 2 (will be replaced by LINAC 4 which is under construction). The protons travel from there into the Booster, before they enter the Proton Synchrotron (PS), which was the first accelerator built at CERN. From there, the protons are transported into the Super Proton Synchrotron (SPS), accelerated to a top energy of 450 GeV and sent to the LHC. The accelerator complex at CERN is shown in Figure 2.2.

There are four collision points around the LHC, where the main experiments in each

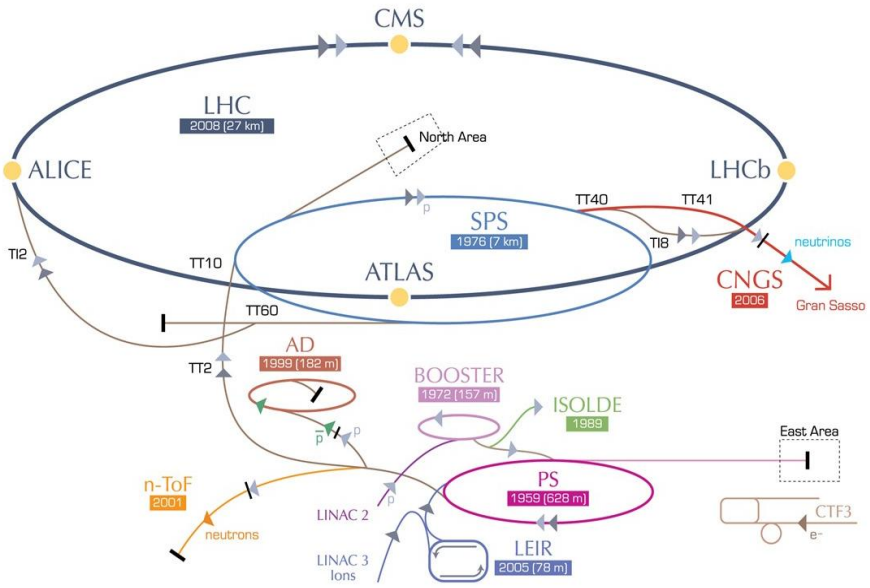

Figure 2.2: The CERN accelerator complex, copyright CERN.

collision point are ATLAS [10, 11], ALICE [12], CMS [13], and LHCb [14]. ATLAS and CMS are general purpose high luminosity detectors, designed for the maximum collision rate that the LHC can provide. LHCb is specially designed for studying rare decays, which implies that they must limit themselves to a maximum of about one collision per particle bunch crossing. That results in a maximum collision rate about 1-2 orders of magnitude less than ATLAS and CMS. ALICE is specialised for ion physics, but operates during proton physics as well with a maximum collision rate about 4 orders of magnitude lower than nominal LHC performance. The limitation for ALICE is due to limitations in the maximum radiation that can be accepted, and the detector is forced to turn off either partly or in its entirety if the total radiation exceeds that limitation.

We will look more into the details of the LHC layout and the experiments in Chapter 4.

2.4 Motivation for This Work

> *Taking this new machine under control, including establishing optimal conditions for physics, will require much expertise and the ability to solve problems as they emerge.*

The above quote is taken from the summary of the April'08 LHC Workshop on experimental conditions and backgrounds [2]. A direct outcome of this workshop was that funding for the thesis work presented here was requested.

The main parameters of a particle collider is the particle type, the beam energy and the luminosity — the number of collisions per cross section. As for any physics experiment, lowering the background and noise levels will improve the quality of the data obtained, allowing for a better analysis.

The term background can have several meanings for a particle collider. For the search for e.g. the Higgs boson, any collision not producing a Higgs boson can be considered background to this search. Electrical noise on the detector signal is another source of background for the experiments. In this thesis we consider the machine induced background, which we will define as:

Particles showering towards the experimental cavern originating from the interactions between the beam and its environment, but not originating from particle collisions at the interaction point.

As a result, if there is no beam in the machine, there is no machine induced background as we define it.

The background level will impact both the quality of the triggering system which is responsible for selecting which events are interesting enough to store, and for the quality of the data that are stored. There is not necessarily a hard upper limit for the background levels, or a lower limit under which there is no point to reduce the background further. Depending on the detector design, there might be a point at which the radiation levels are too high, and the detector cannot function or cannot efficiently trigger/store data anymore. There will always be a need to improve the understanding of the background sources in order to minimise them and to be better prepared for the future when the situation might worsen.

The combination of high luminosity and low luminosity experiments poses a further challenge for background in the LHC. Machine induced background sources typically scale with beam intensity and/or energy, sometimes with a highly non-linear dependence (e.g. electron cloud). It is of particular importance for the low luminosity experiments ALICE and LHCb to fully understand the background conditions and to know what the sources of background are. Even if the background is kept very low

relative to the beam intensity, challenging conditions for ALICE are not necessarily excluded.

The LHC has a complex three stage collimation system [15], which performance has been studied extensively. The collimators act as the limiting aperture in the machine, which is the origin of what is called beam halo background. The beam halo background estimates have been an important input for background simulations of the experimental detectors. A significant part of the total machine induced background that is not considered in the collimation studies, is the beam colliding with rest gas in the vacuum chamber (beam-gas background). In particular the elastic or quasi-elastic collisions can in principle produce showers to the experiments from beam-gas collisions anywhere in the machine. Particle tracking with accurate optics is required for a good knowledge of this background source.

2.5 Work Presented in This Thesis

Prior to the start of this work, a need was found for a dedicated study of background conditions on the machine side. Each experiment have a group of people dedicated to background studies. A collaborate effort between the machine and the experiments was found beneficial for an optimal understanding of machine induced background. Vacuum conditions, beam optics, detector response, and trigger algorithms all play important roles when the rates and effects of background should be determined.

In the context of this PhD we have investigated machine induced experimental background, with the aim to get a first overall picture of the background conditions in the LHC. We generally consider three categories of background: collisions between the beam and the rest gas in the vacuum pipe (beam-gas background), particle showers from the halo of the beam colliding with aperture close to the detectors (beam-halo background), and in the case of multiple experiments in one accelerator, collision residues from one experiment which are transported close to another experiment before hitting an aperture restriction and then shower into the detector (cross-talk).

The rest gas in the LHC beam pipe consists of mainly H_2, CO_2, CO, and CH_4 with the relative densities varying depending on pumping efficiency of different vacuum systems [16]. Since the beam has a very high energy, the collision between a proton in the beam and a rest gas molecule will produce secondary particles which gets a small angular spread with respect to the beam direction. As a result some of these residues can travel for long distances before they end up in an aperture restriction elsewhere in the machine. Some elastic and diffractive scattered protons will stay within the beam and contribute to the halo growth. A part of these residues will end up in the detector region. This can produce a significant amount of background, depending on

parameters. In general the beam–gas background does not necessarily change much with changing optical parameters, but scales with pressure and beam intensity.

A proton or ion beam will always have a certain amount of transverse and longitudinal blow-up from non-conservative forces that act on the individual particles. In order to reduce the radiation levels on sensitive cold masses, the LHC requires a complex system of collimators that effectively remove the halo of the beam so that it does not heat up and damage the cold components. The collimation system has several stages, where what is called the tertiary collimators are located around 60 to 140 m from the interaction points (IP). Their purpose are to protect the final focusing quadrupoles, which are sensitive to radiation and close to the beam when it is strongly focused. As a consequence the tertiary collimators serve as the smallest aperture restriction in the straight sections around the experiments. There will then be a flux of protons from the halo of the beam hitting these tertiary collimators. The showers from these hits produce particles that can reach the experimental cavern. Differing from beam–gas, the beam-halo background we have described depends to a larger degree on optical parameters, because the openings of the tertiary collimators are decided based on the focusing strengths. The beam-halo background will depend strongly on the beam lifetime, since a lower beam lifetime is directly translated to a faster production of beam halo particles.

The final machine induced background component we take into account is the cross-talk between experiments. Collision residues from elastic and quasi-elastic collisions at one interaction point can reach aperture restrictions close to other experiments and produce a certain amount of background. This cross-talk is dependent on the number of collisions at the other interaction points, which means that this kind of background is more important for the low luminosity experiments like ALICE and LHCb. Under normal circumstances one could argue that this background component should be low compared to the luminosity where the background is originating, but depending on the particular optics between two experiments, the cross-talk can still be of importance in some occasions.

In the case of the LHC, the simulation of machine induced background is done in several steps, something we described at length in [17]. After obtaining the machine parameters like the beam intensity, the optical parameters, and the vacuum conditions, there is a tracking stage where one simulates the loss rates on aperture restrictions around the ring. The losses close to an experiment are then transported into a particle shower simulation code which can transport all particles from the aperture restrictions and through the different materials up to the experimental cavern. From this stage on there is another simulation code taking over which can simulate the detector response on the given background. The detector response must then be inserted in a software that can predict the trigger response based on the given detector hits, trigger algorithms

and so forth. The final simulation result can be compared to actual data.

2.6 Thesis Outline

In this work, we have focused on the retrieval of the input machine parameters, collision event generation, and particle tracking in the entire machine with accurate optics. We started by establishing a strategy for simulating beam-gas background in the LHC. Initially, we did not have a simulation code suitable for this kind of simulations, and so the first task was to extend an existing tracking code to fit our purpose.

The first part was focused on selecting the right tools and extending those to cover beam-gas simulations. After this was implemented, simulated vacuum distributions and other input parameters was obtained and simulation of the nominal machine was initiated.

In the following, we extended our developed code to simulate interaction region cross-talk, and we used it to simulate some special cases not directly related to experimental background. We obtained loss maps from localised obstacles [18], and studied the losses from a beam hitting some special detectors called Roman pots [19]. These studies allowed us to directly compare results with data, providing a higher confidence in our simulations.

In the later part of the thesis work, a significant effort was put into retrieving and analysing available data to get a good grip of the machine performance on a regular basis. We developed an extensive analysis tools package, which automates the work of obtaining the relevant information that are vital in order to be able to know how the experimental background and more generally machine parameters varies over time.

We start by introducing some general accelerator physics and terminology in Chapter 3, and then present the LHC design and layout in Chapter 4. In Chapter 5 we discuss at length the beam-gas background, a central part of this thesis. We then cover IR cross-talk and other background sources in Chapter 6, before we describe our fill analysis tools and background observations so far in the LHC in Chapter 7. Here we cover calculations of total beam lifetime and compare to observations. Finally, we will present our conclusions and outlook in Chapter 8.

2.6.1 Publications

The publications related to this thesis work are given in Appendix D. Appendix D.1 and Appendix D.2 cover our studies of beam-gas background. In Appendix D.3 the studies of interaction region cross-talk background are presented. Our fill analysis tool was first published in Appendix D.5 together with some early analysis examples. In

Appendix D.4 we published our full simulation chain together with some collaborators from the LHCb experiment. A revised version of this paper will be published to Transactions of Nuclear Science. In addition to the publications, there were two CERN project notes published that contain results from this work. These are summarised in Appendix D.6.

Chapter 3

Accelerator Physics and Optics

In this chapter we will present briefly the basic principles of accelerator physics. The interested reader is suggested to look for a more comprehensive coverage in Refs. [20, 21, 22]. We will start by introducing the linear optics theory, before we look at the dynamics of particle tracking in accelerator physics, which is of high relevance to the work presented in this thesis.

3.1 Magnets

The basic components in a modern particle accelerator are radio-frequency (RF) cavities where an electromagnetic field accelerate the particles in a synchronous manner, as was demonstrated by Wideröe. In addition, magnets steer and focus the beam. The first magnet is the dipole which steers charged particles along the beam orbit. Quadrupole magnets focuse and defocuse the beam, keeping the beam stable. The importance of the accelerating cavities depends on the accelerator type. For a high energy lepton collider like LEP, the beam would not stay in the machine for a full turn without the accelerating cavities. For a hadron storage machine like the Intersection Storage Rings (ISR), they did not need accelerating cavities after the beams were at top energy.

The magnets control the movement of the individual particles transverse to the beam direction, as can readily be seen from the Lorentz force law Eq. (3.1).

$$\mathbf{F} = Q(\mathbf{E} + \mathbf{v} \times \mathbf{B}) \tag{3.1}$$

Here, **F** is the force, **v** is the velocity vector, **B** is the magnetic field vector, Q is the charge and **E** is the electric field vector. A static magnetic field can only give a force

normal to the direction of the beam, and as a consequence, it can do no work on the particles in the beam. Hence we need an electric field component for the acceleration. We also note that even though it is theoretically possible to steer the beam with electric field as well, it is not feasible for most machines due to the fact that the speed is close to the speed of light. To get an equivalent electric field to 1 T magnetic field, one would require an electric field of 300 MV/m. In the LHC we have a nominal dipole field of 8.3 T.

For comparison, in the Compact Linear Collider (CLIC) project, the design accelerating field gradient is 100 MV/m. A superconducting RF cavity has a theoretical maximum electric field of around 50 MV/m. Using magnets for the beam steering is both a necessity and more convenient.

Magnets are defined by their magnetic strength, which we denote B given in Tesla. The particles will as a result of the magnetic field be deflected along a radius of curvature R which at a given location follows the relation

$$\frac{1}{R} = \frac{e}{p}B. \tag{3.2}$$

Here, e is the particle charge, and p is the particle momentum. A Taylor expansion of the magnetic field gives

$$\begin{aligned} \frac{e}{p}B(x) &= \frac{e}{p}B(0) + \frac{1}{1!}\frac{e}{p}\frac{\partial B(0)}{\partial x}x + \frac{1}{2!}\frac{e}{p}\frac{\partial^2 B(0)}{\partial x^2}x^2 + \ldots \\ &= \frac{1}{R} + \frac{1}{1!}\frac{e}{p}\frac{\partial B(0)}{\partial x}x + \frac{1}{2!}\frac{e}{p}\frac{\partial^2 B(0)}{\partial x^2}x^2 + \ldots \end{aligned} \tag{3.3}$$

In this expansion, we get the magnetic components for ideal multipoles. The first term is the bending field of a dipole, the second shows the quadrupolar focusing field, the third term is the sextupolar field and so on. We define the focusing strength k of a quadrupole as

$$k \equiv \frac{e}{p}\frac{\partial B(0)}{\partial x}, \tag{3.4}$$

and the sextupolar in similar manner is denoted m, so that we can rewrite Eq. (3.3) as

$$\frac{e}{p}B(x) = \frac{1}{R} + \frac{1}{1!}\,kx + \frac{1}{2!}\,mx^2 + \ldots \tag{3.5}$$

In Eq. (3.5) we have defined magnetic strengths that have included the particle charge, and momentum. Using these relations we can then develop beam optics which are invariant to beam energy and particle mass/charge ratio.

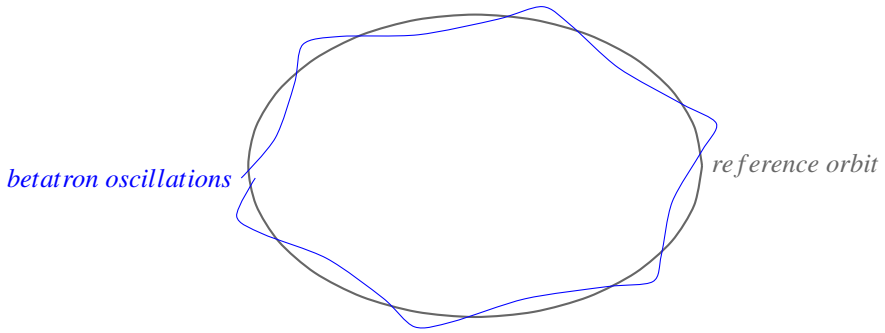

Figure 3.1: The particle trajectories do small oscillations about the reference orbit of a circular accelerator. These transverse oscillations are referred to as the betatron motion.

3.2 Coordinate System

In an accelerator, the particles move along a trajectory which is more or less in the centre of the beam pipe. Since the spread of the particles is small relative to the size of the machine, it makes sense to use a different coordinate system than Cartesian. For a stable machine, the particles oscillates around a fixed point in phase space which we call the reference orbit (see Figure 3.1). A particle perfectly on the reference orbit will stay on this orbit. We define the position of the reference orbit by the vector $\mathbf{r}_0$, and a position which deviates from the reference orbit with the vectors $\mathbf{x}$, $\mathbf{y}$, and $\mathbf{z}$. $\mathbf{z}$ is pointing in the direction of motion, while $\mathbf{y}$ is pointing upwards. $\mathbf{x}$, $\mathbf{y}$, and $\mathbf{z}$ forms a right-handed coordinate system, as shown in Figure 3.2. This is known as the "Frenet–Serret" coordinate system.

As derived in Appendix A, the linear equations of motion in the Frenet-Serret coordinate system are

$$\begin{aligned} x'' + x\left(\frac{1}{R^2} - k\right) &= \frac{1}{R}\frac{\Delta p}{p_0} \\ y'' + ky &= 0, \end{aligned} \tag{3.6}$$

where $'$ denotes derivation with respect to the position s along the orbit. p_0 is the reference momentum for a particle on the orbit. k is the quadrupolar strength defined as positive when the quadrupole is focusing in the vertical plane, and R is the radius of curvature at a position s.

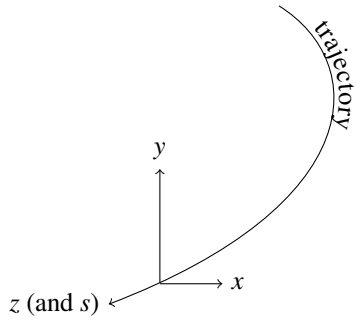

Figure 3.2: Schematic view of the Frenet–Serret coordinate system. In this convention we follow a right handed coordinate system. The z coordinate is pointing in the same direction as s.

In Eq. (3.6) we have made several assumptions. First of all we have assumed that the acceleration is slow, which generally holds for storage rings. Furthermore we have assumed that the longitudinal momentum multiplied by the transverse magnetic field is much larger than the transverse momentum multiplied by the longitudinal field,

$$p_z \, B_T \gg p_T \, B_z.$$

While it is always true that the transverse momentum is much lower than the longitudinal momentum, it is not always the case that the longitudinal field is much smaller than the transverse. In e.g. a solenoid, the longitudinal field is much larger, and the approximation might not hold inside such a magnet. For most part of an accelerator though, this assumption holds. Finally we have ignored second order terms in x, y and $\frac{\Delta p}{p_0}$, which means that for e.g. highly off-momentum protons this equation might not be sufficiently accurate.

3.3 Matrix Elements

Eq. (3.6) in the vertical plane we recognize as second order differential equations. A general linear differential equation of the second order reads

$$a(x) \, f''(x) + b(x) \, f'(x) + c(x) \, f(x) = d(x). \tag{3.7}$$

Eq. (3.7) is homogeneous if $d(x) = 0$. If we assume the functions a, b, c to be constants, we have the general solution

$$f(x) = k_1 e^{\lambda_1 x} + k_2 e^{\lambda_2 x}. \tag{3.8}$$

where k_i, λ_i are constants. If we now assume at first that $\Delta p = 0$, we have a homogeneous differential equation in both planes. We have $b = 0$ in our case, which in the vertical plane gives us the solution

$$y(s) = c_1 e^{\sqrt{-k}\, s} + c_2 e^{-\sqrt{-k}\, s}, \tag{3.9}$$

with c_1, c_2 as constants. What we want to know is the coordinates after a particle has passed through an element from a given initial condition. If we do this we can get out the constants c_1, c_2 and write $y(s)$ as a function of y_0 and y_0', the position and the derivative of the position (i.e. angle) before the element. If we define $s = 0$ before the element, and $s = l$ after the element of length l, we have the relation between the constants

$$y_0 \equiv y(0) = c_1 + c_2 \tag{3.10}$$

$$y_0' \equiv y'(0) = \sqrt{-k}\,[c_1 - c_2]. \tag{3.11}$$

Inserting into Eq. (3.9) we then get

$$\begin{pmatrix} y \\ y' \end{pmatrix} = \begin{pmatrix} \frac{e^{\sqrt{-k}\, l} + e^{-\sqrt{-k}\, l}}{2} & \frac{e^{\sqrt{-k}\, l} - e^{-\sqrt{-k}\, l}}{2\sqrt{-k}} \\ \sqrt{-k}\frac{e^{-\sqrt{-k}\, l} - e^{-\sqrt{-k}\, l}}{2} & \frac{e^{\sqrt{-k}\, l} + e^{-\sqrt{-k}\, l}}{2} \end{pmatrix} \times \begin{pmatrix} y_0 \\ y_0' \end{pmatrix}. \tag{3.12}$$

$$\tag{3.13}$$

We recognize the fractions as the trigonometric cos, sin when k is positive (focusing in the vertical plane), and hyperbolic cosh, sinh when k is negative (defocusing). For the horizontal plane we get the same result, but with

$$-k = k - \frac{1}{R} \equiv k_x. \tag{3.14}$$

We note that the focusing strength in the horizontal plane, k_x, is different from zero also for a dipole. This is known as *weak focusing*.

What we have developed here is called the hard edge model, since we have assumed that the magnetic field regions abruptly changes. The fringe field effect is usually a small effect, discussed more in detail in e.g. [23, Ch. 4.2].

3.3.1 Betatron Motion

If we place the quadrupoles in alternating horizontal and vertical focusing, we will have an oscillation of the particle trajectories as they move along the orbit. At first one might think that if the alternating quadrupoles would presumably be equal in strength, there would be no net effect from the quadrupoles focusing and defocusing the beam. However, since the focusing is dependent on the position of the particles, one can obtain a net effect by having the beam more compact in the defocusing quadrupole for the given plane, and hence obtain a net focusing effect. The simplest ordering of quadrupoles and dipoles is what we call a FODO cell, which stands for focusing-drift-defocusing-drift (O = zero/empty). The drift space is then typically filled with a dipole in the arcs. Using the matrix definition fromn Eq. (3.13), with an appropriate magnet strength and eight FODO cells, we obtain the particle trajectories shown in Figure 3.3. The FODO cell is used in the LHC.

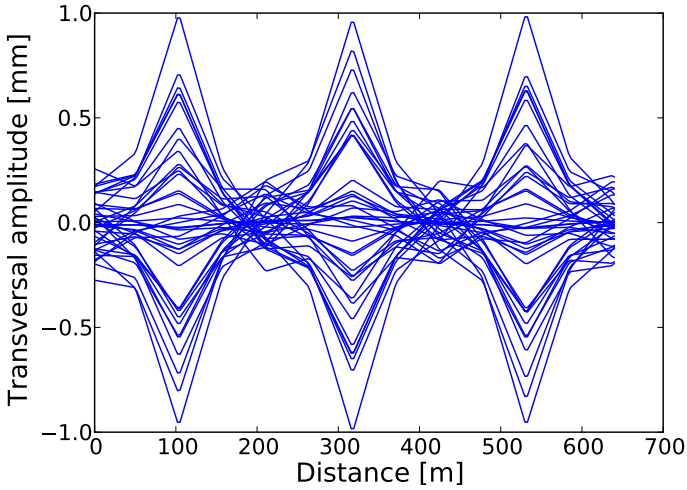

Figure 3.3: Particle trajectories through arch, showing the amplitude in one transverse plane. The results are for a basic thick lens 4D tracking.

The particles oscillate transversally as they move through the accelerator. This is called “betatron motion”. It is possible to have an unstable transverse motion where the transverse position grows out of bounds. Finding the right magnetic (optical) strenghts

for a stable beam is known as matching.

If higher-order magnetic multipoles are introduced, one obtains regions of the transverse phase space where the motion is stable, and other regions where the motions is unstable. It is desirable to keep the stable region as large as possible. The border between the stable and unstable region in the transverse phase space is known as the dynamic aperture.

If we are using transfer matrices for particle transport, we have the following relation:

$$\begin{aligned} X_i &= M_{i-1}\, X_{i-1} = M_{i-1}\, (M_{i-2}\, X_{i-2}) \ldots \\ &= M_{i-1}\, M_{i-2}\, M_{i-3} \ldots\, X_0. \end{aligned} \tag{3.15}$$

In other words, to get the coordinates at one point based on the coordinates at another point, we multiply the initial coordinates with the product of the matrices of each element in between. For a circular collider we call the transfer map for a complete cycle the "one-turn transfer matrix". In Appendix B, we develop the TWISS parameters, α, β, γ, which interpretation can be seen in Figure 3.4.

We define the phase advance μ between two points as the number of betatron oscillations between the two points. In Appendix B we show that by solving the Hill's equations we get

$$\mu = \int_{s_1}^{s_2} \frac{\mathrm{d}s}{\beta(s)}. \tag{3.16}$$

In a circular acclerator we define the tune Q as the phase advance for one complete turn, divided by 2π

$$Q = \frac{1}{2\pi} \oint \frac{\mathrm{d}s}{\beta(s)}. \tag{3.17}$$

Together with the tune, Q, we can write the one-turn transfer matrix as

$$\begin{pmatrix} \cos(Q) + \alpha\, \sin(Q) & \beta\, \sin(Q) \\ -\gamma\, \sin(Q) & \cos(Q) - \alpha\, \sin(Q) \end{pmatrix} = \cos(Q) \cdot I + \sin(Q) \cdot J, \tag{3.18}$$

where I is the identity matrix, and

$$J = \begin{pmatrix} \alpha & \beta \\ -\gamma & -\alpha \end{pmatrix}. \tag{3.19}$$

The derivations can be found in e.g. [20, 24].

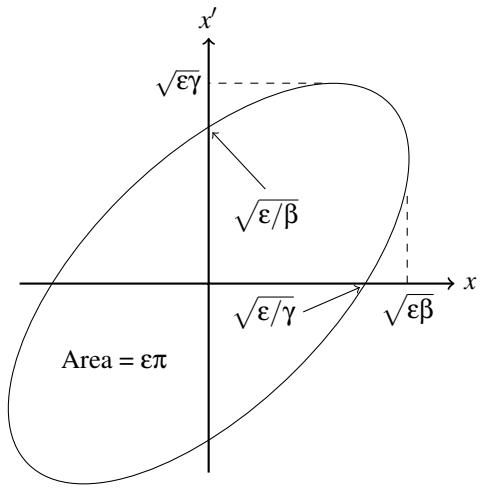

Figure 3.4: The TWISS parameters define the transverse shape of the beam in phase space. The area covered by the beam is defined by the emittance ε, while the physical size is defined by the square root of the β-function times the emittance. The divergence is similarly defined by the γ-function and the emittance.

3.4 Machine Imperfections

A real machine has magnetic field imperfections in the magnets, alignment errors, mechanical vibrations and so forth, which all have to be taken into account in order to get an accurate picture of the beam's behaviour.

3.4.1 Dispersion

The dipolar strength $1/R$ is a function of the particle energy. As a result, a particle with lower energy will see a stronger dipolar strength, and will follow a slightly different orbit in the machine. We define the dispersion function as the orbit for a particle with

$$\frac{\Delta p}{p} = 1.$$

This is a purely fictive orbit, as a particle with that high energy offset will not survive inside a machine.

Dispersion cannot be cancelled out everywhere in a circular machine, but dispersion free regions are needed. The insertion regions in the LHC are dispersion free except for the region dedicated to dispersion collimation. Correcting dispersion can be a complicated matter. An off-momentum particle will not go through the centre of the magnet in dispersive regions. That means the dispersion function will oscillate through the quadrupoles, shown in Figure 3.5. The dispersion function can be found by varying the radio frequency field and measure the change in orbit as a function of frequency.

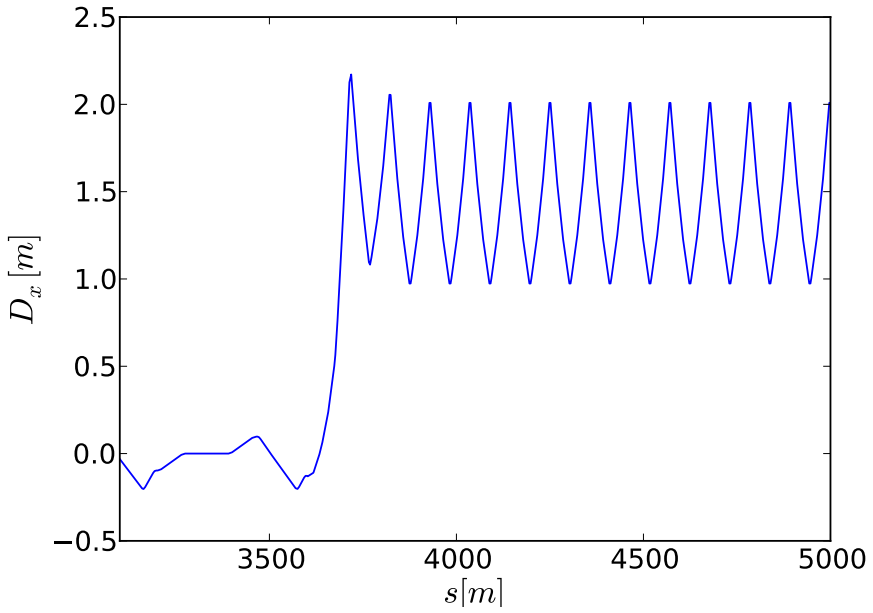

Figure 3.5: An example showing the dispersion for beam one downstream of ALICE in the LHC. ALICE is located in the dispersion free region around 3300 m. In the regular arc you see that the dispersion function oscillate regularly according to the length of the FODO cell. The dispersion is computed using Mad-X, with nominal injection optics.

3.4.2 Coupling

So far we have only considered two fully decoupled transverse planes. A rotated quadrupole will (de-)focus vertically a particle with a horizontal amplitude and vice versa. As a result, with skew quadrupolar field, there is a *coupling* between the two planes. A solenoid field will add coupling as well, since it will transfer some horizontal momentum to vertical momentum. In short, coupling means that the number of betatron oscillations in one plane depends on the particle amplitude in the other plane. There can also be coupling between the longitudinal and transverse planes.

Coupling can be corrected using skew quadrupole corrector magnets. A large machine like the LHC will have several skew quadrupoles distributed around the ring for this purpose.

3.4.3 Chromaticity

We mentioned that particles of different energies will see a different dipolar strength and hence follow a different orbit. The focusing strength k will also be different. That leads to a different number of betatron oscillations for different energies, resulting in a tune spread ΔQ of the beam. The chromaticity ξ is defined as the change in tune spread per relative change in momentum

$$\xi = \frac{\Delta Q}{\Delta p/p}. \tag{3.20}$$

Under the assumption that the relative change in momentum is small, it can be shown [20, Ch. 3.16] that the chromaticity equals the closed integral

$$\xi = \frac{1}{4\pi} \oint k\, \beta \, \mathrm{d}s.$$

Allthough one would initially think that the chromaticity should always be kept small, it is sometimes found beneficial to increase the chromaticity. If the chromaticity is larger, it means that a particle on a resonance will move away from the resonance as it drifts out of the beam envelope. If the chromaticity is small, this change in tune will be smaller and the particle might stay on the resonance until it is lost. Small chromaticity is beneficial in the absence of resonances.

3.5 Diffusion Processes

Single particle dynamics cannot explain why the particles in the core of the beam diffuse towards higher amplitudes, causing an increase of the emittance and particle losses

in the machine. For circular lepton machines, synchrotron radiation is responsible for loss of transverse momentum, which together with the RF cavities keeps the emittance at an equilibrium. For hadron machines, the synchrotron radiation is not large enough to have a significant impact. Even at LHC energies, the synchrotron radiation is barely strong enough to have an influence at all. As a result, various diffusion processes that we will briefly describe here are responsible for a loss of beam particles, and constant emittance growth. The number of particles lost divided by the number of particles in the beam defines the beam lifetime.

3.5.1 Beam-Gas Scattering

An important process for machine induced background is beam-gas scattering. The particles in the beam collide with the rest gas molecules left in the chamber. For elastic collisions, the particles might stay in the beam with a slightly increased transverse momentum (emittance growth), or they might be lost on aperture somewhere. The same is true for diffractive events with small momentum transfer. The rate of beam-gas scattering will be directly proportional to the vacuum pressure. We will look into beam-gas scattering as a source of machine induced background in Chapter 5.

3.5.2 Electron Cloud

Several dynamical processes can increase the vacuum pressure, and an important process to consider can be electron cloud. We illustrate the electron cloud process in Figure 3.6.

When the bunches travel through the beam pipe, they attract oppositely charged particles. Electron cloud can hence be produced by positively charged beams. When the beam trajectory is bent, the particles emit synchrotron radiation. If the energy of the emitted photons is large enough to kick electrons out from the wall, the number of electrons in the vacuum will increase significantly. These primary electrons are also denoted photoelectrons.

The electrons will be accelerated in the field produced by the bunches, and impact on the opposite wall with an increased energy. The impacting electrons will have a probability of sending off a secondary electron from the wall. If this probability is larger than one, and the second bunch arrives in time to accelerate the secondary electrons, this effect can be amplified further.

The probability of creating secondary electrons upon impact is denoted “Secondary Electron Yield (SEY)”, and has been studied extensively in e.g. [25] for different coatings. SEY depend on both the wall material and the history of the vacuum pressure and

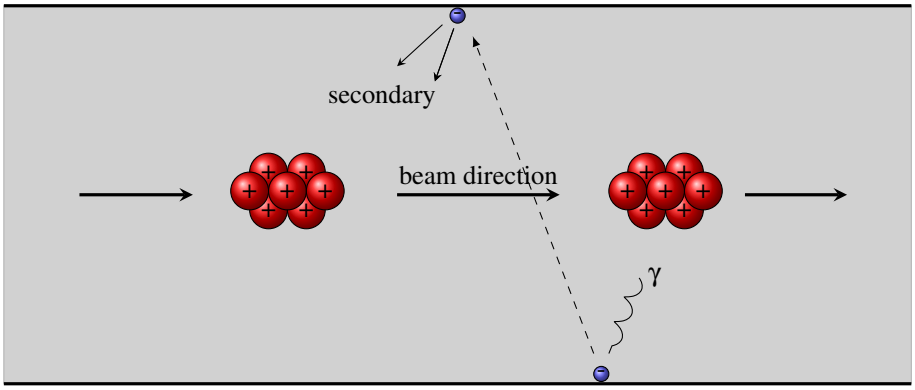

Figure 3.6: Electrons in the vacuum chamber are accelerated by the beam, and hit the wall on the adjacent side with an increased energy. Depending on the secondary electron yield of the vacuum chamber, a number of electron are scattered out from that location. If the next bunch arrives in time to accelerate the secondary electrons, a cascade effect occurs, called electron cloud.

temperature.

Luckily, the sputtering of particles on the wall of the beam pipe reduces the secondary electron yield over time. One way to mitigate electron cloud problems is to increase the beam intensity and vacuum pressure to greatly increase the amount of particles impinging on the wall. This process is known as “scrubbing”. The first “scrubbing run” in the LHC was performed in the spring of 2011.

3.5.3 Intrabeam Scattering

The accelerated beam consists of charged particles densely packed, which have both a longitudinal and transverse momentum relative to the beam movement. As a result, these particles will collide and exchange momentum within the beam. This leads first and foremost to an emittance growth, but if the bunch charge density is high enough it can also lead to significant particle loss. The loss of particles due to intrabeam scattering is known as the Touschek effect, and was first observed in the electron storage ring AdA in Frascati, Italy.

Intrabeam scattering is a function of both the bunch volume and the bunch intensity. Larger volume and/or lower bunch intensity will reduce scattering. Two models, Piwinski and Bjorken-Mtingwa are commonly used to describe the effect, and they both

agree well at higher energies [26, 27].

Intrabeam scattering is typically too weak in an electron storage ring to have an effect because the radiation damping from synchrotron radiation is usually faster. In high intensity hadron storage rings on the other hand, intrabeam scattering can cause significant degradation of luminosity lifetime. For nominal LHC energies, an IBS lifetime of around 63 h for the longitudinal beam size and 105 h for the horizontal beam size is expected from simulations [28, ch. 5.5.2].

3.5.4 Burnout from Collisions

The dominant contribution to the beam lifetime for an ideal accelerator will be the loss of particles at the interaction points due to the collisions themselves. Elastic and quasi-elastic collisions can give small momentum transfers, producing an emittance growth rate in addition to particle losses from the stronger interactions. These collisions can be a source of background which we denote "interaction region cross-talk". We will come back to that source of background in Chapter 6.

The lifetime from burn-out follows

$$\frac{1}{\tau} = \frac{\mathscr{L}\sigma}{N}, \tag{3.21}$$

where σ is the cross section, N is the number of particles in the beam and $\mathscr{L}$is the luminosity. For LHC, which has a luminosity of $1 \times 10^{34}\mathrm{cm}^{-2}\mathrm{s}^{-1}$, a beam intensity of about 3×10^{14}, and an inelastic cross section of around 70 mb, the lifetime from burnout will be around 130 h per high luminosity experiment, or 65 h in total.

3.5.5 Beam-Beam Interaction

When the beams are colliding, they inherently kick each other due to the electromagnetic interactions between the beams. These are separated in two main categories, head-on and long-range. The head-on beam-beam effect comes from the two bunches that collide with each other, resulting in a focusing effect for oppositely charged beams, and a defocusing effect for equally charged beams like the LHC. The long-range beam-beam effect comes from bunches that pass each other closely. The linear beam-beam parameter is defined as [21, ch.5]

$$\xi = \frac{N\, r_0\, \beta^*}{4\pi\, \gamma\, \sigma^2}, \tag{3.22}$$

where N is the number of particles in a bunch, r_0 is the classical particle radius, β^* is the β-function at collision, and σ is the beam size. This is the generalised case with

round beams. The force from the beam on a test particle is

$$F(r) = \frac{n\, e^2(1+\beta^2)}{2\pi\, \varepsilon_0} \frac{1}{r} \left[1 - \exp(-\frac{-r^2}{2\sigma^2}) \right], \tag{3.23}$$

where n now is the density of particles per longitudinal distance s along the beam direction. The shape of the function

$$\frac{1}{x} \left[1 - \exp(-x^2) \right]$$

is shown in Figure 3.7. x will then be proportional to the radial distance from the beam core, measured in number of beam σ. The beam-beam force has a maximum at around 1.1 σ. Between $\pm$ 1 σ, the beam-beam force changes approximately linearly. The focusing kick given to the particles in this region is the linear beam-beam parameter.

The beam-beam force is not directly a diffusion process, but it distorts the orbit and increases the tune footprint (the spread in the tune among the beam particles). This can then indirectly lead to significant reduction in the beam lifetime.

For the LHC, the beam-beam interactions are expected to be one of the most important parameters that will eventually limit the performance of the machine, and it has been studied carefully in the past [29].

3.6 Machine Aperture

Simulating experimental background evolves around particle tracking and stability analysis to obtain estimates of losses around the machine which then subsequently can produce particle showers towards the experiments, resulting in false detector signals. In order to get proper loss estimates, two things are required. First, you need to have a good model for particle tracking. We will come back to that afterwards. Second, you need a precise knowledge of the aperture restrictions around the machine.

A particle will have a fixed betatron action, but will oscillate about the closed orbit as explained before. The beam will change its size as well, shown previously in Figure 3.3. What stays fixed (on a short time scale at least) is the beam emittance. As a result, what is interesting to know about the aperture is how many beam sigma there is between the beam orbit and the wall of the beam pipe, known as the normalised aperture.

In addition, the beam orbit is not necessarily going through the centre of the beam pipe. The element (be it a magnet, RF cavity or something else) can be misaligned or tilted, or the orbit can be displaced either from magnetic errors or simply by design

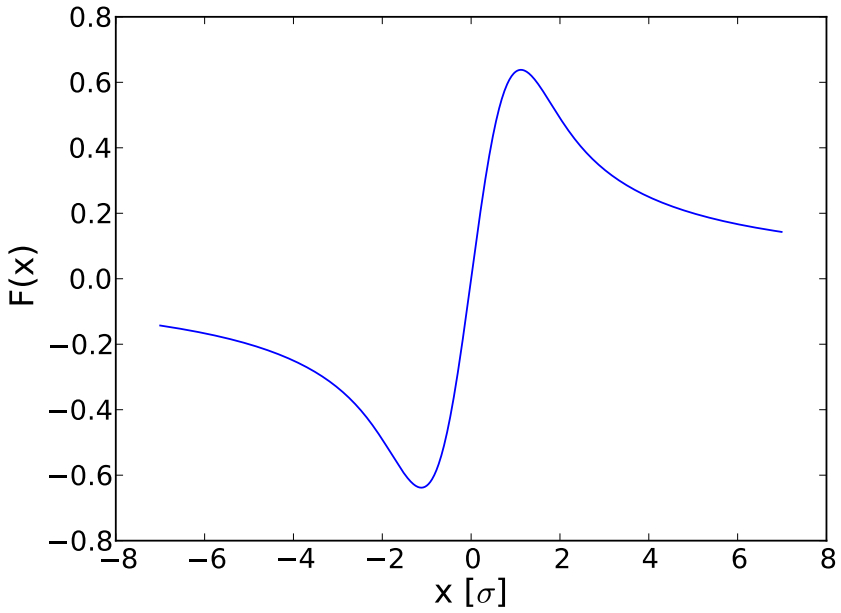

Figure 3.7: An illustration of how the beam-beam force on a particle changes depending on the distance from the beam. This function will be proportional to the beam-beam force, with the horizontal axis measured in units of beam σ.

because you want an orbit bump for some reason. When setting the aperture tolerances, it is important to take these (potential) displacements of the orbit into account, and not merely measure the aperture from the centre of the element.

As we explained earlier, there is dispersion in many places of the machine, which will produce an additional spread of the beam in addition to the transverse beta-function. Both the dispersion and the beta-function must be taken into account when estimating the available aperture in the machine.

The LHC has a very high amount of stored beam energy, around 360 MJ/beam. That means that if the beam is lost on any component in the machine, that component will have to be replaced. Even the energy in the halo of the beam can be dense enough to heat the many superconducting elements producing a magnet quench. To protect the machine, a three stage collimation system is installed [30, 15].

In order to take into account orbit tolerances and the variations of the beam size in the LHC, we calculate the "normalised primary aperture", known as N1. This calculation is explained in [31, 32]. The N1 is essentially the maximum number of beam σ that can fit inside the beam chamber without touching any chamber wall. N1 takes into account the orbit tolerances, alignment of the machine, dispersion and so forth.

In Figure 3.8 we illustrate how the N1 is varying in the LHC for injection optics. We see that it is predominantly governed by the maximum β in either plane. Depending on the collimation system and the protection requirement, one then defines a minimum N1 that can be accepted.

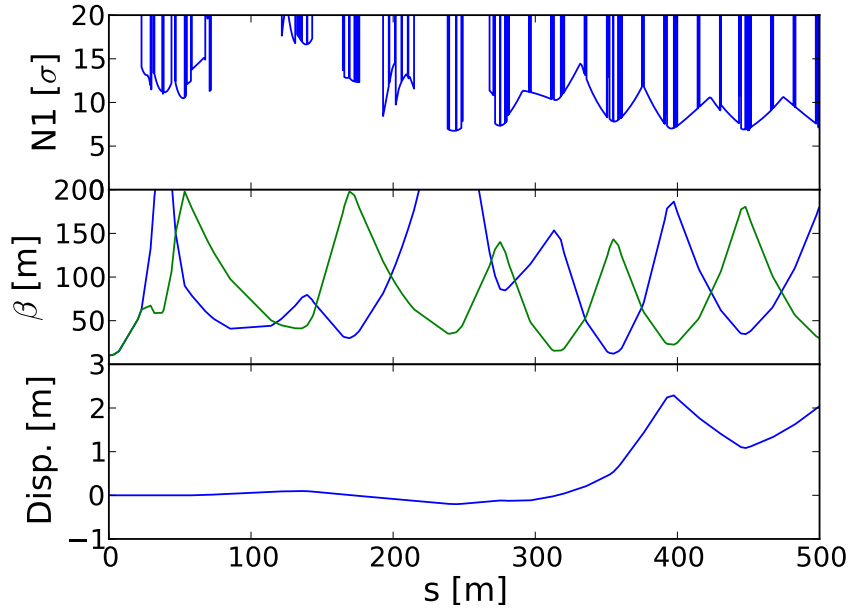

Figure 3.8: Here we illustrate how the normalised primary aperture is varying on one side of LHCb for injection optics in the top plot. LHCb is located at s = 0 m. Between 400 m and 500 m, we see the regular FODO cell in the arc. In the middle plot we see the horizontal beta in blue, and the vertical in green. In the lower plot we see the horizontal dispersion. Computed using Mad-X.

3.7 Particle Tracking

Particle tracking studies require careful consideration. For linear elements like drifts, dipoles and quadrupoles, an exact matrix can be obtained. For non-linear elements, a matrix representation that is independent of the initial coordinates does not exist. We generally call the function representation of an element a "map", which calculate the parameters of a particle at the end of an element based on the parameters at the beginning of an element, as shown in Figure 3.9. For some studies, it is sufficient to

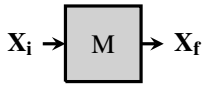

Figure 3.9: The transfer map takes the calculates the final coordinates of a particle, $\mathbf{X_f}$ based on the initial coordinates of a particle $\mathbf{X_i}$.

only study the transverse stability. That means that one only looks at the positions and angles in the horizontal and vertical plane, and ignores movement in the longitudinal plane. This is known as "4D tracking" (two parameters per plane, four in total). In other cases, it is required to also take the longitudinal stability into account, which introduce the longitudinal position with respect to the centre of the beam, and the RF phase the particle has with respect to the synchronous phase. This gives a total of 6 coordinates. For instance, this can be relevant when you want to study intrabeam scattering, or when you expect coupling between the planes. This is known as "6D tracking". In general, you can learn a lot in many situations from looking at one plane only, since the three planes should normally be more or less decoupled.

3.7.1 Symplecticity

For long term tracking, it is of high importance that the transfer map used are symplectic. Symplecticity means that the transformation should not increase or decrease the action of a particle. Magnetic fields alone can not do work on a particle, which would be required in order to change the momentum of the particle (momentum can still be shifted from one plane to another when you have coupling). As a result, our representation of the magnet – the transfer map – should neither do any work on the particle. Mathematically, it means that the transfer map $\mathbf{M}$ should obey the relation [21]

$$\mathbf{M}^T \, \mathbf{J} \, \mathbf{M} = \mathbf{J}, \tag{3.24}$$

where T denotes transpose of the matrix and $\mathbf{J}$ is the matrix

$$\mathbf{J} = \begin{bmatrix} 0 & \mathbf{I} \\ -\mathbf{I} & 0 \end{bmatrix}, \tag{3.25}$$

and $\mathbf{I}$ is the identity matrix.

There are several ways to ensure that the symplectic condition is obeyed, and one of them is to represent the accelerator in thin lenses and drifts between. In a thin lens formalism, the particle positions can only change in the drift sections. The kick from a thin lens can only change direction of the particle, and the change in direction can only be a function of the position. Hence, the general matrix for a kick is

$$\begin{bmatrix} 1 & 0 \\ a & 1 \end{bmatrix}, \tag{3.26}$$

where a can be a function of the input coordinates. Eq. (3.26) obeys the symplectic condition, which means that a thin lens representation will always be symplectic.

3.7.2 Off-Momentum Tracking

In Appendix A we develop the linear equations of motion under the assumption that the transverse momentum and energy offset of the particles were small. The same assumption is used for most formalisms developed in tracking codes, because it allows transfer maps that are faster to calculate, and they are simpler to implement and understand. The relative momentum deviation in a beam is typically not more than 1 ‰, which makes this assumption satisfactory. There are tracking codes which will allow for arbitrary momentum deviation, but the increased computing resources needed are for many applications unacceptable.

For most studies the limitations are satisfactory, but for background studies we are interested in particles which are actually lost and then produce showers into the experiments. These particles can have much higher momentum offset, and special care should be taken to ensure that the simulation results will be reasonable. Allthough the accuracy of the tracking simulation worsens, there is a benefit in that these particles are not tracked for long, which means the tracking accuracy becomes less important.

Chapter 4

LHC Layout

The Large Hadron Collider is designed for colliding proton beams of 7 TeV energy at a luminosity of $1 \times 10^{34}\,\mathrm{cm}^{-2}\mathrm{s}^{-1}$. It has eight insertion regions, comprising four interaction points, two collimation regions, one insertion for accelerating cavities and one for beam extraction (beam dump).

The four main experiments are ATLAS, ALICE, CMS and LHCb, located in insertion regions 1, 2, 5, and 8 respectively, as shown in Figure 4.1. The other four long straight sections are used for collimation (IR3 and IR7), RF cavities for acceleration (IR4) and for the beam extraction (IR6). In order to understand the machine induced background we need a good knowledge of the layout around the experimental regions, as well as the machine optics, orbits and aperture.

This chapter will give a description of the interaction region layouts and a brief introduction to the four main experiments with background protection and monitoring in mind. We will in later chapters use this for reference. The machine parameters serve as input parameters for simulations in Chapter 5 and Chapter 6, and the understanding of how the experiment measure the background is important in Chapter 7 which covers machine performance and analysis.

4.1 General Parameters

The nominal (design) parameters for the LHC consists of 2808 bunches, each consisting of 1.15×10^{11} protons per beam. The normalised emittance ε is expected to be

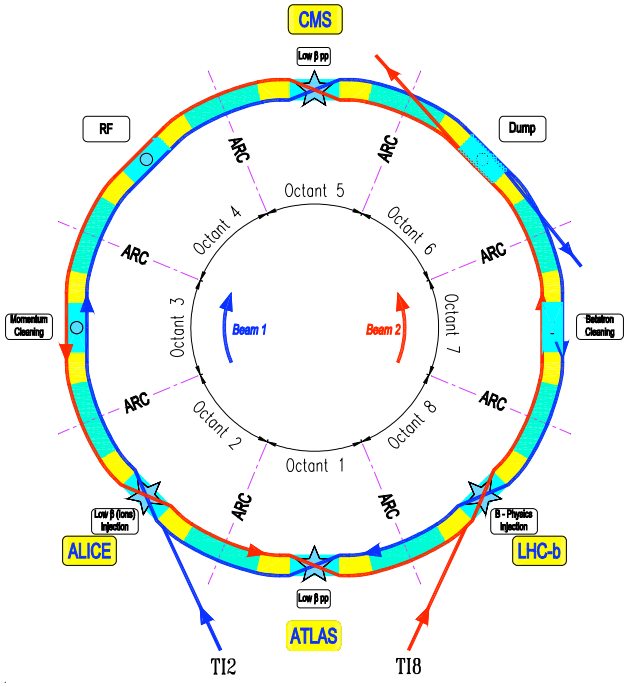

Figure 4.1: The overall layout of the LHC. The LHC is split in eight octants. Each octant is comprising of an insertion region, and separated by a regular bending region (arc).

3.75 μmrad. The luminosity of a machine is defined as

$$\mathscr{L} = \frac{1}{4\pi} \frac{f_{\text{coll}}\, I_1\, I_2\, F_{\text{geom}}}{\sqrt{\sigma_x\, \sigma_y}}. \tag{4.1}$$

f_{coll} is here the bunch collision frequency, i.e. number of bunch collisions times the revolution frequency. In the LHC, the nominal bunch spacing is 25 ns. The entire ring cannot be filled however, as there need to be room left for the dump kicker rise time, and there will be one gap per injection according to the rise time of the injection kicker as well. In total, 2808 of the total 3564 possible buckets will be filled with a proton bunch. We then get

$$f_{\text{coll}} = \frac{2808}{3564} (25\text{ ns})^{-1} = 31.5\text{ MHz}.$$

Table 4.1: The nominal crossing angles in each interaction point. Negative values means crossing against the beam 1 axis direction.

IP	Angle [μmrad]	Plane
1	142.5	ver
2	±150.0	ver
5	142.5	hor
8	-200/-65	hor

I_1 is the bunch intensity in beam one, and I_2 the bunch intensity in beam two, 1.15×10^{11} protons for the nominal LHC parameters. σ_x is the horizontal beam size, and σ_y is the vertical beam size. The beam size at collision is defined as

$$\sigma = \sqrt{\varepsilon\,\beta^*},$$

where $*$ simply denotes the value at the interaction point.

In Eq. (4.1) we assume that beam one and beam two have equal Gaussian shape and equal size. The more general luminosity function is the overlap integral of the transverse density functions of the two beams

$$\mathscr{L} = f_{\text{coll}} \int_x \int_y \rho_1(x,y)\cdot\rho_2(-x,y)dxdy. \tag{4.2}$$

Since the horizontal x-axis is inverted for the two beams, we add a minus sign for beam two. If the beams are colliding at an angle, this has to be applied to the coordinate system transformation as well.

Finally, F_{geom} is a geometrical correction factor. F_{geom} is around 1 for the nominal LHC parameters. For the high luminosity upgrade there are plans to squeeze the beams even further, which results in a significant reduction in the geometrical factor. This can then be mitigated with crab cavities [33]. Studies of the LHC luminosity was covered in detail in the thesis of S. White [34].

In each interaction point, the beam orbits are on top of each other for about 120 m (see Figure 4.3), providing about 30 additional collisions. Having these collisions head-on would produce unacceptable tuneshift and too high radiation levels in the experimental region from all the added collision residues. To avoid the additional collisions, a crossing angle is introduced. The crossing angles for nominal optics are given in Table 4.1. These crossing angles are a combination of external crossing angle and the internal crossing angle arising from the spectrometer dipoles in LHCb and ALICE. In

Figure 4.2 we show how the two polarities for the internal spectrometer changes the crossing scheme. More details can be found in [28, Ch. 4.2]. Due to the large amount of long-range collisions, the tune shift from these collisions is still significant even if the contribution per bunch crossing is reduced [29].

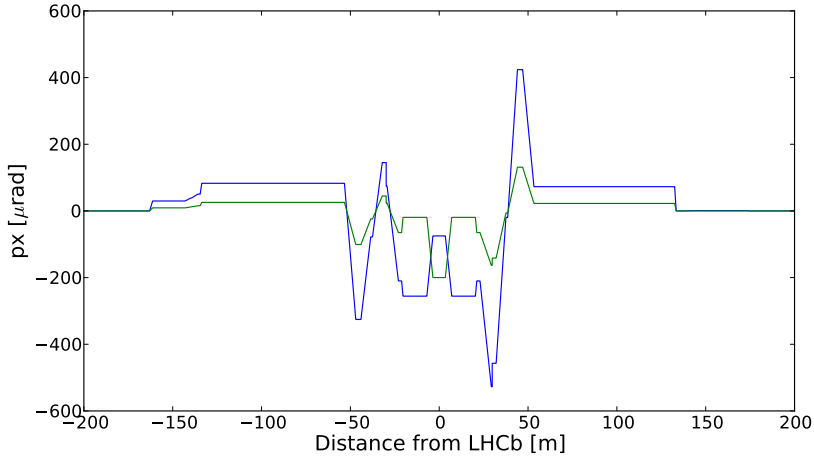

Figure 4.2: The two crossing angle schemes in LHCb. Only beam 1 horizontal shown. The blue curve shows the disfavourable spectrometer dipole polarity, which requires a larger external compensation.

The nominal LHC parameters are listed in Table 4.2. In addition to a new world record in beam energy, the unprecedented amount of bunches and stored energy are of particular importance. The LHC peak luminosity is expected to be two orders of magnitude above the previous record holding machine Tevatron [9]. The small β values in the ATLAS and CMS experiments means tight aperture and alignment tolerances in these interaction regions. In Table 4.3 we show the parameters at the end of the 2011 run for comparison, which already result in a peak luminosity which is 35% of the nominal value.

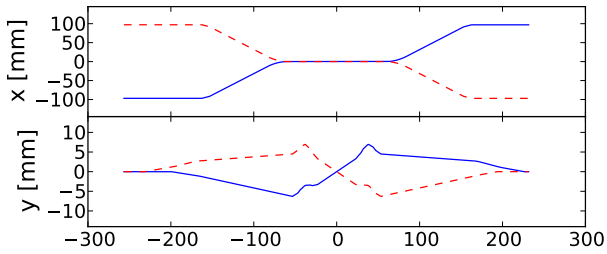

(a) ATLAS

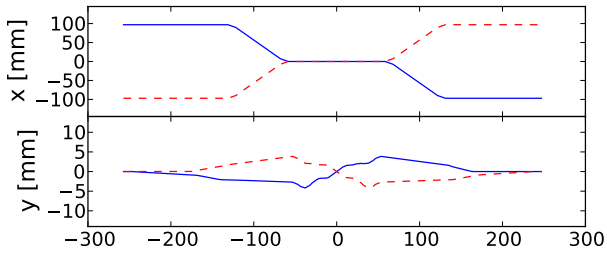

(b) ALICE

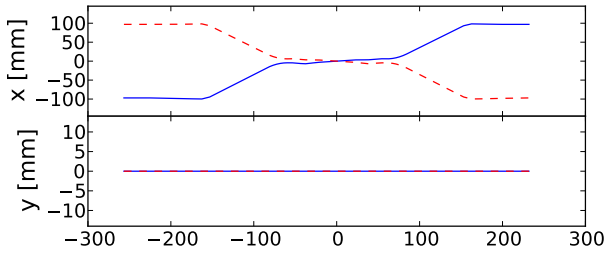

(c) CMS

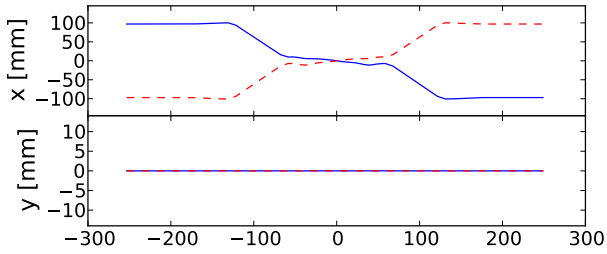

(d) LHCb

Figure 4.3: The orbit of the two beams for nominal optics, including the crossing angle. Beam 1 in blue/solid moving in positive direction, beam two in red/dashed. We have added what is called the "survey", which shows how the orbits of the two beams are separated outside the interaction region.

Table 4.2: The nominal parameters for LHC at injection and collision (proton physics), as given by [28].

	Injection	Collision	Unit
Beam energy	450	7000	GeV
Particles per bunch	1.15×10^{11}		
Bunches per beam	2808		
Bunch spacing	25		ns
Stored energy	23	362	MJ/beam
Beam current	0.584		A
Transverse emittance	3.5	3.75	μm rad
Peak luminosity (ATLAS/CMS)		1×10^{34}	$cm^{-2}s^{-1}$
β^* ATLAS/CMS	11	0.55	m
β^* ALICE	10	10	m
β^* LHCb	10	10	m

Table 4.3: The LHC parameters at end of the 2011 proton physics run [35].

	Collision	Unit
Beam energy	3500	GeV
Particles per bunch	2×10^{11}	
Bunches per beam	1380	
Bunch spacing	50	ns
Transverse emittance	~ 2	μm rad
Peak luminosity (ATLAS/CMS)	3.5×10^{33}	$cm^{-2}s^{-1}$
β^* ATLAS/CMS	1.0	m
β^* ALICE/LHCb	10	m

4.1.1 Nominal Optics

The nominal optics are described in Table 4.2, which has one optics for ATLAS/CMS, and another for ALICE/LHCb. In Figure 4.4, we show the β-functions for both optics.

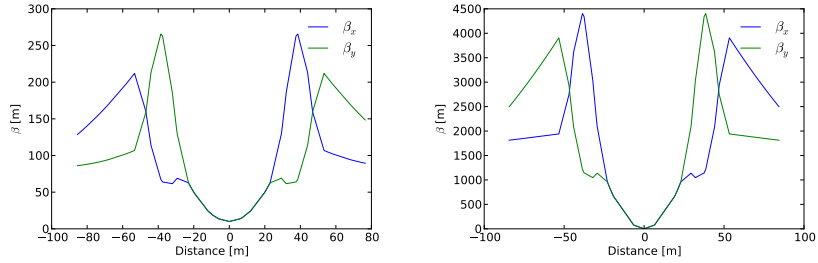

(a) ALICE, beam 1

(b) CMS, beam 1

Figure 4.4: The β-functions for the nominal optics, with a β^* of 0.55 m in CMS, and 10 m in ALICE, for beam one. Beam 2 optics is similar, but the x- and y-planes are inverted. ATLAS has similar optics as CMS but inverted for the same beam. Similarly, LHCb and ALICE are also antisymmetric.

4.1.2 Interface Plane

An interface plane between the machine and the different experiments is defined for all background simulations, and given in Table 4.4. This interface plane is typically chosen after the last shielding element at the entry of the experimental cavern.

4.2 The Interaction Regions and Experiments

The LHC consist of two general purpose, high luminosity experiments. These are ATLAS and CMS. In addition, two other experiments are aiming for less than maximum luminosity. Hence we call them low luminosity experiments, which should be considered a relative term. LHCb in particular, will still obtain the same luminosity as the CDF and D0 detectors in Tevatron. We start with the low luminosity experiments and their interaction regions.

Table 4.4: The positions of the interface planes are defined as an infinite transverse plane upstream of the interaction point, approximately at the entrance of the cavern after the last shielding.

Exp.	Beam 1 [m]	Beam 2 [m]
ATLAS	22.6	22.6
ALICE	19.5	19.5
CMS	22.6	22.6
LHCb	2.1	19.9

4.3 Low Luminosity Interaction Regions

The low luminosity experiments ALICE and LHCb are located in the same insertion regions where the beams are injected, which means that the insertion regions are asymmetric. Beam one is injected in IR2 where ALICE is located, and beam two in IR8 where LHCb is located. In Figure 4.5 we show the interaction region 8. Q1-Q7 are the main quadrupoles. The inner triplet, Q1-Q3 is about 30 m long, located about 23 m from the interaction point. Q1 and Q3 are the same kind of magnet (MQXA), while Q2 consists of two magnets which are slightly shorter (MQXB). The D1 and D2 are the dipole magnets responsible for bringing the beams onto the same orbit. There is a set of injector magnets (MSI) between Q5 and Q6 and the MKI between Q4 and Q5. In addition, there is a 4 m long collimator called the TDI which sits between D1 and D2, responsible for catching failed injections.

The vertical tertiary collimator (TCTVB) sits in the recombination chamber between D1 and D2, 73 m from the interaction point. It is a special collimator which is seen by the outgoing beam as well, allthough at a larger aperture. The horizontal tertiary collimator sits 118 m from the interaction point, still in front of D2. Differing from the vertical collimator though, this is not in the common beam pipe, which means that it is not seen at all by the outgoing beam. The TDI and TCTVB are shown in Figure 4.5(b).

4.3.1 ALICE

The ALICE detector is shown in Figure 4.6. ALICE is a general purpose heavy ion physics experiment. The experiment is operational during proton physics as well. It has a maximum luminosity of around 2×10^{30} cm^{-2}s^{-1} before some sub-detectors must be

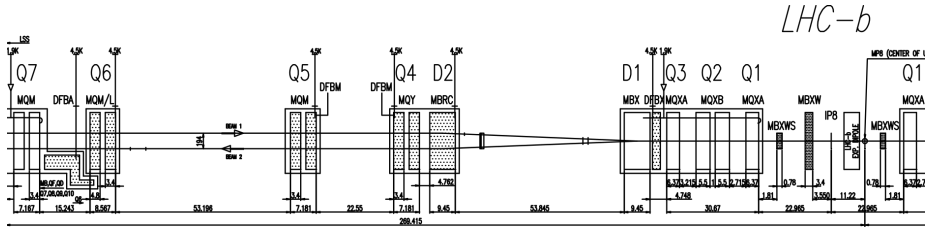

(a) IR8 left

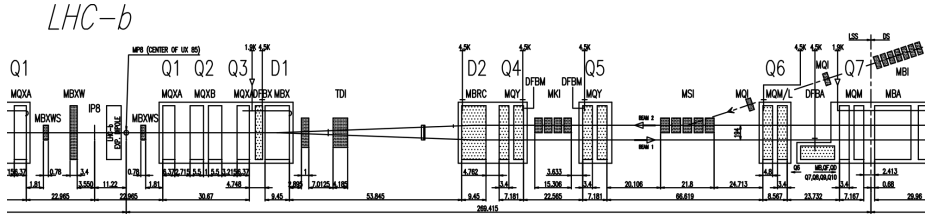

(b) IR8 right

Figure 4.5: The layout of the interaction region where LHCb is located. The beam injection in the same region makes e.g. the pressure profile asymmetric. The ALICE interaction region looks similar but mirrored since the injection is on the left hand side. Figure from [36].

turned off for protection. That is four orders of magnitude less than ATLAS and CMS for the nominal machine parameters. As a result, it is perhaps the most challenging experiments in terms of controlling the background.

ALICE is an asymmetric detector. The central barrel chamber is surrounded by a solenoid magnet (red) which stretches 6.2 m to each side of the interaction point. Downstream of the interaction point for beam one, a dipole magnet and several muon tracking stations are installed. The detector stretches almost 19 m away from the interaction point on this side.

ALICE has zero degree calorimeters (ZDC) located in front of the D2 dipoles on each side of the interaction point. It is situated behind the vertical collimator, and it was found in tracking studies that it is partially shadowed by this collimator [37].

The V0 detectors are useful for background detection [38]. These are two sets of scintillator counters located asymmetrically about the interaction point. The V0A detector is located 3.55 m upstream for beam one, while the V0C detector is located 0.9 m downstream of the interaction point for beam one.

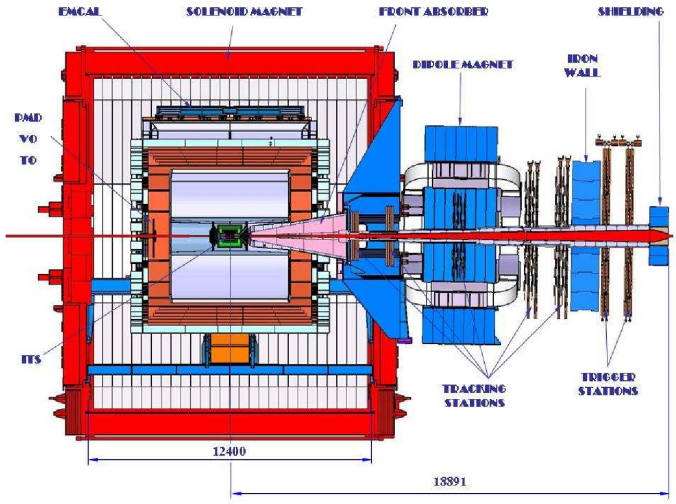

Figure 4.6: The ALICE detector. Figure from [12]

If one then considers time 0 when the bunches collide, one can identify collision signals and background signals by looking at the time difference of the two signals (V0A-V0C), and the addition of the timing signals (V0A+V0C). This is illustrated in Figure 4.7. We see that this method will better disentangle beam one background from the collisions than beam two background. The method then assumes that all signals arrives on time, not considering e.g. debunched beam. In [39, pp. 5] an example using real data is shown.

4.3.2 LHCb

The LHCb detector is optimised for B-physics. Due to the fact that b hadrons are predominantly produced in the forward cones at high energies [14], the LHCb detector is an asymmetric forward detector. It is the only of the four larger experiments in the LHC without a central barrel detector. The layout of the detector is shown in Figure 4.8, where the collision point can be seen in the left of the figure. Beam one is coming from the left, which is referred to as the beam one side or the left side of the experiment.

The rare decays which LHCb are looking for, are more difficult to study if the

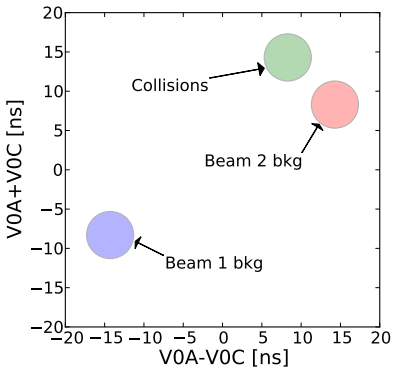

Figure 4.7: The timing of the collision events and background events at the V0 detectors in the ALICE experiment, with respect to the bunch arrival time.

pileup[1] is higher than one. Hence, the LHCb luminosity is limited by keeping the pileup low, while ATLAS and CMS are designed for about 20-25 particle collisions per bunch crossing.

The central part closest to the interaction point comprises of a high precision vertex locator (VELO). This is a series of silicon modules of 8.4 cm diameter, designed to cover the pseudorapidity range $1.6 < \eta < 4.9$ [14, Ch. 5.1]. The VELO has proven very interesting for detecting beam-gas events [40]. By collecting the vertices from non-colliding bunches, the VELO is capable of estimating both the beam profile and the crossing angle.

The main detectors for background monitoring are the beam condition monitors (BCM) [41], and the beam loss scintillators (BLS) [42] to detect fast losses. The BCM's consist of 8 diamonds at an angle of about 1° with respect to the interaction point, covering an angle of about 0.2°. Both the BLS's and the BCM's are located about $2-3$ m away from the interaction point, installed on both sides. The rest of the experiment comprises of a dipole magnet, followed by two Cherenkov counters (RICH 1 and 2), calorimeters and finally muon chambers farthest from the interaction point.

LHCb has published studies of machine induced background in several papers, and as a part of this work we presented in detail the full simulation chain which is set up, see Appendix D.4. Recently, a paper was published which showed good agreement between simulations and background data [43].

[1] Pileup is defined as the number of collisions per bunch crossing.

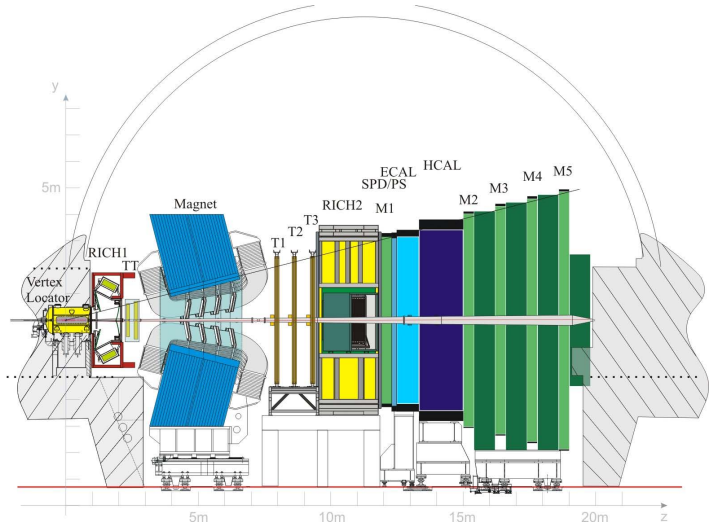

Figure 4.8: The LHCb detector. Figure from [14]

This thesis work is intended not to be specific to any one experiment. However, as LHCb is currently the only experiment with the complete simulation chain available, it has been natural to use the results of the LHCb background studies in our discussions later on. For ATLAS and CMS complete FLUKA models of the long straight sections have not been available, and for ALICE the main challenge has been transporting the simulations from the interface plane towards the detector and evaluate the expected detector response.

4.4 High Luminosity Experiments

The high luminosity experiments ATLAS and CMS are located in interaction regions 1 and 5. These interaction regions are approximately symmetric. In Figure 4.9 the interaction region left of CMS is shown. The inner triplet Q1-Q3 is the same as for the low luminosity experiments. The D1 dipole is here a set of six shorter magnets, while in the low luminosity interaction regions the D1 was one longer magnet. Both tertiary collimators are located just after the D2, $145 - 147$ m from the IP. A TAN (target absorber neutrals) is located about three meters closer to the interaction point, responsible for collecting neutral particle residues from the collisions.

The TOTEM Roman pots stations are named XRP1-3 in Figure 4.9. The first station is right behind the TAN, the second between Q4 and Q5, while the last is between Q5 and Q6. The ALPHA project is a part of the ATLAS collaboration, and consists of two stations four metres apart, located just behind Q6 in the ATLAS insertion region.

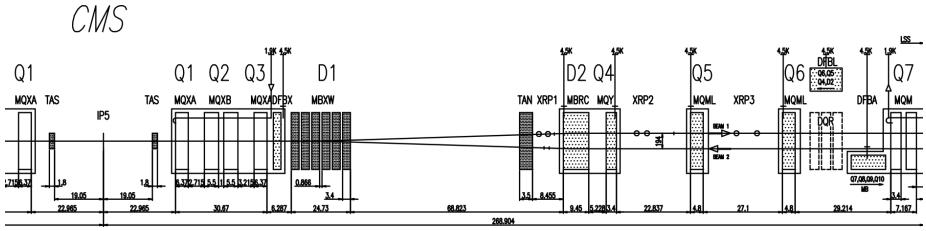

Figure 4.9: The layout of the interaction region where CMS is located, right hand side only. The interaction region is symmetric about the interaction point. Figure from [36].

A collimator type named TAS (target absorber secondaries) is installed on each side of the interaction point close to the first quadrupole magnet, Q1, to reduce the heat load from secondary particles from the collisions.

4.4.1 ATLAS

ATLAS is a general purpose barrel detector designed for the nominal LHC luminosity of 1×10^{34} cm^{-2}s^{-1}. It is a symmetric barrel detector comprising of a central tracking system, a solenoid magnet, electromagnetic and then hadronic calorimeters, and in the outer part a toroid magnet and a muon detector system. The basic layout can be seen in Figure 4.10.

In order to mitigate the high level of background, a multi-layered shielding system is installed in the forward regions of the ATLAS experiment, as is outlined in Figure 4.11. A total of more than 2800 tonnes of metal, concrete and plastic has been used [10].

For background monitoring, beam condition monitors (BCM) are installed at $\pm$ 1.8 m from the interaction point. ATLAS has the perhaps most extensive muon detector system, and special care has been taken to track the background in the muon system as well. Proportional tubes and various scintillators are installed in the inner, middle, and outer muon endcaps [10].

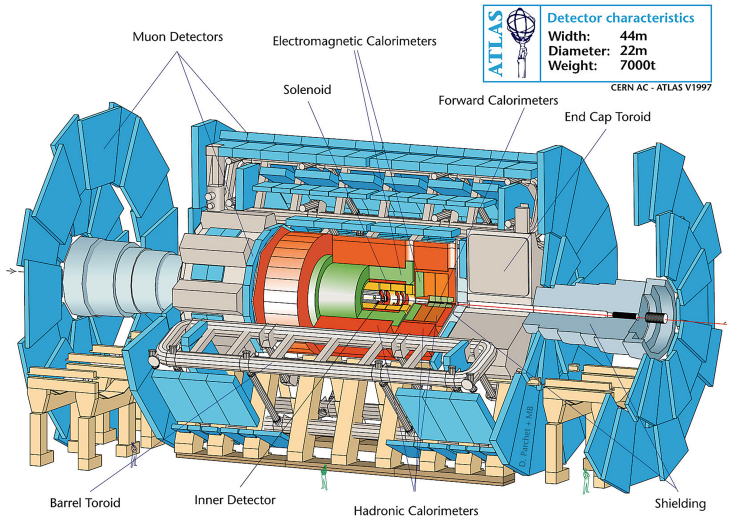

Figure 4.10: The ATLAS detector. Figure from [44]

4.4.2 CMS

CMS is the second general purpose high luminosity detector at the LHC. As can be seen in Figure 4.12, the overall design principle is similar to that of ATLAS. The main differences are that the solenoid is located outside of the calorimeters, and a more compact muon system is implemented (hence the name Compact Muon Solenoid).

The main background monitors in CMS are beam condition monitors. There are the BCM1(L) located 1.8 m from the interaction point on both sides, and the BCM2(L) located 14 m from the IP. The L stands for leakage current, referring to the measurement type. The BCM1 have a sampling time of 5 μs, and the BCM2 a sampling time of 40 μs. This is comparable to the LHC revolution time which is 89 μs, but not fast enough to resolve the individual bunches. The BCM1 sees collision products as well, while the outer part of the BCM2 is hidden from the collision spot and sees beam halo products [13].

A BCM1F (F for fast) is installed in the same location as the BCM1, with a sampling time on the order of 1 ns. The location is optimal for measuring the difference between halo and collision products, which will arrive at this location with a time difference Δt of about 12.5 ns.

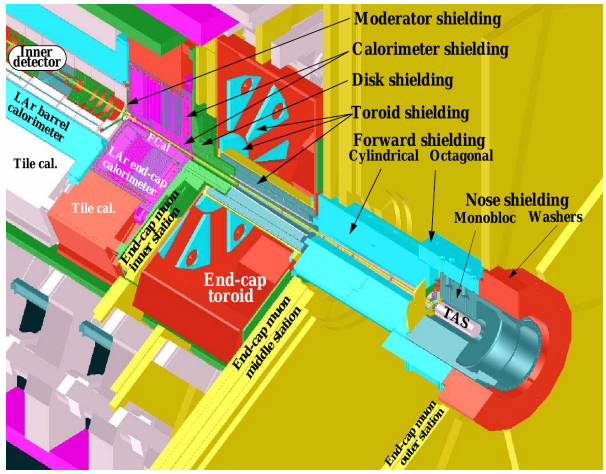

Figure 4.11: The shielding in the ATLAS forward region. Figure from [10].

Since the CMS experiment is close to the beam dump region in IR6, there is a larger concern for particle sprays coming from particles in the abort gap. The BCM1(L) is a good monitor to track the population in the abort gap, with its resolution time.

In addition to the BCM's, beam scintillator counters (BLS) are installed at 10.9 m and 14.4 m from the interaction point. These are responsible for counting hit and coincidence rates.

4.5 Machine Aperture

The machine aperture is of great importance for the machine induced background. The closer the beam is to the aperture, the larger fraction of the beam will be scraped away producing more showers towards the experiments. Previously in this chapter we showed the optics in the interaction regions. The β-function relates to actual beam size according to the function

$$\sigma = \sqrt{\varepsilon\beta},$$

where ε is the beam emittance. In the horizontal plane we generally have a non-negligible dispersion. Taking into account the momentum spread of the particles σ_p, we have the horizontal beam size defined as

$$\sigma_x = \sqrt{\varepsilon\,\beta + (D_x\,\sigma_p)^2}, \tag{4.3}$$

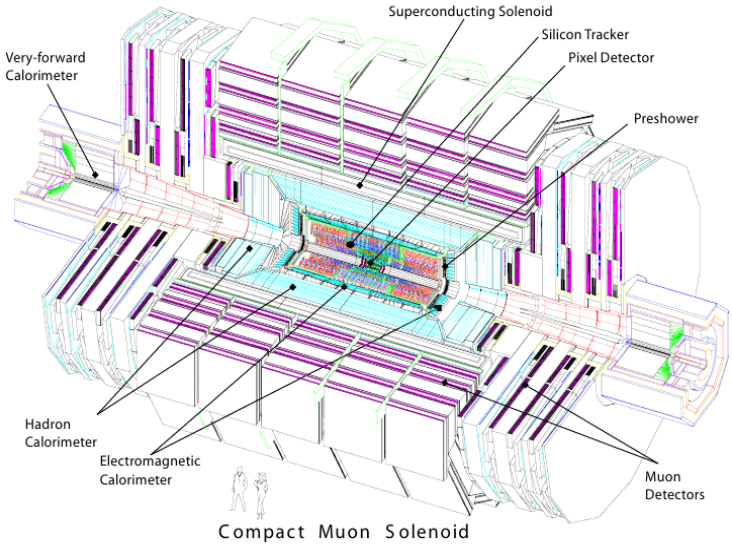

Figure 4.12: The CMS detector. Figure from [13]

since the momentum distribution and transversal spread are independent.

The minimum aperture in the ring is the primary collimators which are set at a half gap opening of 5.7 σ in the nominal settings [15]. The minimum aperture in the interaction regions is the tertiary collimators, which are set at a half gap opening of 8.3 σ. In Figure 4.13 we show these two beam envelopes in the four interaction regions. We have added what is called the survey, which gives the beam orbit in actual Cartesian coordinates instead of in the Frenet-Serret coordinate system described in Chapter 3.

In Mad-X, a simple aperture model is defined for most machine elements. In Figure 4.14 we show the same envelopes with the added aperture model from Mad-X. We see that the aperture model is missing information in the recombination chamber between the two dipoles D1 and D2. We see the tertiary collimators in both cases which are barely touching the outer envelope. Notice that the crossing angle in CMS in particular make the aperture restriction much tighter on one side of the final focusing triplets. We further note that the aperture is significantly more constrained for low-β optics.

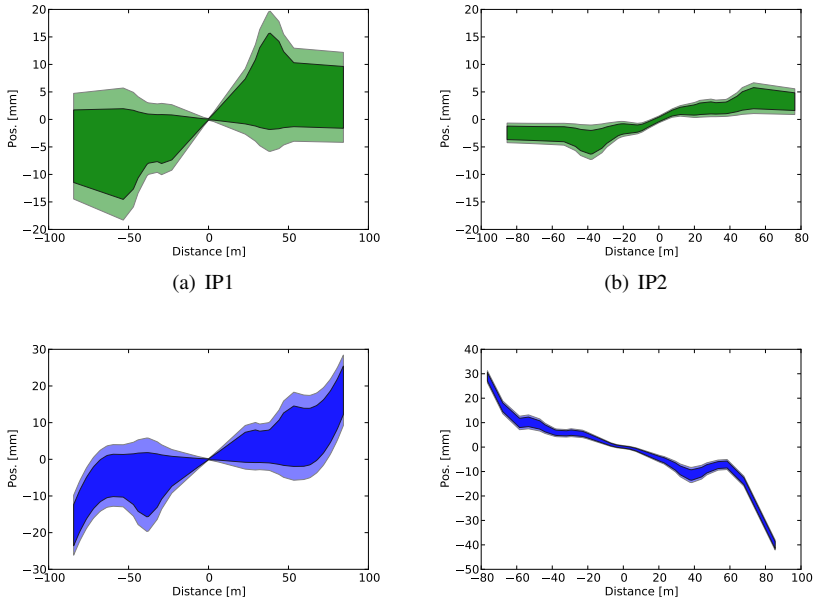

(a) IP1 (b) IP2

(c) IP5 (d) IP8

Figure 4.13: The beam envelope which passes through the primary collimator openings in the nominal machine, and the envelope passing through the tertiary collimator openings in transparent. We show the plane with the crossing angle for the different interaction points, for beam one. Blue is used for the horizontal plane, green is for the vertical plane. The dark band show the 5.7 σ primary halo, the lighter band show the tertiary halo which goes to 8.3 σ.

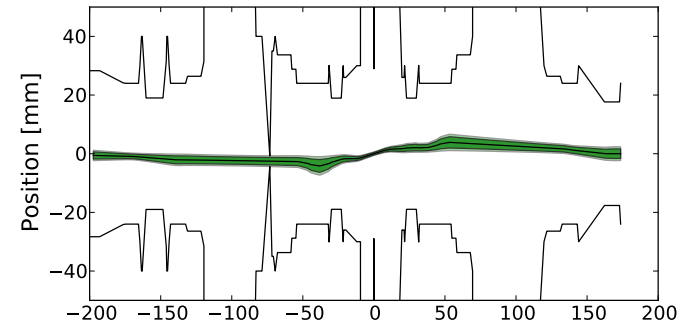

(a) ALICE

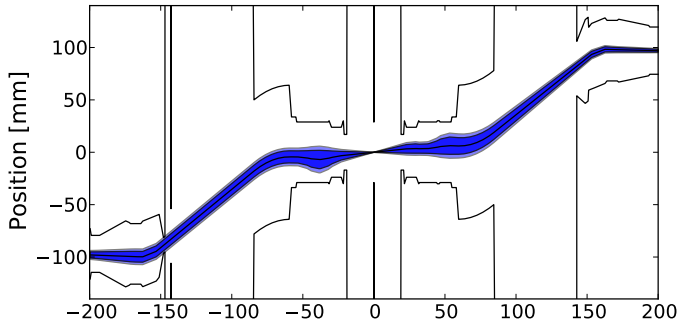

(b) CMS

Figure 4.14: The beam envelopes as shown in Figure 4.13 with the aperture model from Mad-X included. The tertiary collimators set the minimum aperture in each region. The aperture is significantly tighter in CMS (and ATLAS) than in ALICE (and LHCb) due to the lower β^*.

4.5.1 Collimator Settings

The tertiary collimator defines the minimum aperture restriction in the experimental regions. By extension, they then define the rate of beam halo background, elastic beam-gas background and IR cross-talk.

For the nominal optics parameters the tertiary collimators are set to 8.3 σ [15]. In the 2010 run however, the beams had lower intensity and the β^* was higher, which allowed for a more relaxed setting. The tertiary collimators were set at 15 σ, leaving a 2.5 σ margin to the minimum aperture in the triplet quadrupole [45]. In 2011, the beams were squeezed to a β^* of 1.5 m, and the tertiary collimators were as a result moved in to 11.8 σ for all experiments but ALICE which increased β^* to 10 m.

In the nominal settings [15], the tertiary collimators in front of LHCb and ALICE are set to 8.3 σ, even though the β^* is 10 m. As the main purpose of the tertiary collimators are to protect the final triplet against asynchronous beam dumps, one could imagine that these collimators could be set in a more relaxed position in order to mitigate some of the machine induced background.

Chapter 5

Studies of Beam–Gas Scattering

As the beam travels through the beam pipe, particles in the beam collide with the rest gas left in the chamber. The official LHC vacuum design requirement is to keep the lifetime of the beam due to beam-gas interactions above 100 h [46]. With a nominal intensity of 3×10^{14} protons/beam [28], that means about 10^9 protons lost every second. With a 7 TeV beam energy, it amounts to 1 kW of power. Beam–gas collisions can be a significant source of background to the experiments.

In this chapter we will first describe the beam-gas background in general. We will then discuss the input parameters and simulation strategies. Afterwards the simulated results for the nominal machine are presented and analysed.

The publications given in Appendix D.1, D.2, and to some extent D.4 are related to this work. In addition, we presented the simulation of beam-gas background for 2009 in [47], and expected backgrounds for ALICE for the nominal machine in [48]. The two notes are summarised in Appendix D.6.

5.1 Rates and Lifetime

The rate of beam-gas collisions from a region s_0–s_1 for one beam follows the formula

$$\dot{n}_{\text{coll}} = I\, f_{rev} \sum_i \sigma^i \int_{s_0}^{s_1} \rho^i(s) ds, \tag{5.1}$$

where i denotes the different gas species present in the vacuum chamber. I is the beam intensity (number of protons), while f_{rev} is the revolution frequency, equal to the speed of the particle divided by the circumference of the beam orbit. The gas density $\rho(s)$

of the particular gas species is integrated along the beam trajectory. To get a good measure of the total pressure, we can define a H_2 equivalent density as

$$\rho(s)_{\mathrm{H}_2 eq.} \equiv \sum_i \frac{\sigma^i}{\sigma^{\mathrm{H}_2}} \rho^i(s). \tag{5.2}$$

This definition of equivalent pressure/density should not be confused with the equivalent pressure in terms of pressure gauge reading. A pressure gauge has a different efficiency for measuring the pressure of different gas components. A calibration factor must be applied if you know that the gas composition is significantly different from air, which is the case for the LHC vacuum chamber. The two definitions of equivalent pressure have little to do with each other, but the conversion factors can in some cases be similar.

Only a proton which is kicked out of the stable region of the beam will be lost, which means that not all beam-gas collisions will produce a lost proton. If the stable angular region (divergence) is small, the probability that a given angular kick is sufficient to lose the particle is increased. From Liouville's theorem, the divergence is small when the beam size is large, so the probability will be inversely dependent on $\beta(s)$. We define the "survival ratio" as

$$r_s(\beta(s)) \equiv \frac{1 - \dot{n}_{\mathrm{lost}}}{\dot{n}_{\mathrm{coll}}}.$$

Note that we are here talking about the number of losses that originates from a given location, not the number of losses at that location. The rate is a function of the beam size which again is a function of the location and the optics. The "effective" cross section for hydrogen is then

$$\sigma_{\mathrm{eff}}^{\mathrm{H}_2}(s) = \sigma^{\mathrm{H}_2}\ (1 - r_s). \tag{5.3}$$

To know precisely the effective cross section, tracking simulations are needed.

The beam lifetime if beam-gas was the only source of particle losses is then defined from

$$\frac{1}{\tau_{BG}} = f_{rev} \sigma^{\mathrm{H}_2} \oint (1 - r_s)\ \rho(s)_{\mathrm{H}_2 eq.} \mathrm{d}s. \tag{5.4}$$

The integral of the H_2 equivalent density is now for one complete turn.

The equivalent pressure reduces the calculation of beam-gas event rate for one beam to

$$\dot{n}_{\mathrm{coll}} = I\ f_{rev}\ \sigma^{\mathrm{H}_2} \int_{s_0}^{s_1} (1 - r_s) \rho(s)_{\mathrm{H}_2 eq.} \mathrm{d}s. \tag{5.5}$$

With a cross section of about 100 mb, a lifetime of 100 h in the LHC corresponds to an average H_2 equivalent density of around 10^{15} H_2/m^3 [28, Ch. 12]. Using Eq. (5.5), that gives us the rate of 9×10^8 proton/beam/s if we assume the survival ratio to be 0.

5.2 Pressure Distribution

The gas composition in the LHC consists mainly of CH_4 in the warm regions, and H_2 in the cold regions. In addition, there is a partial pressure of CO and CO_2 [16]. The relative magnitude of these partial pressures can change significantly based on the input parameters chosen. The relative total cross section for the relevant species are given in Table 5.1 for 7 TeV beam energy. This has been calculated by simple addition of the atomic cross sections for hydrogen, carbon, and oxygen, simulated using DPMJET III [47].

Table 5.1: The total cross section of the four main components of the residual gas in the LHC. Values are simulated using DPMJET III, summarising the cross section for the different atoms. The beam energy is set to 7 TeV.

Species	σ_{tot} [mb]	$\sigma_{tot}/\sigma_{tot}^{H_2}$
H_2	92	1
CH_4	578	6.28
CO	895	9.73
CO_2	1400	15.2

The vacuum pressure has been simulated in detail for the nominal and early machine parameters [16, 49, 50]. In our work we use the hydrogen equivalent densities. As can be seen in Figure 5.1, the momentum transfer from proton colliding with a proton at rest, or a proton colliding with a carbon atom at rest is quite similar, with proton on proton giving a slightly higher cross section in the very forward region. Using hydrogen equivalence should then be safe for a conservative estimate.

In order to improve the vacuum quality, the machine will be scrubbed in several stages. Scrubbing is done by letting the pressure increase as much as possible, by reducing the pumping speed and/or increasing the beam intensity. The result is a higher beam-gas rate which produces high energy particles impinging on the wall of the beam pipe. These particles will clean the wall from impurities, which in turn reduces the desorption rate from the surface. This reduces the secondary electron yield (SEY), which is important if the machine is experiencing electron-cloud problems. Scrubbing in the LHC is of particular importance in the cold sectors and the cold–warm transitions, where bake-out is not possible. For what is defined as the early machine parameters in the vacuum pressure simulations, a beam energy of 7 TeV is still assumed, but 1/3 of

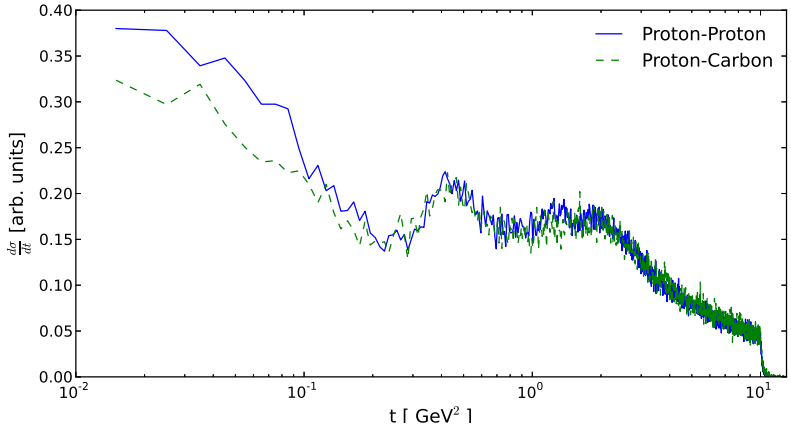

Figure 5.1: Qualitative difference between proton-proton (solid) and proton-carbon (dashed) collisions, simulating single diffractive events in DPMJET III.

nominal beam intensity and a scrubbing which is not yet fully effective is implied.

Since the beam lifetime during a scrubbing run is expected to be dominated by beam-gas scattering losses, one could imagine a dedicated study which to some extent could verify the simulations that are presented here. However, one would then need dedicated simulations of the vacuum during these runs in order to get a decent knowledge of the dynamic pressure distribution. Further, one has to take into account other effects as electron cloud, beam impedance and wakefields which become much stronger with the increased beam intensity. Finally, for background considerations these conditions are quite far from normal physics operation, and most of the detector components are switched off as a protective measure.

The molecular densities from the simulation of the nominal machine are given in Figure 5.2. For the beam-gas simulations, we have assumed that the pressure in IR2 and IR8 is similar but inverted, since the asymmetry about the interaction point mainly comes from the injection region. We assume that IR1 and IR5 are similar, and that the pressure is symmetric about the interaction point in these regions. These assumptions are expected to be OK for our studies.

H_2 is the dominating species in the cold regions due to its relatively high vapour pressure at low temperatures. However, due to the relatively larger size of the CO_2 molecule, it is the dominating term in terms of scattering cross section in the cold

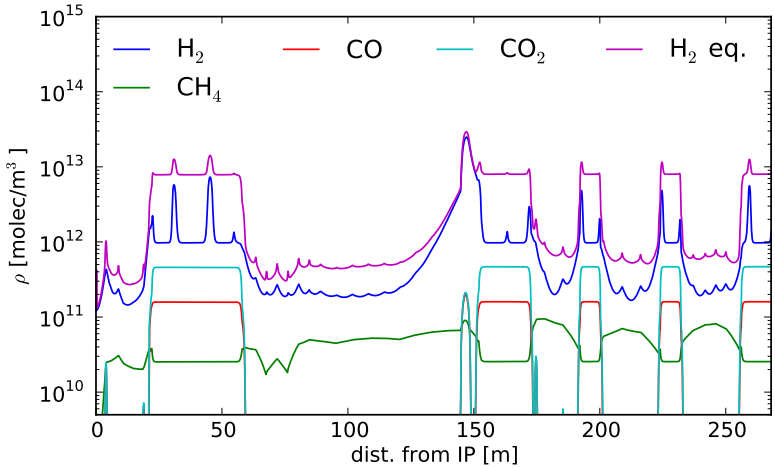

(a) IR1 and IR5, symmetric about the IP.

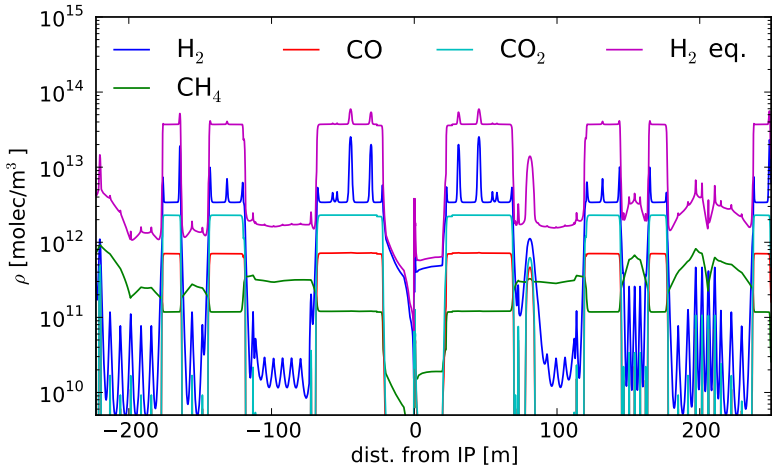

(b) IR2 and IR8

Figure 5.2: The simulated molecular density for the nominal machine parameters, for the four common species present in the LHC vacuum chamber. Simulation data from [16, 49].

regions. CH_4 is dominating in the warm regions regions since it is not pumped by the NEG coating unless it is ionised [16].

5.3 Physics Processes

The interactions taking place when two hadrons collide can be divided in some main categories, which we will briefly describe here. For more information, see e.g. [51, 52].

Classical mechanics divide collisions into elastic and inelastic collisions, of which the former requires that kinetic energy is conserved. In all collisions, the total momentum before and after the collision is conserved. Elastic scattering is the first category of collisions which we will discuss here.

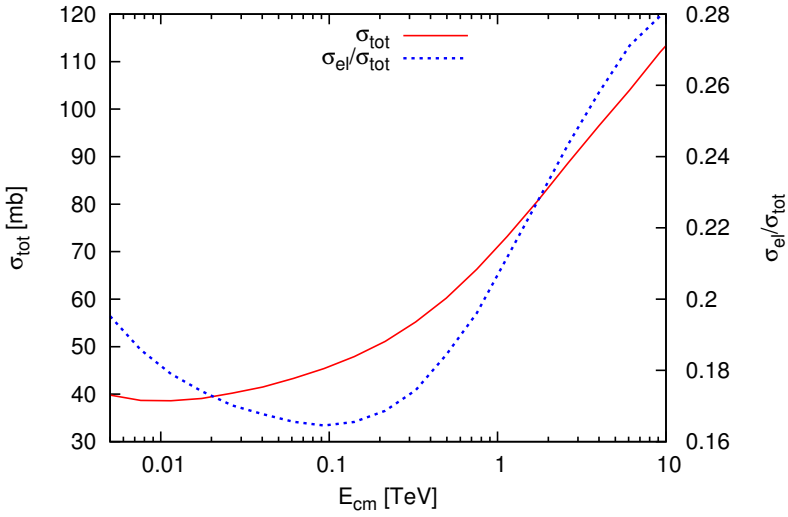

Figure 5.3: The total cross section as a function of the centre of mass energy in red solid. The blue dashed line shows the elastic cross section divided by the total cross section, with values on the right hand side axis. The relevant energy for beam-gas is around 0.2 TeV, where the elastic cross section is low compared to the total cross section.

The leading process in elastic scattering at high energies is the exchange of a

pomeron, a hypothetical particle which consists of quarks and gluons [53]. A pomeron has the same quantum numbers as vacuum, which means no charge, colour or flavour exchange. The interaction is shown in Figure 5.4(a). It should be noted that the pomeron exchange is one way to describe the process, and other theories exist. It is the most widely used approach for modelling elastic scattering at high energies. Elastic scattering is expected to have a cross section of around 30 mb at nominal LHC energy [54]. In Figure 5.3 we show the elastic cross section divided by the total cross section as a function of energy, simulated using DPMJET III.

We do not consider Coulomb scattering in these DPMJET simulations. As can be seen in e.g. [55], the importance of Coulomb scattering becomes important at momentum transfers lower than 0.005 GeV^2 for centre of mass energy of 100 GeV. It was found in similar background studies for the Tevatron [56] that Coulomb scattering gave a small contribution to the background rates. Similarly, ionization processes are disregarded, because single kicks are too weak to cause direct losses. These processes lead to slow emittance growth and halo population. As a consequence, these protons will always hit the primary collimator first, with a small impact parameter, and are part of the halo background.

Inelastic scattering is divided in diffractive and non-diffractive events. Non-diffractive events are expected to account for approximately 56 % of the total cross section at LHC energies [54]. Diffractive events are described in a similar manner as elastic events, by the exchange of a pomeron (at high energies). The definition of diffractive events is the presence of one or several gaps in the rapidity distributions, similar to the diffraction pattern from photons through a slit. The simplified pseudo-rapidity is defined as

$$\eta \equiv -\ln\left(\tan\frac{\theta}{2}\right),$$

where θ is the angle the outgoing particles make with the initial particle trajectory. In diffractive scattering, the energy exchanged remains small, and no quantum numbers are exchanged between the protons [52].

The first category of diffractive events is single diffractive, which is expected to have a cross section of about 10 mb at nominal LHC energy [54]. Single diffractive is shown in Figure 5.4(b). It is similar to elastic scattering, but one proton is dissolved and a multi-particle final state is produced. In double diffractive events, both protons are dissolved, producing two multi-particle final states. The cross section for double-diffractive events at nominal LHC energy is expected to be 7 mb [54]. Double diffractive event is shown in Figure 5.4(c). Other types of diffractive events exist, like e.g. double pomeron exchange, but the cross section for these processes is small.

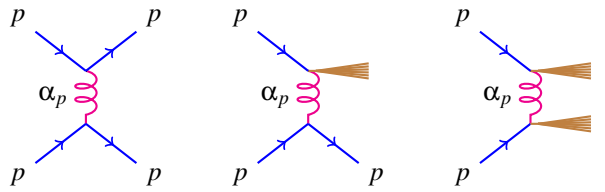

(a) Elastic scattering. (b) Single diffractive scattering. (c) Double diffractive scattering.

Figure 5.4: A Feynman diagram of the elastic process (a), the single diffractive process (b), and the double diffractive process (c) by the exchange of a virtual pomeron, α_p. In single diffractive events, one proton stays intact while a jet of final state particles are created from the other proton. In double diffractive scattering, none of the initial protons are intact, but the final state can still contain a high energy proton.

In Figure 5.5 we show a 2D histogram of the energy and angular kick of the scattered protons. This is from a simulation using DPMJET III, with proton at 7 TeV colliding with a proton at rest. A clear separation is observed between the primary protons (the curved band), and the secondary protons from diffractive events. In Figure 5.6 the cross section for elastic and diffractive scattering as a function of the momentum transfer t is shown. We see that for low t, the cross section is dominated by the elastic scattering, while single diffractive is more dominant at higher t.

To understand the significance of t with respect to aperture limitations, we need to consider the TWISS parameters. The primary collimator are set with an opening of about 6 beam σ from the beam centre in the LHC in normal operation. Since the β-function varies along the orbit, so does the size of the beam. A momentum transfer of 0.1 GeV^2 equals an angular kick of

$$\frac{\sqrt{0.1}}{7000} = 45\mu\text{rad},$$

assuming fully elastic collision. In the LHC arcs, an approximate TWISS γ of 0.05 rad/m can be used. With a normalised emittance of 3.75 µm, one beam σ equals

$$\sigma = \sqrt{\frac{\varepsilon_n}{\gamma_{\text{relativistic}}}\gamma_{\text{twiss}}} = \sqrt{\frac{3.75\times10^{-6}}{7000/0.938}0.05} = 5.0\ \mu\text{rad}. \tag{5.6}$$

In other words, the average kick from elastic scattering is on the order of 10 beam σ, comparable to the aperture restrictions in LHC. In some regions the beam divergence

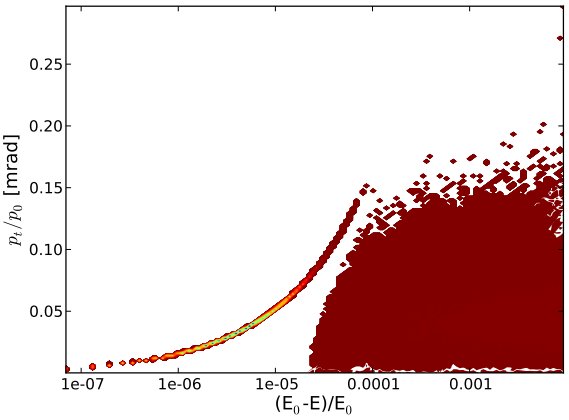

Figure 5.5: Angle vs. energy of scattered protons with a momentum loss of less than 1 %, simulated using DPMJET III. All processes available in the simulation software are turned on. The colour scale is logarithmic.

will be larger, and the scattering angle will be smaller in number of beam σ. In ATLAS and CMS the TWISS γ equals 1.8 rad/m when the beams are fully squeezed, which means a beam size of 30 μrad. In other words, a large fraction of elastic collisions in the interaction point will result in emittance growth and not particle losses directly.

With that in mind, we realise that only a full simulation of beam-gas scattering distributed around the ring, including the beam profile, will give an accurate prediction of the survival ratio and halo growth from elastic scattering.

5.4 Local, LSS and Distant Beam-Gas

The elastic and diffractive collisions will to some extent contribute to the halo production [57]. The halo should be cleaned by the collimation system, which means that this part of the beam-gas background is a part of the normally produced halo. A common definition of beam halo is all particles which are more than three σ away from the centre of the beam.

Losses from particles with large angular kicks are distributed around the ring according to the vacuum pressure. Particles with a large difference in momentum com-

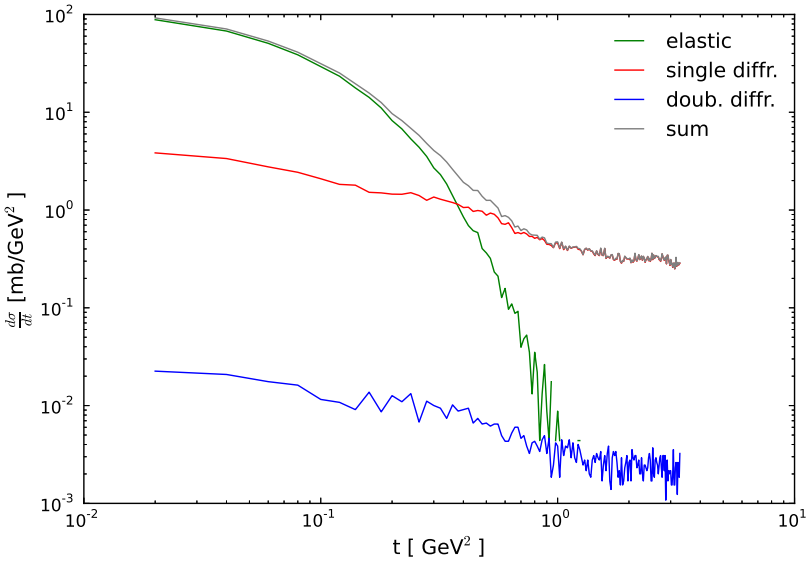

Figure 5.6: Simulation of elastic, single- and double-diffractive scattering as a function of the momentum transfer t, using DPMJET III. The simulation is of a proton of 7 TeV hitting a proton at rest. The sum of elastic, single- and double-diffractive cross sections is shown in grey.

pared to the beam, undergoing a small angular kick will typically be deflected at the next location of a strong magnetic field. Finally, the particles which are in the range between these extremities stay within the beam for a while before being lost on aperture restrictions. These losses can be concentrated in certain areas due to phase advances, pressure bumps, and particular aperture restrictions for the optics that are used. That makes it a potential problem for radiation and quench protection, and it can be a significant source of background. In this work we have focused on estimating the background, but the results can be found useful for machine protection studies as well.

We generally split the beam-gas background in three categories. The categories are defined based on where the origin of the beam-gas event took place, with respect to the experiment. Local beam-gas is considered beam-gas collisions within the experimental beam-pipe. Elastic events can cause problems for forward physics detectors like roman pots, and event counters like the BRAN [58]. The experiment is not shielded from this

beam-gas background, and as a result the inelastic events are of large importance in this region.

The second part is denoted the LSS beam-gas, which is originating from the last long straight section upstream of the experiment but before the entrance to the experimental cavern. A larger part of this background will have to traverse some level of shielding before reaching the detectors. Showering through material can increase multiplicities, while the overall energy deposition is reduced. The number of tracks will usually be reduced. Differing from local beam-gas, this background produces particles with trajectories more or less parallel to the beam.

The trackers are aligned in a few layers around the interaction point. Hence, a particle traversing this region parallel to the beam-pipe can hit a high number of these tracker channels. We say that the "occupancy per tracklet is high", where occupancy is defined as the number of detector channels activated, and tracklets are defined as potential particle tracks. This is a typical signature of the machine induced background coming from outside of the detector region – a higher number of activated channels per track than for collisions at the interaction point [59].

Beam-gas collisions originating from further away than the last LSS upstream of the experiment are denoted long-range or distant beam-gas. Sometimes it is referred to as elastic beam-gas, since it is in large part elastic or quasi-elastic events that cause particles to survive in the beam-pipe for long enough to produce secondaries in the experimental region. The long-range beam-gas events are particles which are essentially in the halo of the beam. That means they will for the most part hit the smallest aperture restrictions. In the LSS, that means the tertiary collimators (TCT). Additionally, the muon secondaries becomes increasingly important, since muons can traverse a large amount of material without being stopped.

The aperture of the TCT's can vary depending on how much the beam is squeezed, since their main objective is to protect the final focusing system. For nominal optics, which means a β^* of 0.55 m in ATLAS and CMS, they are placed at $8.3\,\sigma$ [15]. In 2010 and 2011, the β^* was 3.5 m and $1.5/1.0$ m respectively, which meant TCT openings of $15.3\,\sigma$ and $11.8\,\sigma$ [60]. Since the minimum aperture in the region around the experiments depend strongly on the collision optics, the elastic beam-gas background will depend on the optics as well. One will usually expect a higher background level for smaller β^*.

5.5 Earlier Studies

Previous simulation studies of the beam-gas background have predicted that beam-gas background in the LHC is expected to be a very significant contribution to the total

background, possibly the most significant [61, 62]. Experience in previous machines such as Tevatron and HERA show similar importance of beam-gas background [7, 56].

The expected rate of particles entering the experimental cavern is on the order of MHz for the nominal machine parameters. That is comparable to the number of bunch collisions, which is 32 MHz for nominal LHC parameters [28, Ch. 2].

A main limitation for the precision of these simulations is the knowledge of the pressure distribution. In general, a factor 2 difference is to be expected when measuring the absolute pressure, with added uncertainty from extrapolating a few measurements to a full pressure profile. The measurements depend on accurate calibration of the pressure gauges, which measures the local pressure at the gauge location.

For a complex machine like the LHC, a simulation including locations of pressure gauges and vacuum pumps together with other relevant information is needed to know what a gauge reading correspond to in pressure inside the actual beam chamber. Relevant information for these simulations include conductivity, location of cold and warm elements, coatings, quality of bake-out, known vacuum leaks, material desorption rates and so forth. Unexpected small vacuum leaks, or unsuccessful bake-out are examples that can significantly alter the vacuum pressure in a different way than what is expected from simulations. A limited set of parameters can be included in one simulation, and an experienced judgement is necessary to decide what information is essential when simulating a large vacuum system.

For this work we have received data from several simulations from the vacuum group [63, 49], some of which have not yet been published elsewhere [50, 64].

5.6 Simulations

The three components of the beam-gas background require different simulation procedures. In [17], we presented in detail how the the full simulation chain was implemented for all background components for the LHCb experiment. The implementation is similar for the other experiments.

The simulation of the local beam-gas inside the experimental cavern can be directly fed into the standard simulation software for the different experiments. The inelastic interactions are expected to be most important, in particular for low β^* optics. Since the angular deflection of the residues are significantly larger, the importance of the beam optics is reduced. Some parameters like e.g. the crossing angle can still play a significant role for the local beam-gas background. In fact, beam-gas events can be used to measure the crossing angle and even the beam profile if the vertex location detection in the experiment is good enough [65].

The LSS beam-gas is simulated using particle shower codes like FLUKA [66],

MARS [67], or BDSIM [68]. A fairly detailed model of the geometry and materials inside the tunnel is required. FLUKA has an extensive library of highly detailed models of most of the LHC elements, and is used for radiation studies in the LHC. As a result, FLUKA has been chosen for most studies of LSS beam-gas background in the LHC so far [47, 69].

The geometric model typically extends for a few hundred meters, and earlier studies have shown that the muon flux from beam-gas events up to around 500 m upstream of the IP could reach the experimental cavern [62]. Simulating particle showers through such large geometries requires a large amount of computing power. Biasing is often needed to get sufficient statistics. Biasing is a term which here means we increase the statistics of important processes that have low cross sections, and/or reduce less important processes that consume a lot of processing power. The secondary particles from the simulations will then have a weight attached to them — they are not all equally probable. Biasing is beneficial to reduce computing power needed, but it requires a larger effort in order to make sure one does not lose important information in the process.

When particles from the shower simulations reach the interface plane as defined in Table 4.4, the simulation is stopped and particle information is written to file. This information is then used for detector response simulations, including the full model of the experiment's detectors and materials. For maximum flexibility, the information includes transverse position and direction, momentum, particle type, event tag and the origin where the beam-gas interaction took place. The latter is needed in order to be able to rescale for different pressure distributions without the need for a new simulation. Sometimes you will still need a new simulation, e.g. in the case when you have a pressure bump in a location where you normally have a very low pressure. In this case, the statistics in this region will probably be too low. An alternative strategy is to assume a more or less flat pressure distribution, in order to have decent statistics from all regions of the LSS.

Beam-gas events further upstream than the LSS can also produce secondary particles reaching the experimental cavern. These get a low angular kick and/or a small momentum deviation, which leaves them in the halo or close to the halo of the beam. These residues can stay in the beam pipe for several turns, but it is expected that if they survive for many turns they will behave in a similar manner as the normal halo, and cleaning these residues will have similar efficiency as the cleaning efficiency for the beam halo. The cleaning inefficiency is defined as [15, Ch. 5.3]

$$\eta = \frac{\dot{p}\tau}{I\Delta x}. \tag{5.7}$$

Here, $\dot{p}$ is the rate of particles hitting a given element (e.g. a collimator), τ is the lifetime of the beam, I is the total number of particles in the beam (beam intensity),

and Δx is the length of the element.

Simulation Code

For multi-turn tracking simulations, precise optics description is necessary. The SixTrack simulation code [70] offers full six-dimensional thin-lens tracking, and developments in recent years provides a full aperture description [71], together with elastic and single-diffractive scattering for protons through some material types [72]. The code has been used extensively for dynamic aperture studies in the LHC [73, 74, 75], and for collimation studies [15, 30]. These simulations require accurate tracking of the beam over many turns without artificial blow-up of the beam (non-symplecticity). As a result, the code is optimised for speed and accuracy. Due to its advanced level of sophistication and physics validation through earlier studies, it was chosen as the particle tracking code for the proton residues from long-range beam-gas events.

In addition to tracking and comparison with aperture model to produce loss maps, it is necessary to produce the initial collisions between beam and rest gas particles (event generator). Collision events are simulated and results are written to an ASCII file. Afterwards this file is read when the tracking code has decided that a collision should take place. The approach makes it easy to replace or extend the event generator if that would be deemed necessary at any point. For a more in depth explanation of how the interface between DPMJET and SixTrack works, see Appendix C.

The full simulation chain which these studies are a part of, is described in Appendix D.4. A full simulation chain including all background sources and detector response is only available for LHCb thus far. We have adopted for a highly modular approach, which allows for a better understanding of the quality of the various parts of the simulation.

A simulation of the various background sources up until the interface planes have been performed in the past using MARS/STRUCT15 for the high luminosity experiments [76]. Since these studies are using independent codes, the comparison between the two will give further insight into the quality of the results.

Aperture Model

The aperture model used in these studies is identical to the one used for collimation studies [15, 30]. The model is similar to the standard model that is used for most optics studies for LHC (V6.503 in the optics database), but it is optimised and extended for collimation studies. In Figure 5.7, we show an example in the interaction region 2 (ALICE). The SixTrack model we used in our simulations was last changed in January 2008. Comparing the models, we see some minor differences. Since collimator losses

make up for the largest fraction of the losses in the interaction regions, the differences in the models are not expected to produce dramatically different results for our studies.

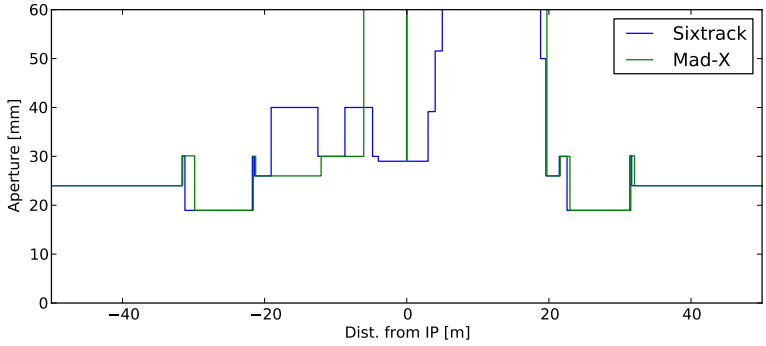

(a) Horizontal

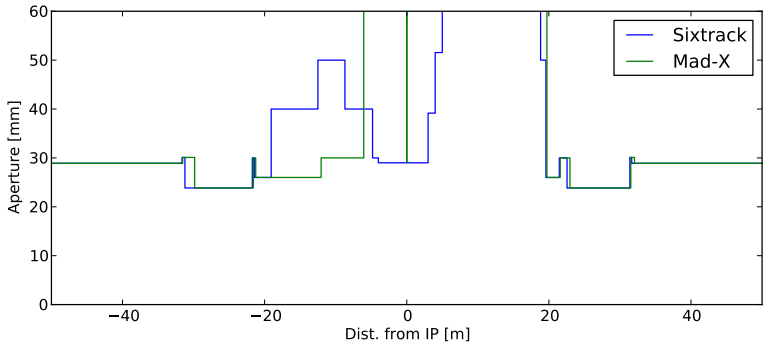

(b) Vertical

Figure 5.7: The aperture in Mad-X in green, compared to the one used for the SixTrack simulations in blue in the region around ALICE for beam 1.

5.6.1 Nominal Machine

The LHC design parameters were presented in Section 4.1. Main features are a β^* of 0.55 m in the high luminosity experiments ATLAS and CMS, 10 m in ALICE and LHCb, and a beam energy of 7 TeV.

The tertiary collimators are set at an opening of $8.3\,\sigma$ in all interaction points. As the purpose of the tertiary collimators is to protect the final focusing quadrupole triplets, they might not need to be placed that close to the beam in the low luminosity experiments. The β^* is large enough in ALICE and LHCb so that the aperture of the final focusing magnets are not a major aperture restriction anymore. If the background originating from the tertiary collimators become too large for these experiments, one might consider to set the tertiary collimators with a larger gap. In this work we will assume nominal settings.

The first simulation results were presented in [77], where we used the nominal optics. Since then, several improvements have been made to the code, so we present new simulations here with a more in depth look at the results.

Pressure Map

In Figure 5.8 we show the pressure map for beam 1 used in these simulations. For beam 2 the map is identical, but the beam is then moving from right to left in the figure. We show the pressure in units of particle density. In [47] you can find an explanation on how one can calculate the molecular density from a pressure. The regions around the experiments have more detailed simulations, as was shown earlier in Figure 5.2. For the rest of the machine we use an approximated average pressure, one value for the arc and one for the other insertion regions. The pressure in the arc is estimated to be around 20 times higher than in the cold parts of the insertion regions, due to synchrotron stimulated desorption [50]. The simulation of the vacuum pressure are based on nominal machine parameters and a completed scrubbing period.

The average pressure from this map is 1.2×10^{14} H_2 /m^3, which results in an estimated rate of beam-gas events of

$$\dot{n}_{\text{coll}} = 1.2 \times 10^8 \text{proton/beam/s}. \tag{5.8}$$

We simulated about 2.6 million beam-gas collisions. By dividing $\dot{n}_{\text{coll}}$ with the number of simulated collisions, we get a normalisation factor of 42.9 to this simulation set if we want to know the proton hit rate per second. From Eq. (5.4) that implies a beam lifetime of

$$\frac{1}{\tau_{BG}} = 11.25\ \text{kHz}\ 95\ \text{mb}/\text{H}_2\ 1.2\times10^{14}\ \text{H}_2/\text{m}^3\ 26\,658.9\ \text{m} = \frac{1}{800\ \text{h}}. \tag{5.9}$$

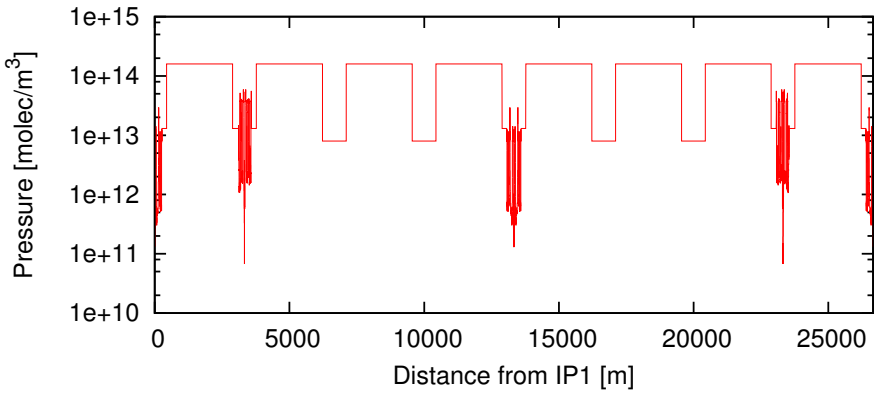

Figure 5.8: Hydrogen cross section equivalent pressure profile for the nominal machine.

If we for one reason or another end up with a higher pressure (e.g. scrubbing less effective than expected), we then have about one order of magnitude of margin before we approach the limit set in the design report, which is a 100 h lifetime from beam-gas collisions. If that were to happen it might still be that such a rate can be accepted, depending on machine protection and the resulting experimental background rates. If not, then the rates can be drastically reduced by reducing the beam intensity, since the rates scales quadratically with beam intensity for a fixed energy [50].

Scattering Locations

We distribute the beam-gas collisions in the ring so that the probability of a collision is proportional to the local pressure. In Figure 5.9 we show the number of scattered particles compared to the pressure in the region upstream of ATLAS/CMS. We show the hydrogen equivalent pressure for comparison, which is here as described before an equivalent pressure in terms of total cross section. In our simulation we have one scattering location every three meters around the ring, with a total of about 2.5 million events. That gives an average of about 300 events per location, which as can be seen in the example figure still gives low statistics in some regions.

For the nominal machine energy, the pressure is higher in the arcs than in the long straight sections. For the beam-gas background the losses coming from the long

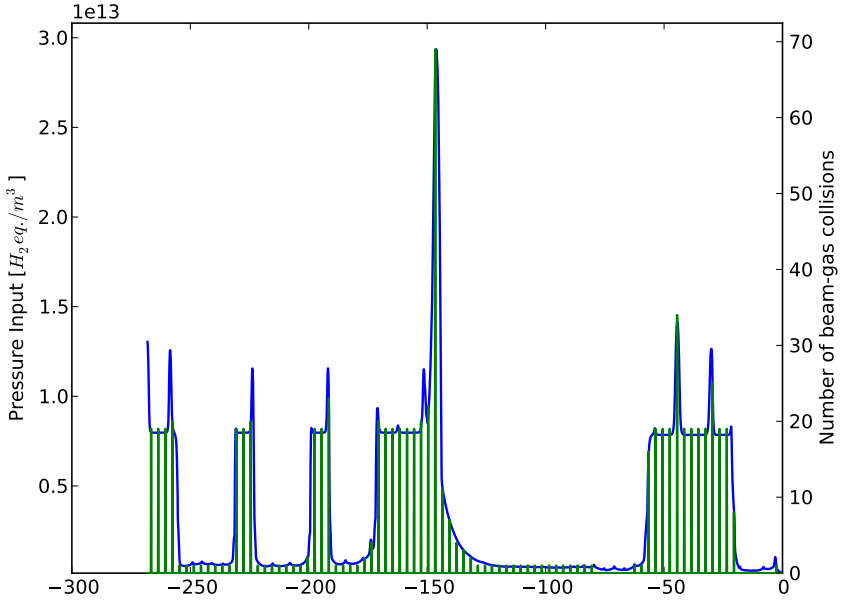

Figure 5.9: An example of how the pressure distribution (blue, left hand y-axis) correlates to the distribution of scattering locations (green, right hand y-axis). This is for the nominal machine, in the region upstream of ATLAS/CMS for beam 2.

straight section can still be more important because they have a higher multiplicity[1] at the interface plane. Here we are primarily focused on studying elastic and quasi-elastic collisions that survive for a long time in the machine. Losses in the long straight sections upstream of an experiment can in principle be directly simulated using e.g. FLUKA or BDSIM, and there is less need for a fast tracking tool like SixTrack.

We distribute the events around the ring during the first turn of the simulation, and then track for a total of five turns. As we show in Appendix D.1, the major part of the losses occur during the first two or three turns of the simulation.

[1] number of particles per originating event

Survival Ratio

From our simulation, we define the survival ratio as the number of particles still in the beam after the simulation has ended, divided by the number of scattering events. In our simulation of 2.595 million beam-gas events, 74 000 protons stayed in the beam pipe for all five turns. That gives a survival ratio estimate of

$$\frac{74}{2\,596} = 2.85\ \%.$$

Loss Maps

There are three main categories in the output from our simulation. The first category are the protons which hit a collimator after the beam-gas scattering event. These are of main interest when looking at long-range interactions, since protons travelling close to the beam orbit have a significantly higher probability of hitting the collimators than other aperture restrictions. In Figure 5.10 we see the losses on the various collimators. Of particular interest are the losses on the tertiary collimators (TCT's), displayed in red. These collimators are located about $60 - 140$ m upstream of each interaction point, and showers from these collimators will produce background towards the experiments. For beam 1 we see the largest losses in front of CMS.

One should note that the TCT's are about two meters apart in front of CMS/ATLAS, so it is difficult to see in Figure 5.10 the actual rates on the two sets of collimators separately. The beam-gas collision rates for each tertiary collimator are provided in Table 5.2.

The second category are losses on other aperture restrictions. These are worse for machine protection reasons, in particular in cold regions where small rates can induce enough heat to quench a superconducting magnet. In Figure 5.11 we show the losses on aperture restrictions. Excluding a few spikes, the losses on aperture stay three orders of magnitude below the losses on collimators. In the arc we see an increased amount of losses, which is caused by the increased pressure in the arc. This will be a feature for all optics at 7 TeV, because of the synchrotron radiation which is a function of the energy and not the optics. For lower energies the losses will be significantly differently distributed, and overall the losses should be lower.

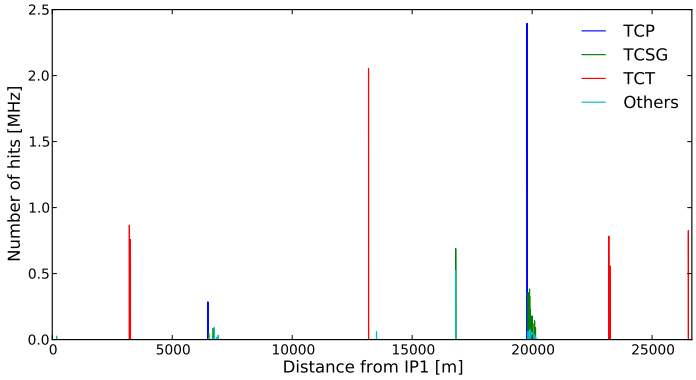

(a) Beam 1

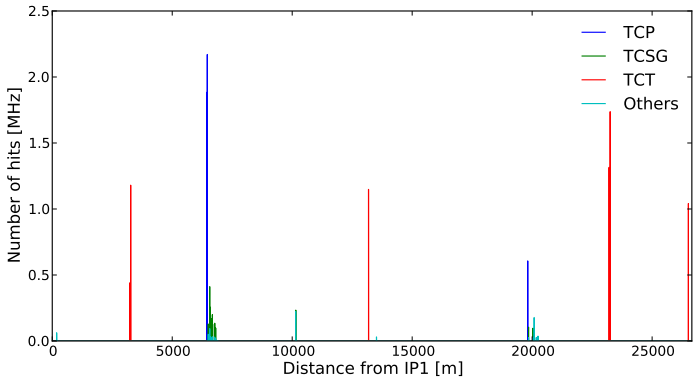

(b) Beam 2

Figure 5.10: Losses on collimators for the nominal LHC machine. In blue the primary collimators, in green the secondary collimators, and in red the tertiary collimators. For background considerations, the hits on tertiary collimators are of particular interest. Horizontal axis follows the beam direction.

Table 5.2: The loss rates on the tertiary collimators in front of the four experiments for the nominal LHC optics at 7 TeV.

Experiment	Orientation	Rate [MHz]	
		Beam One	Beam Two
ATLAS	H	1.07	1.13
	V	0.76	1.04
ALICE	H	0.92	1.75
	V	0.76	1.75
CMS	H	2.06	1.15
	V	1.61	1.01
LHCb	H	0.81	0.81
	V	0.56	1.19

There are a few interesting spikes in Figure 5.11 in front of ATLAS and CMS. In Figure 5.12 we show the actual loss coordinates of the aperture losses upstream of CMS. The losses on the collimators are excluded from this figure. The spike is precisely at 200 m, which is the location of Q5. The losses seem to be evenly distributed on both sides of the magnet, and the aperture limitation looks to be horizontal. The vast majority of the losses are in the horizontal plane in this region. If we look at the beam size in the same region, we note that the horizontal β-function is significantly larger than the vertical, which is the most probable explanation for the difference.

If we calculate the available aperture in this region for the 0.55 m optics, we find the origin of this peak. The aperture restriction in question is at around $15\,\sigma$, while the minimum aperture restriction in the arc is between $25-30\,\sigma$. The aperture in the region for these optics is shown in Figure 5.13.

Hence, a large fraction of the protons that get an angular kick which place them in between these two extremities, will end up on this particular aperture restriction. The rate is high because these losses are integrated over a very long region. For ALICE and LHCb, the optics are different and they do not have a similar sudden aperture restriction in this region.

This rate is still expected to be to small a rate to be confirmed by observations. Based on FLUKA simulations from [78] we expect that this is equivalent to less than 1×10^{-7} Gy/s. The expected quench rate for these magnets is around 1×10^{8} protons/s

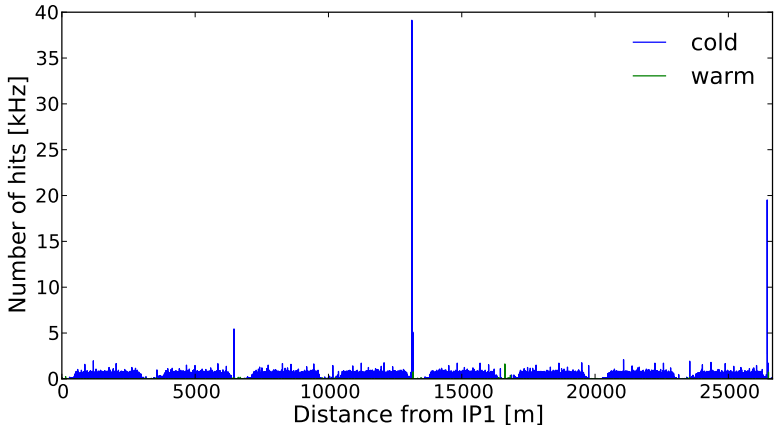

Figure 5.11: Losses on aperture restrictions other than collimators. In green the losses on warm elements are shown, while the blue line shows losses on cold elements.

for steady-state losses.

ATLAS has one octant between itself and the tertiary collimators in front of LHCb/ALICE. For beam one approaching CMS there are no major aperture restrictions between IR3 (momentum collimation), and the CMS insertion region. Not considering phase advances and other optical differences, one would then expect approximately twice the loss rates in front of CMS, since the losses have twice the length to develop.

5.6.2 Loss Origins

Depending on how the experiment is located with respect to other aperture restrictions in the machine, and the available aperture for the given optics, the distance travelled for the protons can vary from experiment to experiment, and between the two beams. We already saw in Table 5.2 that for ALICE, the losses from beam 2 is significantly greater than the losses from beam 1.

In Figure 5.14 we show the distance the protons travel on average after a beam-gas collision before they are lost on some aperture restriction that is not a collimator. We see that these protons on average does not travel much more than a few hundred meters,

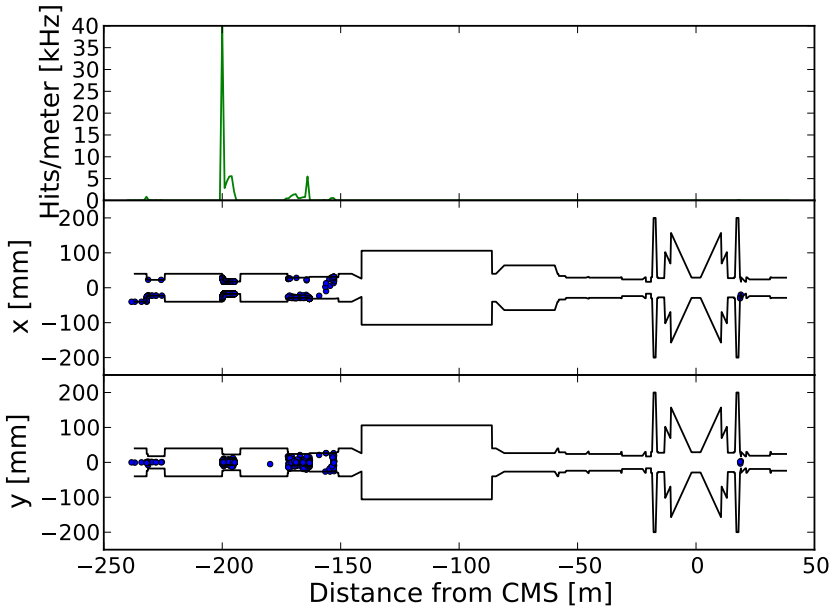

Figure 5.12: Aperture hits in the region upstream of CMS for beam 1. In the upper plot we show the loss rates, in the middle the horizontal locations of the lost particles, and in the lower plot the vertical positions of the lost particles.

with a maximum at around $30 - 50$ m.

In Figure 5.15 we show the same plot for the losses on any of the collimators in the machine. Here we see a rather different pattern. First of all the losses can come from much further away. This is shown better in Figure 5.16. In the arcs, the phase advance increase by one unit in about 400 m. The distance between the peaks in Figure 5.16 is about half of that, equal to a phase advance of 180°.

The origins of the beam-gas events that produce hits on the various tertiary collimators around each experiment can be found in Figures 5.17 - 5.20. In some cases, nearly all losses are coming from the preceding arc (e.g. beam 1 background for LHCb). In other cases the losses tend to come from almost the entire machine (e.g. beam 2 for ALICE and ATLAS).

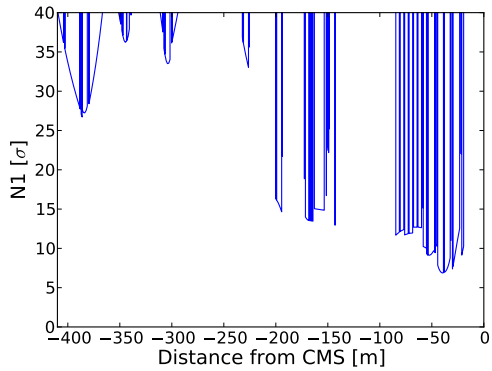

Figure 5.13: The aperture measured as N1, upstream of ATLAS/CMS for the nominal 0.55 m β^* optics, and a 7 TeV beam energy.

The betatron collimation region is located in the interaction region next to LHCb (IR7). The betatron collimation is effectively stopping these particles in all cases. The momentum collimation is located in the interaction region next to ALICE (IR3). The same effective cleaning is not observed in this region. This implies that it is the betatron amplitude and not the momentum deviation after the beam-gas collisions which causes these losses. Since the dispersion is low at the TCT locations by design, this is expected.

It is worth noting how effectively other experimental regions are cleaning the losses in some cases, e.g. for beam 2 horizontal for ALICE, where the losses seem to be abruptly stopped in the CMS interaction region. Another interesting thing to observe is the horizontal/vertical asymmetry observed in particular for beam 2 for LHCb and ALICE. This can be understood from the fact that the tertiary collimators in these two regions are far apart, as described in Section 4.3.

For ATLAS, the beam 1 losses come from the last two octants. It is interesting to note that in the octant 7-8 (upstream of LHCb), the horizontal and vertical losses have a different shape. The horizontal losses comes from the middle of the arc while the vertical losses comes more from the end of the arc. Looking at the integrated losses, horizontal losses are somewhat higher overall. The beam 2 losses are dominated by the first upstream arc, but all of the machine up to the betatron collimation contributes. ALICE TCT's are catching some of the losses here, an effect which would be reduced if the ALICE TCT's are further retracted. No important asymmetries between horizontal

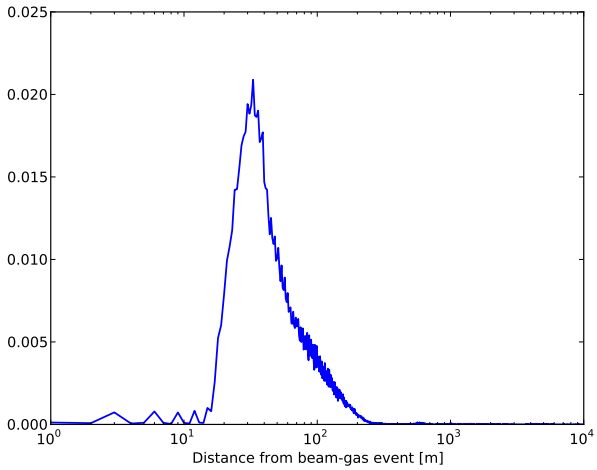

Figure 5.14: The distance the protons travel after a beam-gas scattering before they are lost on aperture restrictions, excluding collimator losses. The data are normalised to the total number of aperture hits per metre. This is from the simulation of the nominal machine for beam 1.

and vertical losses are observed for beam 2. Overall, the beam 2 losses are higher than beam 1 losses for ATLAS.

For ALICE, the beam 1 losses are coming from the three upstream octants, with the last arc being dominant. The cleaning done by ATLAS TCT's seems to be more important in the horizontal plane. Overall the horizontal losses are slightly higher than vertical. For beam 2, the losses come from five octants upstream. An important asymmetry is observed, where the horizontal losses are effectively stopped in the CMS interaction region. Differing from ATLAS losses, it is not the last octant, but the three last octants which give an almost equal amount of integrated losses. For the vertical losses, all five octants give a significant contribution.

For CMS, the beam 1 losses are dominated by the last three octants. The momentum collimation region is to some extent reducing the losses in the horizontal plane. The primary momentum collimators are only installed in the horizontal plane. The ALICE TCT's are doing a better job cleaning vertical losses than horizontal losses for CMS beam 1 losses. For beam 2 we see losses from the last two octants upstream. A very strong asymmetry in the integrated losses from beam 1 and beam 2 is seen for

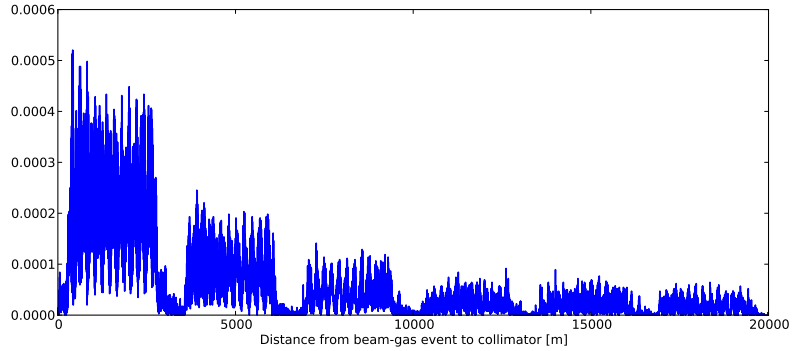

Figure 5.15: The distance the protons travel after a beam-gas scattering before they are lost on any collimator. The data are normalised to the total number of aperture hits per metre. The data are from the simulation of the nominal machine for beam 1.

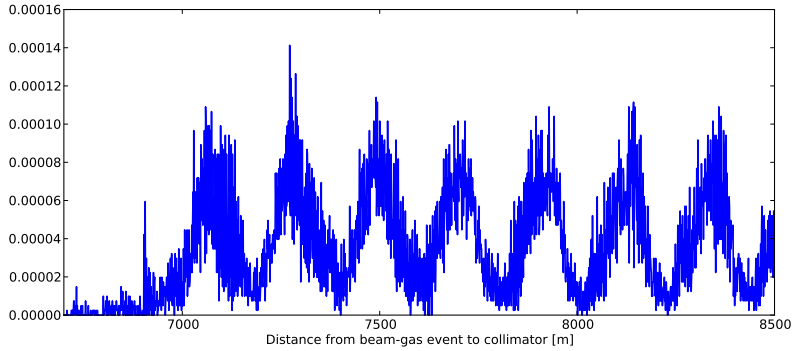

Figure 5.16: A zoom of Figure 5.15 in a region where we see a regular pattern attributed to the phase advance between the loss location and the collimator.

CMS, where beam 1 losses are close to a factor two higher.

For LHCb, the beam 1 losses comes from the last octant only. It clearly is a benefit for LHCb to be close to the betatron collimation in this case. For beam 2, there is a strong horizontal/vertical asymmetry. While the horizontal losses are effectively stopped by ATLAS collimators, the vertical losses comes from all seven octants up-

stream, with some cleaning by the CMS collimators as well. This results in the vertical losses being about double for beam 2 compared to beam 1. LHCb is more vulnerable to beam 1 background, see Section 4.3.2.

With these loss maps we can learn where the potentially problematic pressure bumps can arise. If a pressure bump is generated in a region where we see no losses in the simulations, chances are that this bump will not impact the background for the detector. One should keep in mind that we have not simulated imperfections in the optics (β-beat) or misalignments, something which could have an impact on these results.

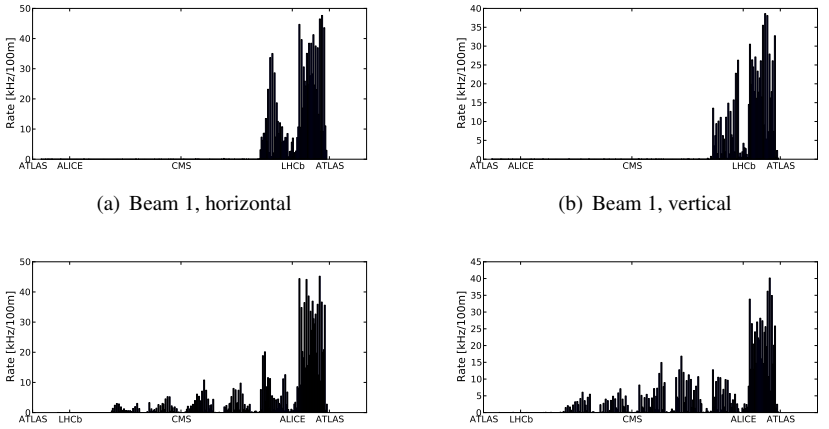

(a) Beam 1, horizontal

(b) Beam 1, vertical

(c) Beam 2, horizontal

(d) Beam 2, vertical

Figure 5.17: The distribution of the origins of the beam-gas events which produce hits on the collimators close to ATLAS.

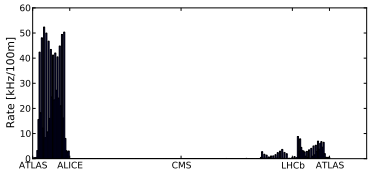

(a) Beam 1, horizontal

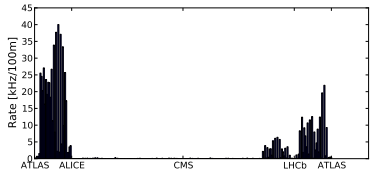

(b) Beam 1, vertical

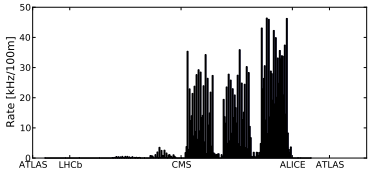

(c) Beam 2, horizontal

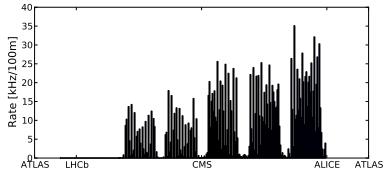

(d) Beam 2, vertical

Figure 5.18: The distribution of the origins of the beam-gas events which produce hits on the collimators close to ALICE.

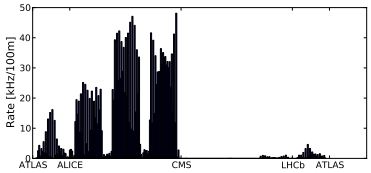

(a) Beam 1, horizontal

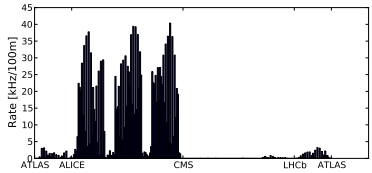

(b) Beam 1, vertical

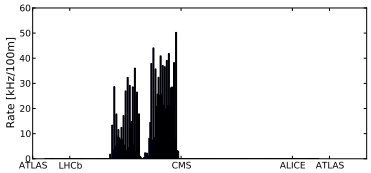

(c) Beam 2, horizontal

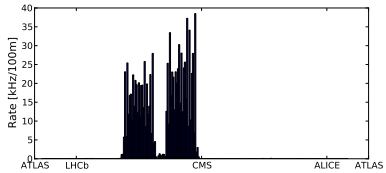

(d) Beam 2, vertical

Figure 5.19: The distribution of the origins of the beam-gas events which produce hits on the collimators close to CMS.

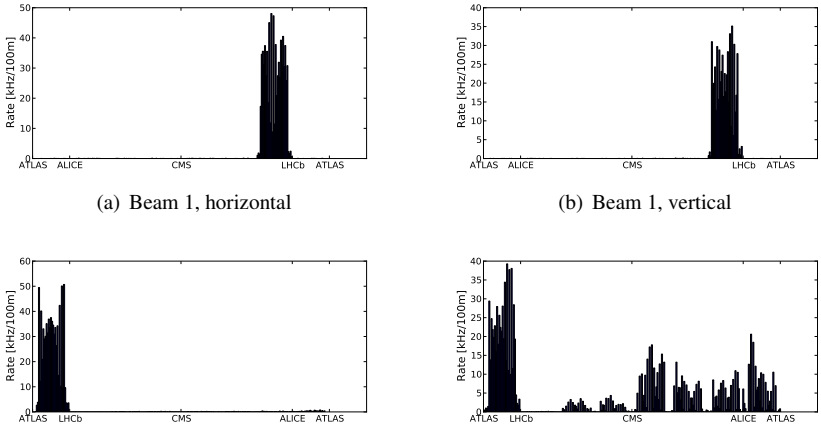

(a) Beam 1, horizontal

(b) Beam 1, vertical

(c) Beam 2, horizontal

(d) Beam 2, vertical

Figure 5.20: The distribution of the origins of the beam-gas events which produce hits on the collimators close to LHCb.

5.6.3 Impact Parameter

When propagating these losses through a shower simulation code, it is important to know the positional distribution of the impacts on the collimator. Protons that hit deep in the collimator jaw, will have a low amount of particles exiting on the adjacent side, and most of the energy will be absorbed in the collimator itself. A proton which is barely gracing the jaw will produce a rather different background signal.

We see a general trend in the distribution that for the high luminosity experiments ATLAS and CMS, the transverse distributions of the hits are more wide spread across the collimator, while it is more peaked at the jaw opening for ALICE and LHCb. This is related to the larger beam size at the collimator positions in the low β^* optics. In Figure 5.21 we show an example for the horizontal collimators in front of ALICE and ATLAS.

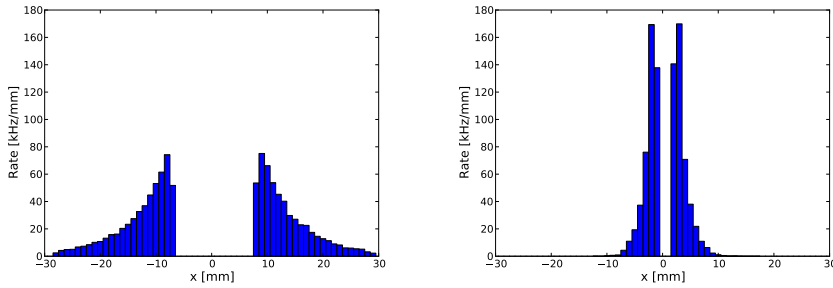

(a) ATLAS (b) ALICE

Figure 5.21: The transverse distribution of particle hits on the horizontal tertiary collimators for beam 1. The distributions are significantly more peaked at the jaw opening for ALICE than for ATLAS.

The depth distribution of the hits does not vary as much, and we show an example in Figure 5.22. The majority of the hits are distributed in the first 20 cm, and after 60 cm there are practically no hits.

Finally, in Figure 5.23 we show the distributions in both dimensions. The particles are spread significantly further out for CMS (and ATLAS) when compared to LHCb (and ALICE). A small stripe of hits can be seen all along the entire collimator jaw, in particular for LHCb. The colour contours follow a logarithmic scale, which means that

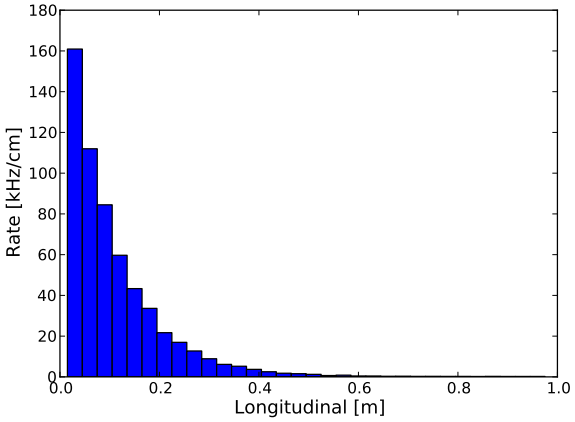

Figure 5.22: The distribution of the depth of the hits on the vertical collimators in front of ALICE for beam 2. A similar distribution is seen on all collimators.

the spread is more peaked than it looks like in the figure.

5.6.4 Summary for the Nominal Machine

In this chapter we have focused on the total background contribution from the full machine. What we should then remember is that all protons with an energy below 80 % of the beam energy, together with all other particle types, are assumed locally lost and not a part of what is shown here. What we in essence have described is what we defined earlier as the distant beam-gas background.

The wast majority of beam-gas collisions are contributing to this background, because of the much longer integrated length where the interactions can take place. However, the cross section for a beam-gas interaction which produces lost protons at one particular experiment becomes significantly lower. Further, most of these protons end up on the tertiary collimator. That means that the protons and the secondary particles will have to travel through 1 m of metal. A significant part of the energy is already dissipated in the collimator itself, which reduce the amount of background reaching the detector.

As a result, what we define as the LSS beam-gas can give a larger background contribution in the end because the cross section for inelastic interactions is larger, and the amount of particles reaching the detector (multiplicity) is greater.

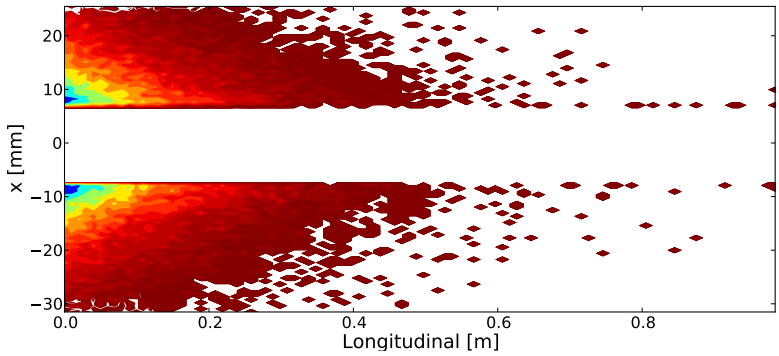

(a) CMS

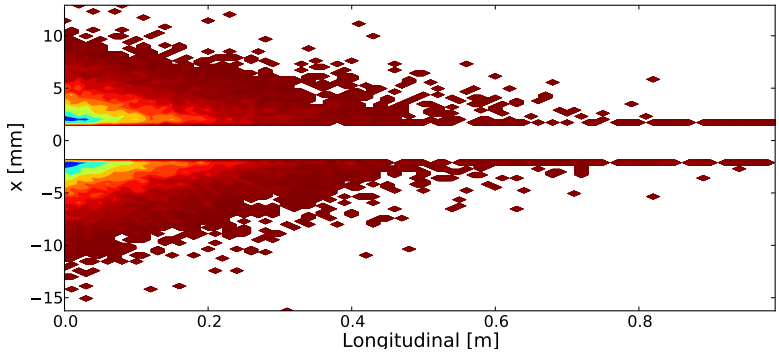

(b) LHCb

Figure 5.23: The distribution of the collimator hits in a 2D histogram. Here showing the hits on the horizontal collimators in front of CMS and LHCb for beam 2. The contours are logarithmic to better see the regions with low rates. The collimators are 1 m long.

Further, one should take note that these pressure maps do not take into account electron cloud and other effects that can significantly increase the vacuum pressure in local regions. The pressure can increase by several orders of magnitude over a limited region, which can completely dominate the overall machine induced background.

A perfect machine has been assumed thus far. Both misalignments and optical imperfections can significantly increase losses. Collimator cleaning studies (using SixTrack as well) have shown that imperfections reduce the cleaning efficiency by a factor 10 [15, Ch. 6.2]. β-beat, coupling and non-linearities were not included. To give a clear estimate on the effects imperfections would have on beam-gas scattering losses is difficult without the full simulation. We do expect beam-gas scattering to be somewhat less dependent on imperfections than the halo cleaning. The reason for this is that the beam-gas residues travel for a shorter distance (mostly less than one turn vs. up to a few hundred turns). Additionally, the collimator impacts are significantly deeper, making the losses less dependent on collimator misalignments. A quick study was performed turning off all sextupoles, and no significant changes in the loss patterns were discovered.

5.7 3.5 TeV

We have now had a detailed look at the expected background rates from beam-gas for the nominal machine energy. If we instead consider a beam energy of 3.5 TeV, and in addition a lower beam intensity which corresponds to the operations in 2010-2011, we get a rather different picture. The main reasons for these differences are the much reduced dynamic pressure, and tertiary collimators with larger openings.

While at full energy we have the highest pressure in the arcs, the situation at 3.5 TeV becomes quite the opposite. In [47] we simulated the background rates for collisions at 450 GeV, where the dynamic pressure can be ignored. In that case the pressure is significantly higher in the long straight section, which means that the beam-gas collisions originating in the long straight sections (LSS beam-gas) and inside the experimental cavern (local beam-gas) becomes increasingly important. With the additional much lower beam intensity, we found a rate from distant beam-gas which was below 1 Hz. The dominant background contribution in this case was found to be the last 60 m before the interaction point.

In Appendix D.2 we describe our simulations for 3.5 TeV and together with the LHCb Collaboration we made the effort to estimate the detector response from the background rates we had simulated. In this work we used a pressure based on a low beam intensity, which still get a dynamic pressure contribution. Our comparison to data was off by a factor ten. An important reason for this was the low background rate

overall (a few Hz), which means the uncertainties increase.

As the intensity increased in 2011, so does the expected pressure, and the beam-gas interaction rate scales fast as the beam intensity increases. Towards the end of 2011, the beam intensity was about 50 % of nominal. At this beam energy and intensity, the dynamic pressure increase was very significant as expected. A paper published by LHCb using data from 2011 [43], had a remarkably good agreement between measurements and simulations. The estimate was off by only a factor 1.6. The main cause of the improved estimate was an increase in beam intensity and a dedicated run without collisions, which resulted in better signal/noise ratio for the background measurements.

For both 2010 and 2011, the collimators were set at a more relaxed position, with the tertiary collimator half gap set at 11.8-15.3 σ. That implies that the background from distant beam-gas will be relatively lower when compared to LSS and local beam-gas. The tertiary collimators primary purpose is to protect the final focusing triplet. Since we did not focus as strongly in these runs, the available aperture in the final triplet was larger and the tertiary collimators could be set more open. This is worth noting for the nominal settings as well, where the tertiary collimators are set at 8.3 σ in all four interaction points, even though β^* is 10 min ALICE/LHCb.

Until the end of this thesis work, the rates from distant beam-gas on tertiary collimators and other aperture restrictions have been expected too low to be measureable by beam loss monitors. As the beam intensity and energy increase, the rates on tertiary collimators in particular, will increase dramatically with respect to rates form normal beam halo. As a result, one will be able to measure the signal on BLM's from the combination of halo background and distant beam-gas background. This is the most direct measurement we have available, but it requires significantly higher rates (order of 100 kHz), and we do not have any clear way to disentangle the signal from halo and beam-gas background. One way one could imagine would be to scrape away the halo for a short while using the primary collimators, but this is considered unsafe operation and cannot be done with the high beam intensities that are required.

In the end, the simulations are using fairly similar procedures to the collimation studies, where measurements by means of loss maps using BLM's are available. As these studies so far show very good agreement between simulations and measurements[79, 80], we feel increasingly confident that our simulations are trustworthy.

Chapter 6

Studies of Other Background Sources

In the preceding chapter we had a look at the beam-gas background, which is always present and is often the most significant machine induced background component. Here we will look at other potential sources of machine induced background, namely interaction region cross-talk and tertiary halo background. We will start by discussing the IR cross-talk in general, and then present our simulations. Afterwards we will discuss the tertiary halo background and how it compares to beam-gas background. We finish by briefly discussing how particle shower simulations including the LSS geometries can be performed. We presented our studies of IR cross-talk in IPAC'10. The article is found in Appendix D.3.

6.1 Interaction Region Cross-Talk

In the LHC we have several experiments running at the same time. As a result, residues from collisions in one interaction point can be a source of background at another experiment. The experiments typically measure the full inelastic cross section, while the cross section for producing a proton with exactly the right parameters to end up in front of another experiment is significantly smaller. As a result, this is not expected to be a problematic contribution to the background when the two experiments are running at a similar luminosity.

For LHC, we have two high luminosity, general purpose experiments. The other two experiments, LHCb and ALICE, are designed for a much lower luminosity, about

2 and 4-5 orders of magnitude respectively. As a result, one can not exclude interaction region cross-talk as a potential source of background for these two experiments, where perhaps ALICE has a greater cause for concern.

Of importance for this source of background is the phase advance between the originating interaction point, and aperture restrictions upstream of the low luminosity experiment which receives the background. In the case of LHC, these aperture restrictions are first and foremost the tertiary collimators. If the phase advance is close to

$$90^\circ + n \cdot 180^\circ, \tag{6.1}$$

then an angular kick from the collision at the interaction point is transformed into a maximum amplitude at the aperture restriction. n is an integer. The one-turn matrix with a fractional tune of 0.5, becomes J as defined in Eq. (3.19). We multiply J by

$$\begin{pmatrix} 0 \\ \sqrt{\varepsilon/\beta} \end{pmatrix}, \tag{6.2}$$

and get

$$\begin{pmatrix} \sqrt{\varepsilon/\beta} \\ -\alpha\sqrt{\varepsilon/\beta} \end{pmatrix}, \tag{6.3}$$

which is the coordinate shown in Figure 6.1.

Hence, if IR cross-talk would become a problem in certain situations, it can potentially be mitigated by modifying the phase advance. However, we expect that this background source will rarely become dominant. Other background sources depend on the beam intensity and will be relatively higher for the low luminosity experiments as well.

6.1.1 Lorentz Boost

Simulating the IR cross talk can be done in a similar way as we simulated the beam-gas background in the previous chapter. Rather than distributing the scattering events along the beam orbit, we have one scattering location per interaction point. Further, we need to change the proton-proton event generation so we now simulate a high energy proton colliding with another high energy proton.

In order to deal with the large amount of bunch crossings in the common chambers of the four interaction points, a crossing angle is introduced which separates the beams and reduce the number of head-on collisions to one per interaction point. That means that the protons collide at an angle, while the proton-proton collisions are simulated head-on.

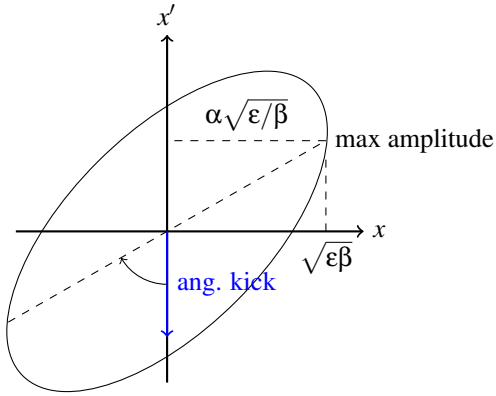

Figure 6.1: A proton which is originally well centred in the beam will receive an angular kick which will be transferred into a maximum amplitude downstream of the collision point.

The crossing angle is varying from experiment to experiment, but it is typically on the order of 100 µrad. That means that the centre of mass is moving at a speed on the order of $10^{-}4$ c. This is significantly below what would be required for relativistic effects, and we can simply apply a normal angular addition to the secondary particles to account for the crossing angle.

We define the 4-vector in natural units as

$$\begin{pmatrix} E \\ p_x \\ p_y \\ p_z \end{pmatrix}, \tag{6.4}$$

where E is the energy and p_i is the momentum component along the i axis. The Lorentz boost can then be defined as

$$\begin{bmatrix} \gamma & -\beta\gamma & 0 & 0 \\ -\beta\gamma & \gamma & 0 & 0 \\ 0 & 0 & 1 & 0 \\ 0 & 0 & 0 & 1 \end{bmatrix}, \tag{6.5}$$

in the special case where the boost is along the x-axis. β is here the speed of the moving

frame in units of c, and the relativistic γ is

$$\gamma = \frac{1}{\sqrt{1-\beta^2}}. \tag{6.6}$$

In the classical approximation, γ becomes one, and the energy in the moving frame is simply an addition to the momentum in the x direction in the rest frame. In Figure 6.2 we show the Lorentz boost for two different centre of mass velocities, and the distribution from collisions with the centre of mass at rest. We see that for 300 µrad, which is a rather large crossing angle in the LHC, the effect of the Lorentz boost can still safely be ignored.

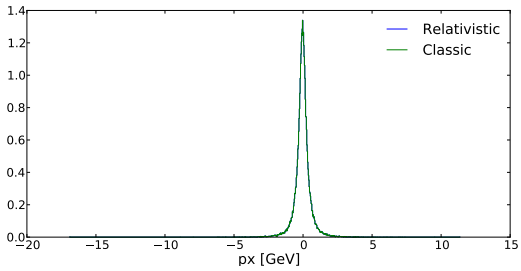

(a) Head-on

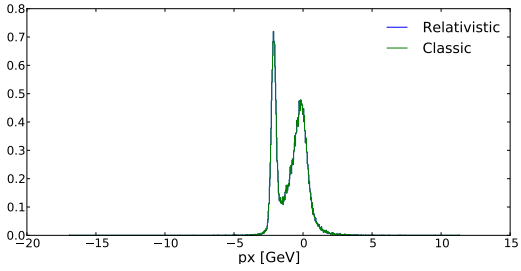

(b) 300µrad

Figure 6.2: Lorentz boost for 0 and 300 µrad crossing angle. The second peak seen when the crossing angle is added is the elastic peak, and is not a relativistic effect. The initial events are 7 TeV head-on proton-proton collisions, simulated using DPMJET III. Take note that it is the energy in the **moving frame** which should be 7 TeV, whereas in the illustration we have set the energy in the **centre of mass frame** to be 7 TeV.

6.1.2 Phase Advances

The phase advances between interaction point and the tertiary collimators in (neighbouring) experiments can give a good indication of the amount of IR cross talk. In Table 6.1, the phase advances between the tertiary collimators in the low luminosity experiments ALICE and LHCb and the interaction points of the higher luminosity experiments are given. We ignore here the background contribution to the higher luminosity experiments. The phase advance between two points is normally given in radians or degrees. In the table we give the phase advance with integers of 2π subtracted, and in units of 2π.

For ALICE, background from CMS for beam 2, and ATLAS/LHCb for beam 1 is of most interest. For LHCb, background from beam 2 is of higher interest. This is due to the location of the betatron collimation in interaction region 7, expected to significantly reduce the halo of the beam passing the region. As LHCb is more sensitive to beam 1 background, there are already strong indications that IR cross talk will not be a major background source for LHCb.

Table 6.1: The "fractional" phase advance in units of 2π between the different tertiary collimators close to ALICE and LHCb and the higher luminosity experiments. A value close to 0.25 or 0.75 indicates maximum cross talk, 0 or 0.5 indicates minimum cross talk.

	Beam 1		Beam 2	
	Horizontal	Vertical	Horizontal	Vertical
		Towards ALICE		
ATLAS	0.70	0.69	0.66	0.68
CMS	0.68	0.34	0.72	0.44
LHCb	0.84	0.78	0.42	0.38
		Towards LHCB		
ATLAS	0.17	0.15	0.93	0.04
CMS	0.15	0.80	0.99	0.81

6.1.3 Simulations

In [81] we presented our simulation results for the 3.5 TeV beam energy, and a β^* of 10 m in ALICE, 3.5 m in LHCb and 2 m in ATLAS and CMS. This implied collimators with larger opening than for the nominal machine, which would presumably reduce the background rate. We assumed that all experiments were colliding head-on and with an equal amount of bunch crossings.

With these assumptions we found a fractional rate on the order of $\times 10^{-3}$ on the tertiary collimators in the ATLAS/CMS region, and $\times 10^{-6}$ in the ALICE/LHCb regions. Fractional rate then means in fractions of the sum of the collision rates at the four experiments. These rates are small when compared to estimates for other background sources.

Table 6.2: The rate of protons hitting various tertiary collimators. The protons are originating from collisions at higher luminosity experiments. The rates are in units of collision rates at the originating experiment.

	Beam 1		Beam 2	
	Horizontal	Vertical	Horizontal	Vertical
Towards ALICE				
ATLAS	3.2×10^{-5}		3.4×10^{-6}	4.2×10^{-6}
CMS			4.2×10^{-6}	3.4×10^{-6}
LHCb	1.2×10^{-3}	4.8×10^{-4}	4.3×10^{-6}	
Towards LHCB				
ATLAS			6.7×10^{-5}	
CMS	9.6×10^{-7}		8.4×10^{-7}	1.7×10^{-6}

In Table 6.2 we show the proton rates on the various tertiary collimators in front of LHCb and ALICE. The numbers are given in units of collisions at the originating interaction point. What we see in the simulation is that the physics debris collimators which are located approximately 180 m downstream of ATLAS and CMS are receiving a large amount of hits in these simulations. Without these in place, the rates coming from ATLAS and CMS would be significantly higher.

The number of simulated events is around 1 million collisions per interaction point, and somewhat lower for LHCb. It means that the statistical error becomes large for rates below $\times 10^{-5}$. We see the highest relative rate on the horizontal collimator in front of ALICE, from LHCb. The rate is about 1 ‰ of the collision rate in LHCb. LHCb has a nominal luminosity of $2-3\times10^{32}$ cm^{-2}s^{-1}, which is about two orders of

magnitude less than ATLAS and CMS. That makes this rate about 10 % of the nominal rate in ALICE, where the maximum luminosity is about 2×10^{30} cm^{-2}s^{-1}.

To summarize, our simulations show that IR cross-talk will most likely not become a significant source of background, with the exception of the low luminosity experiment ALICE, where the rate of this background could become comparable to the collision rate at the interaction point.

Survival Rates

For the beam-gas simulations we found a survival rate of a few percent. The elastic cross section is about 16 % of the total cross section as shown in Figure 5.3 for beam-gas collisions. For proton-proton collisions at 7 TeV, the elastic cross section increases to around 27 %. In addition, all collisions take place in the interaction point, where the β function is smaller than in the arc, and the beam divergence is larger. That means that the same angular kick will have a lower probability of kicking the proton out of the stable region of phase space.

In our simulation for the nominal optics, we find a survival rate of 32 % for ATLAS and CMS, and 26 % for LHCb. That means that a large fraction of the collisions at the interaction points will not produce losses directly, but will be contributing to the emittance and halo growth. In Figure 6.3 we show the angular kick from the collisions in ATLAS and CMS, with the distribution of angular directions in one plane (xp) before and after the collisions. We required a minimum of 99.5 % of the nominal energy in this distribution, which accounts for about 38 % of the collisions. The collisions are simulated using DPMJET III.

6.1.4 Loss Rates During Van der Meer Scans

In order to make an absolute measurement of the luminosity in an experiment, what is called a calibration Van der Meer scan is performed. The beams are transversally separated in a controlled manner, and the luminosity as a function of separation is performed to measure the overlap integral (beam spot) between the two beams. The resulting luminosity as a function of beam separation is shown in Figure 6.4, together with the double Gaussian fit. The method, and the first measurements of the absolute luminosity in the LHC are covered in detail in the thesis by S. White [34].

These scans have an interesting feature for measurements of IR cross talk. Since the cross talk should be directly linearly dependent with the luminosity at the originating interaction point, these scans should also modify the cross talks between the interaction

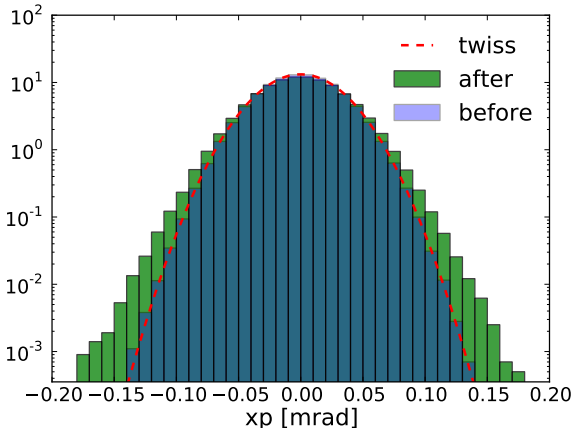

Figure 6.3: The angular distribution (beam divergence) in one plane for all simulated collisions where the proton has at most 0.5 % energy loss from the collision. We only show collisions in ATLAS and CMS here. The original beam divergence is shown in blue. The red line is calculated from the optics table. The divergence of the beam after the collisions in green.

points if there is any. Tracking the loss rates on the tertiary collimators during the calibration scans should enable us to see the cross talk if it is significant enough.

First attempts are described in Appendix D.3. The calibration scans are normally done at reduced beam intensity, in order to minimise the uncertainty in the measurement of the absolute luminosity. The loss rates at the tertiary collimators have been difficult to observe directly as a result.

Our simulations showed that we would receive a very large hit rate on the physics debris collimators, which is not surprising. The purpose of the physics debris collimators is to reduce the heat load from the high luminosity collisions in ATLAS and CMS. For the nominal optics, the simulations show a rate of about 2.5-3 % of the collision rate at the interaction point onto these collimators. In Figure 6.5 we show the luminosity in ATLAS and the loss rate on one of the physics debris collimator next to ATLAS during a high intensity calibration scan. The beam intensity was around 1×10^{14} protons/beam. We see a variation in the loss signal of about 10 μGy/s.

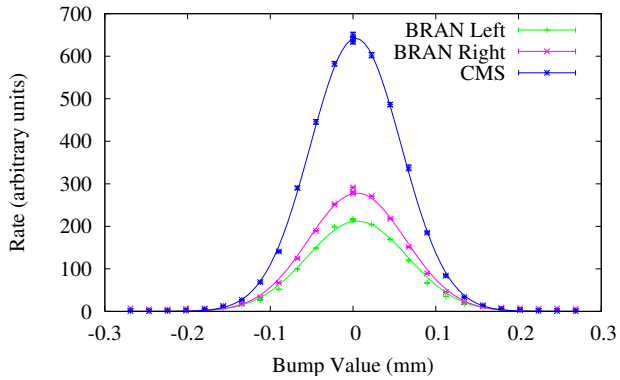

Figure 6.4: The interaction rate during a luminosity calibration scan in CMS [82]. Solid lines show the fit, which is usually a double Gaussian. A scan like this takes about 20 min to complete. Figure courtesy S. M. White.

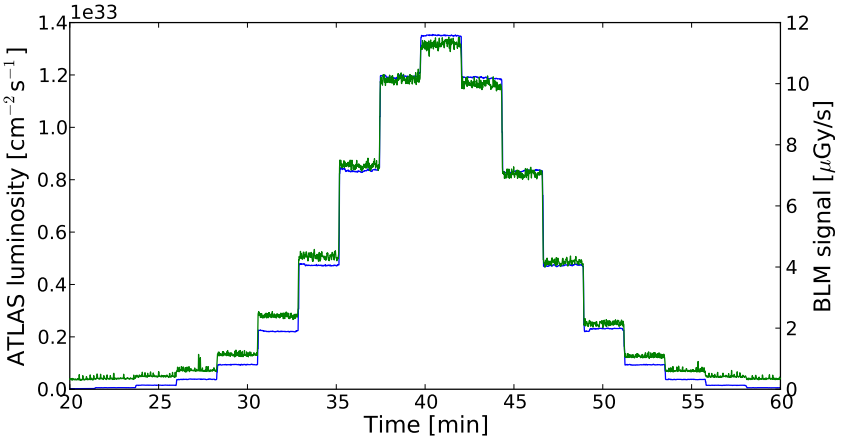

Figure 6.5: Luminosity in ATLAS in blue, and loss rate on beam loss monitor close to the physics debris collimator in green.

If we assume a cross section of 100 mb, then 3 % of the collision rate with a luminosity of 1×10^{33} cm^{-2}s^{-1} corresponds to about 3 MHz of protons on this collimator, or 3×10^{-12} Gy/proton. This fits very well with FLUKA simulations and measurements of the BLM response in the LHC, which estimate $1 - 5 \times 10^{-12}$ Gy/proton for steady-state losses [78, 83].

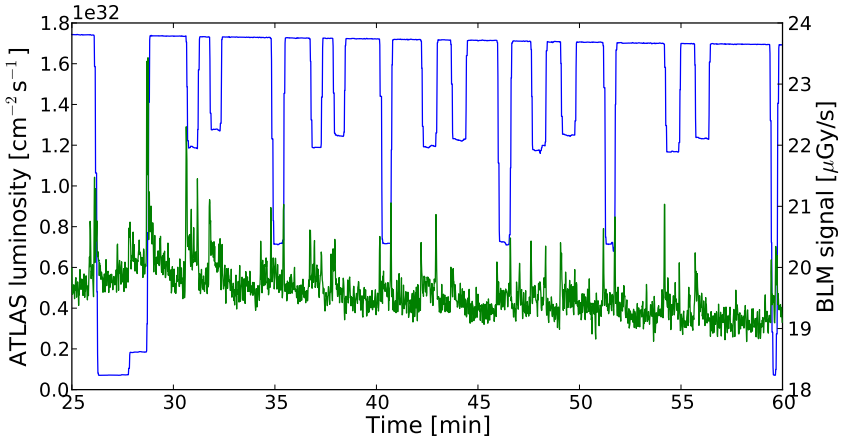

Figure 6.6: Luminosity in ATLAS in blue, and the loss rate close to the horizontal tertiary collimator in front of LHCb in green. Each time the beam is moved in ATLAS, a spike is seen on the loss monitor of the TCTH in front of LHCb (beam 2).

The highest cross talk rates were expected to be almost 3 orders of magnitude lower than the rate on the physics debris collimator, when coming from ATLAS or CMS. In other words, we are talking about order of 10 nGy/s, assuming equal scaling factor for the beam loss monitors. Such a rate would not be detectable, even taking into account that the fractions will be slightly different for the optics in the machine during this scan.

In Figure 6.6 we show the signal from the beam loss monitor connected to the tertiary collimator in front of LHCb for beam 1. This was during a length calibration, where the beams are moved across each other consecutively. We see that there is a peak at most of the locations where the beams are moved. The effect is not from cross talk as such, since the loss rate does not change with the luminosity. Instead, this is an optical or orbit effect. When the beams are separated the beam-beam tune-shift changes which can produce a sudden loss spike when (parts of) the beam is crossing a minor resonance. Such an effect is most likely what we observe here. However, it is the

first time we (knowingly) have observed changes in loss rates on a tertiary collimator due to beam movement in a different experiment. The cross talk from ATLAS to the horizontal tertiary collimator in front of LHCb was also where we expect the highest rate from simulations, according to Table 6.2.

6.2 Tertiary Halo Background

In the LHC, we define tertiary halo as the halo component that has a large enough betatron action to hit the tertiary collimators. The tertiary halo is the main part of the beam halo that will produce background noise for the detectors.

The beam halo generally grows with time due to various slow processes. Elastic beam-gas is one process which we have already discussed that contributes to the general halo growth. Other processes include for example intrabeam scattering, the collisions at the interaction points themselves, and electron cloud.

Once the particle reach the dynamical aperture limit of the machine, the transverse movement becomes chaotic. A chaotic movement can still be bound (think of e.g. a Lorentz attractor [84, Ch. 9]). The dynamics and the distribution of the halo can be difficult to predict. The core and the halo typically follow two different distributions, one common example being a “heavy-tailed” Gaussian distribution.

Since the tertiary halo is produced from slow drifts, the hit distribution on the collimator is expected to be more peaked. We say that the impact parameter – the average distance from the jaw to where the particle hit – is small. In Figure 6.7 an example is shown for the vertical collimator in front of LHCb. The statistics from the collimation studies are usually lower than from beam-gas studies for these collimators. For the collimator in Figure 6.7, there were about 4000 proton hits out of an initial 5 million protons in the halo simulated. The vertical axis for the tertiary halo histogram is normalised to one halo particle. On other collimators the distribution might be wider, but in general it is narrower than the same distribution for beam-gas events.

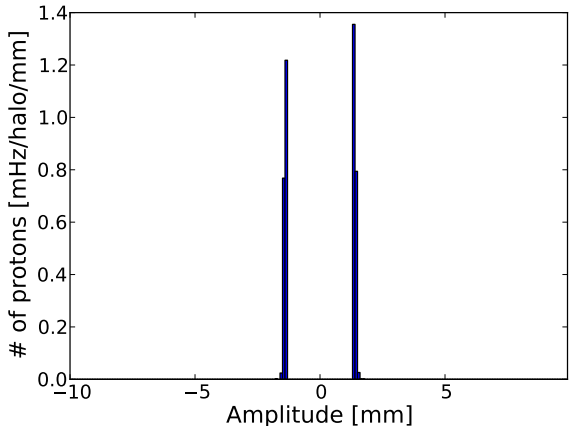

(a) Tertiary halo

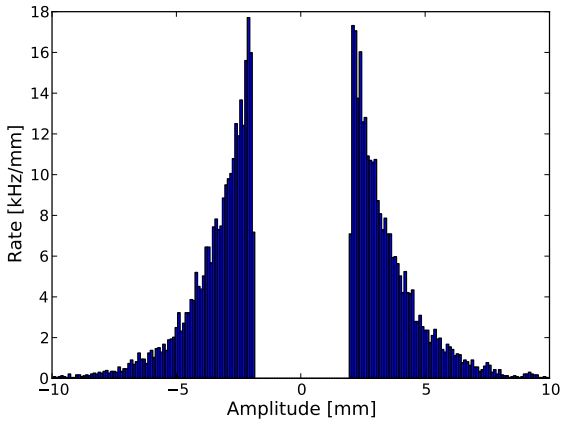

(b) Beam-gas hits

Figure 6.7: The hit distribution on the vertical tertiary collimator in front of LHCb for beam 1 at nominal energy. The distribution is much more peaked for the tertiary halo. The vertical axes are not directly comparable. Collimation simulation done by T. Weiler [85]

6.3 Studies of Particle Showers

The long straight sections need to be modelled in a particle shower code like e.g. FLUKA, MARS, or BDSIM. As input, the data from the beam-gas simulations, tertiary halo simulations and the cross-talk simulations are needed. The first of these sources that were available was the tertiary halo background [86, 15]. In addition, losses from LSS beam-gas can directly simulated by provoking beam-gas collisions while tracking the beam through the particle shower codes. In [62] these two background sources were studied with a model that reached 550 m from the interaction point of ATLAS/CMS. SixTrack was used for the collimation simulations. The model was implemented in MARS15 [87] which was used for beam-gas and shower simulations as well. It was found that in particular high energy muons had a much larger presence in the beam-gas background.

R. B. Appleby et Al. have developed a FLUKA model for the long straight section around LHCb [88], with a priority on beam 1 background which is more important for this asymmetric detector. The model is very similar for ALICE, with beam 1/2 inverted, and we used it to publish our first estimates for the machine induced background for ALICE in [48].

In an ongoing work, the ATLAS and CMS interaction regions are being modelled in FLUKA by R. Bruce [69]. This is very interesting for several reasons. First it serves as a great validation for both the MARS and FLUKA codes. Second, since we now have all four experimental regions modelled in the same code, the relative differences can be better understood. The results from FLUKA are found to be in very good agreement to what was found in earlier studies using MARS [76].

6.4 Summary

Together with the simulations of beam-gas presented in Chapter 5, we have now covered all background sources. Of the three, beam-gas background seems to be the dominant background source for the experiments based on our current knowledge. The same is confirmed from our current understanding of the measured background in the experiment during 2010 and 2011 running. Interaction Region cross-talk looks to be the least significant background source.

IR cross-talk is best compared to the collision rate at the high luminosity experiments ATLAS and CMS. We then get a hit rate on the tertiary collimators in front of LHCb and ALICE which is at least five orders of magnitude lower. For a luminosity of 1×10^{34} cm^{-2}s^{-1} in ATLAS and CMS, that would mean the rate would be comparable to the nominal luminosity in ALICE which is 1×10^{29} cm^{-2}s^{-1}. We should then

keep in mind that ALICE can, and has run with a luminosity one order of magnitude higher. Further, we expect a higher rate of halo background in all circumstances. We do not expect situations where the IR cross-talk will become a problematic background source.

Chapter 7

Fill Analysis and Background Observations

As a part of this work, we developed an automated fill analysis package for continuous monitoring of the LHC machine performance on a fill by fill basis. A vast amount of data is available from beam loss monitors, beam position monitors, vacuum gauges, detector signals and so forth. Our goal has been to present the most important part of this information in a convenient format for quick access by operators and other interested parties.

We will start by discussing the motivation for this work, and how the project is organised. We will then show some data from the machine performance during 2011 running. The background observations during 2011 will be assessed, before we show a detailed analysis example where we look at the beam lifetime. This work was presented at IPAC'11, see Appendix D.5.

7.1 Motivation

The availability of the data is of high importance for a proper understanding of how the machine performs. In order to obtain the data available on the machine side, the TIMBER interface has been developed. TIMBER's graphical interface is shown in Figure 7.1. The TIMBER interface is based on manual extraction of data, which is time consuming to do on a regular basis. Additional information is often needed for a proper analysis. For example, locations of vacuum gauges, or which of the 12 different

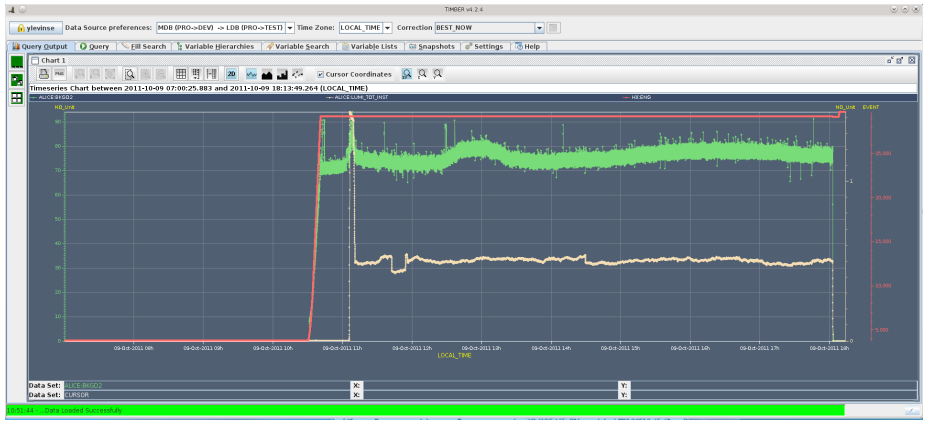

Figure 7.1: An example of the TIMBER interface, here showing the beam energy in red, ALICE luminosity in beige and the ALICE background 2 number in green for fill 2197.

running sums (integration time) to use from the beam loss monitors. To get an overview on a regular basis an automated system that present the essential subset of data and calculate performance numbers is essential. Details of how the project is structured can be found in Appendix D.5.

Our goal was to develop a system which extracts data from the data logging interface (TIMBER), settings from LSA [89], summary from the electronic logbook and so forth. The logging database in its current form does not support correction of wrong data, or addition of missing data without significant effort. Corrections are needed because the experiments can sometimes have difficulties reporting luminosity information online, or there can be an error in the algorithm under certain unforeseen conditions. We wanted to include support for offline correction of data, providing a place where the users could get quick access the most up to date information.

After the data are collected, we calculate and append derived information. As an example, the collision pattern (number of bunch collisions in each interaction point) can be calculated from the fast bunch current transformer (BCT) data available from the logging database, but it is tedious to do manually. Another example is to know the amount of time spent with and without beam present, time spent in stable beams and so on, which give information about machine reliability and effectiveness.

In order to make calculation of derived data more easy, we interpolated all extracted information to common time stamps. This can be done by the TIMBER interface as

well, but the same interpolation routine must be used for all selected data. Machine flags like e.g. beam modes should simply be repeated, while most data should be interpolated linearly or quadratically to the common time stamp. The data are exported to efficient binary formats including the derived data. HDF5 [90] and ROOT [91] export were implemented. These data files are made available to the outside community for their own analysis as well.

7.2 Machine Performance

As stated in the introduction, the main parameters of a particle accelerator is the particle type, particle energy and the luminosity (collision rate). While the two first parameters usually do not change very often, the luminosity changes from fill to fill and even within a fill due to particle losses and emittance growth. An essential measure of machine performance is the maximum (peak) luminosity, and the integrated delivered luminosity.

The peak and delivered luminosity for each fill is calculated including available offline corrections by our analysis package, and presented in a table on the web page as shown in Figure 7.2. In the same table, we give information about the time spent in stable beams, the number of bunch collisions in each interaction point as calculated by the fast BCT data, and the date when the fill started. This table makes it very quick to search for relevant fills for your analysis. For example, one might be curious about *which fills had a stable beams period of longer than X hours recently* or *which fill had the highest peak luminosity in the last week.*

	Fill	Start Date Stable Beams	Duration Stable Beams [hh:mm]	Energy	Scheme [bunches] [P1&5/P2/P8]	ATLAS Peak Lumi [Hz/ub]	ATLAS Delivered Lumi [nb^{-1}]	ALICE Peak Lumi [Hz/ub]	ALICE Delivered Lumi [nb^{-1}]	CMS Peak Lumi [Hz/ub]	CMS Delivered Lumi [nb^{-1}]	LHCb Peak Lumi [Hz/ub]	LHCb Delivered Lumi [nb^{-1}]
	2201	15:27 10.10.2011	3:51	3500	1 1/0/0	4.9	55.3	0	0	4.9	57.4	0	0
	2200	05:27 10.10.2011	4:25	3500	1380 1317/37/1296	3213.4	43418.9	1.5	15.7	3292	43611.7	364.8	5199.4
	2199	01:44 10.10.2011	0:31	3500	1380 1317/37/1296	0.1	5505.3	1.4	1.1	3167.2	5577.7	342.5	355.1
	2197	11:11 09.10.2011	6:55	3500	1380 1317/37/1296	3422.5	64691.8	0.5	12.4	3346.6	63911.9	365.8	8294.7
	2195	11:41 08.10.2011	17:17	3500	1380 1317/37/1296	0.2	114912.8	3.5	58.5	5798.7	120134.7	358	21289.9
	2194	04:33 08.10.2011	0:38	3500	1380 1317/37/1296	3267.6	7072.5	1.9	2.4	3258.1	7015.6	351.2	421.7

Figure 7.2: The table showing the most essential data for each fill.

A separate project was initiated at about the same time as this fill analysis project, called the "LHC Supertable". The LHC Supertable is a similar table to that shown in Figure 7.2, but with more columns (around 80 when this thesis was finalised). The project was inspired by a similar project at Fermilab, where the final version contained more than 200 columns [92]. A significant difference in the design philosophy between the LHC Supertable and the fill analysis project that we started is that the supertable was meant to limit itself to single values per fill. Variations within a fill does not fit in a table. At the moment of writing this thesis, the two projects are in the process of being merged.

Other important figures for machine performance monitoring include the time spent in different operational modes (stable beams, setup, ramp, pre-cycle...), beam intensity variations during the fill, and luminosity during the fill. In Figure 7.3 we show the time spent in various operational modes for 2011. The figure is continuously updated and displayed on the web page.

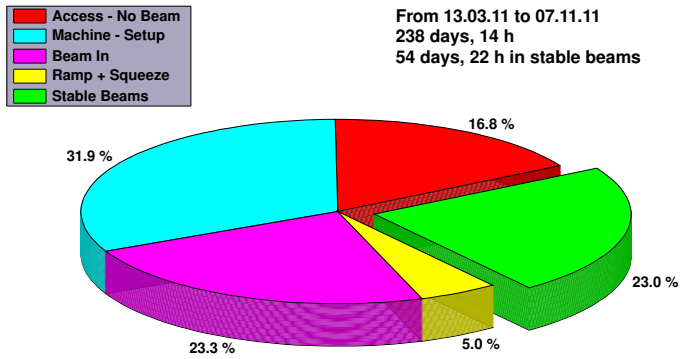

Figure 7.3: The time spent in various operational modes for the 2011 proton run. More than 20 % of the total amount of time available has been spent in stable beams this year. Figure courtesy A. Macpherson [93].

7.3 Background Observations

In the following section, we will make a brief summary of the background experience during the 2010 and 2011 running. More details can be found in the references.

During the 2010 run, the experimental background was generally low, typically below 1 % during proton physics, somewhat higher for ion physics. To define the background in percentage of luminosity can be done in various ways, typically it is the rate measured by a given background trigger divided by the rate of all triggers. Pixel occupancy for non-colliding versus colliding bunches may be another definition.

An increase in relative background was observed when increasing the single bunch intensity towards the nominal 1.1×10^{11} protons/bunch, when reducing the bunch spacing, and when increasing the total intensity further [59]. The increased background could to a large extent be correlated to increased vacuum pressure in the upstream long straight sections of the different experiments.

Interestingly and a bit surprising, electron cloud effects were observed already at 150 ns bunch spacing in the common beam chamber. Electron cloud was not predicted at such large bunch spacing [94]. It was found that the arrival time of a bunch from the second beam could be in such a way as to provoke electron cloud. The effect was thus only present with both beams in the machine, and it could be mitigated by means of installing solenoids in critical regions. If bad vacuum conditions are mitigated by the presence of solenoid fields, it is a strong indication that the source of the problem is electron cloud.

The first attempts with 50 ns bunch separation showed a significant pressure buildup, expected to be caused by electron cloud as well. Thus, the 2011 run was started with 75 ns bunch spacing. After a successful scrubbing run of about 17 h of efficient beam time in April 2011, normal operation with 50 ns bunch spacing became possible [94]. This allowed for a record peak luminosity at the end of the year within 35 % of nominal luminosity, even at half the nominal beam energy.

7.3.1 ALICE Background Challenges

Already during the 2010 run, the luminosity in the ALICE experiment was reduced from maximum by reducing the number of bunch collisions, larger β^* in 2011, and eventually transverse beam separation as well. While the luminosity goes down, the beam intensity stays the same, and some parts of the background scales with the intensity rather than luminosity. One good example being the beam-gas background, in particular the local and LSS beam-gas.

ALICE observed at the end of 2010 an increase in the relative background, which was strongly related to the vacuum conditions in the interaction region [95]. The beam

intensity continued to increase in 2011, and in a period after a technical stop, ALICE had a period of about 13 fills where the detector was forced to turn off as a consequence of the increased background [39].

The experimental magnet polarity had just been changed after the technical stop, which means that the synchrotron light from the beam hits some new locations. It has been suggested that this was partly the reason for the increased background.

The understanding of these problems are still under investigation, but seem to be related to increased vacuum pressure. The conditions improve over time, which is expected to be an effect of beam scrubbing. The exact correlation between background levels, beam intensity and number of bunches is still unclear. A doubling of the energy and beam intensity will further increase the dynamic vacuum pressure, which means it is important to understand the origin of this background and what can be done to mitigate the problems.

7.3.2 ATLAS, CMS, and LHCb Background

The other experiments have not observed background levels as dramatic as for ALICE, much due to the fact that they can handle larger background levels and run at a higher luminosity which makes the relative background smaller.

LHCb publish the fast losses observed by the beam loss scintillators (BLS) in the 2. background number to the LHC logging database. The BLS's saw a higher rate for negative magnet polarity than for positive [96], an effect that is not yet fully understood. LHCb has since the beginning had a very advanced level of comparison between background data and simulations. In a recent publication [43], they showed a good agreement between data and simulations. The simulated background for LHCb is currently dominated by the vacuum pressure in the last 60 m from the interaction point, producing beam-gas background.

CMS had some fills during the end of 2011 where some issues with the vacuum on one side of the interaction point was reducing the detector efficiency [96]. The vacuum spike was located to around 18 m from the IP, which place it near the entrance to the experimental cavern. Some possible improvements have been suggested, including an activation of NEG coating in the region, and vacuum leak checks during the winter shutdown. The origin of the vacuum spike has not been understood.

ATLAS recently published a detailed summary of the background conditions during the 2010 run [59]. ATLAS did not experience problematic background levels in 2011 [96].

7.4 Vacuum in the LSS

Most of the background observations we have described have been related in some way to the vacuum conditions in the long straight sections. As we showed in Appendix D.5, the analysis tool package we have developed is well suited to provide information about the vacuum conditions on a regular basis. The vacuum gauges give a pressure measurement at one location, while simulations give expected pressure distributions along the entire straight sections. Combining the two gives a good overall estimate of the pressure distribution for each fill.

We first take the simulated expected pressure as a basis for the pressure distribution. At each gauge location we have a correction to this base. The relative correction is then assumed to vary linearly between each pressure gauge. Hence, we make a linear interpolation of the relative pressure difference at each gauge. The interpolated relative difference is then mapped on top of the simulated pressure distribution, and we end up with a pressure map for that measurement.

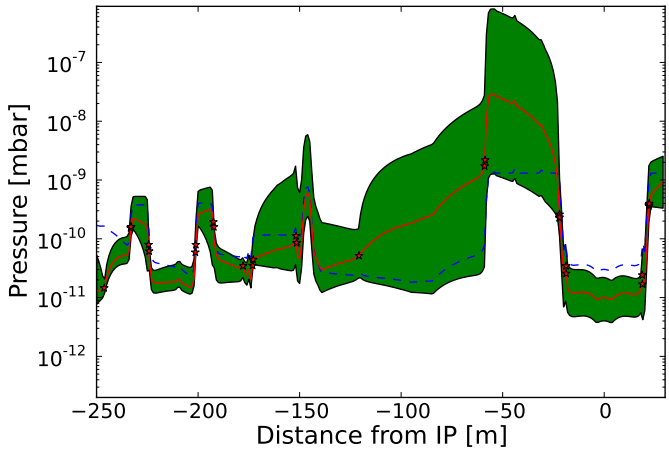

Figure 7.4: The vacuum pressure around ATLAS for beam 1 in fill 2028, 17. of August 2011. In red we see the average pressure. In blue stapled the simulation for the same parameters, courtesy G. Bregliozzi. The green show the max/min span during the fill. The red stars mark the location of the gauges.

In Figure 7.4 we show the simulated and measured pressure during a fill from the

fall of 2011. The simulation was made specifically including the parameters from the same fill. The simulation is directly estimating the pressure that is expected to be read on the gauges, taking into account the calibration factors for the gas composition in various parts of the machine. This is shown in Figure 7.5. The conversion factor between the two axes in the figure is for hydrogen, which is 5.9×10^{22} molecules/m^3/mbar. This conversion gives the pressure that is expected to be read on a vacuum gauge calibrated for nitrogen, not the hydrogen partial pressure. For hydrogen, the difference between the partial pressure and the gauge reading is a factor 2.4 in our case [64].

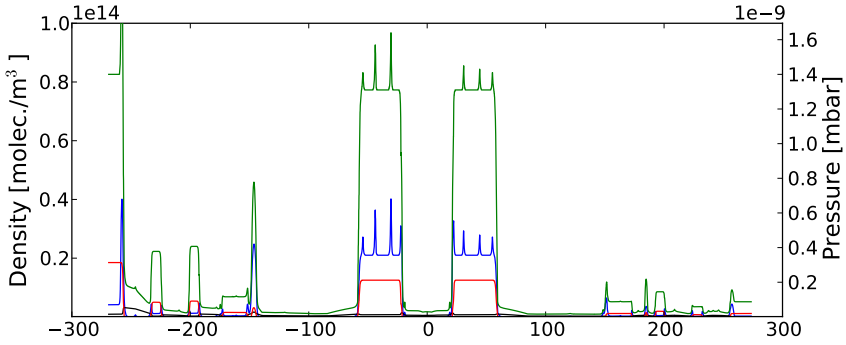

Figure 7.5: The estimated H_2 density in blue, CH_4 density in black, and CO_2 in red from the simulation [97]. The expected pressure to be read in green from the combination of all gas species present, with values read on the right hand side. The factor used between the two axes are taken from the conversion for hydrogen, which makes the blue and green line comparable.

7.5 Beam Lifetime

The beam lifetime is important for the determination of the machine induced background rates. If the lifetime is short, the background is expected to be higher. We will in the following look more in detail at the beam lifetime for and use a record fill during the 2011 proton physics run as an example.

7.5.1 Burnout

The burnout lifetime is equal to the inverse of the sum of the collision rates at each interaction point times one minus the survival ratio R_{sr} for p-p collisions, divided by the beam intensity. In terms of measurable units, that becomes

$$\frac{1}{\tau_{bo}} = \frac{\sigma_{tot}}{I_{\text{beam}}} \sum_{exp} \mathscr{L} \left[1 - R_{sr}(\beta^*)\right]. \tag{7.1}$$

The survival ratio is a function of how strong the squeeze is. For smaller β^*, the divergence of the beam becomes larger, and so the survival ratio increases. From our simulations of beam-gas collisions, we found that R_{sr} was a few percent when β is around 100 m. In our interaction region cross-talk simulations, we found that R_{sr} was around 32 % for 0.55 m β, and 26 % for 10 m β at 7 TeV beam energy. For 3.5 TeV the rates are expected to be somewhat smaller, since the beams are larger.

The burnout lifetime will be dominated by the losses from ATLAS and CMS since the luminosity in these experiments is significantly higher. For online measurement of burnout lifetime at 3.5 TeV we can then use

$$\frac{1}{\tau_{bo}} = \frac{0.7 \cdot 98\text{mb} \left[\mathscr{L}_{\text{ATLAS}} + \mathscr{L}_{\text{CMS}}\right]}{I}, \tag{7.2}$$

where we take the total cross section from [98].

Higher burnout rates will increase the IR cross-talk background. If the burnout rate is high enough, the radiation in the vacuum chamber can increase the vacuum pressure, which again can increase the amount of beam-gas background towards the experiment.

We will use fill 2219 as an example, which was the fill in 2011 that produced the largest amount of integrated luminosity, with a bit more than 120 pb^{-1} of integrated luminosity per experiment, during less than 16 h of stable beams. The fill started in the afternoon 16. of October. In Figure 7.6 we show the burnout lifetime during this fill. The burnout lifetime at the start of the fill is slightly above 100 h, increasing to more than 200 h at the end of the fill.

7.5.2 Beam-Gas

The beam-gas lifetime is found by integrating the vacuum pressure around the full ring, and using Eq. (5.4) to calculate the lifetime. We found in our simulations that the survival ratio was only a few percent, which is within the error margins. We can then safely assume a survival ratio of 0.

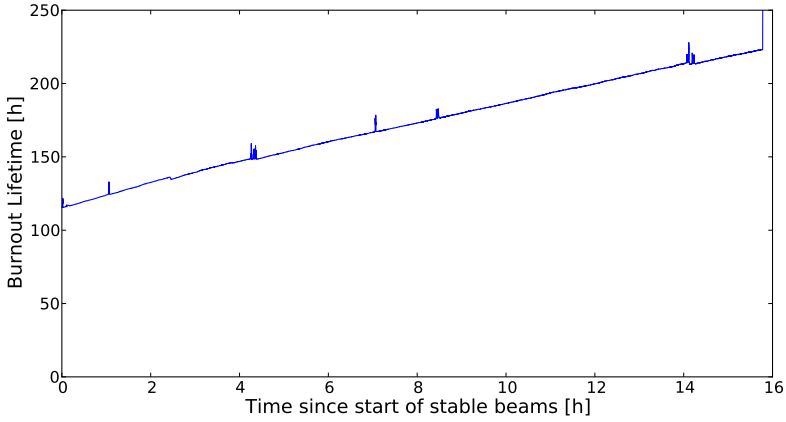

Figure 7.6: The burnout lifetime during stable beams in fill 2219, on 16. of October 2011. We have used the average intensity for beam 1/2.

Ideally we should then have a tool ready which takes data from all functioning gauges, interpolates the pressure and converts it to molecular densities using knowledge of the vacuum and cryogenic system. Since this is not available (we only have it for the long straight sections currently), the latest available simulated pressure profile can be used instead. Some simplified modifications taking into account that the dynamic pressure scales approximately linearly with the beam intensity can be added.

The elastic beam-gas scattering part that does not produce particle losses still contribute to the emittance growth of the beam. We looked at the estimated emittance growth from our simulations of beam-gas scattering by looking at the emittance before and after the simulation through 100 turns and then rescaled to real parameters, and found that it was insignificant for the total emittance growth, on the order of 0.01 μradm.

7.5.3 Total Beam Lifetime

The total beam lifetime is easiest to calculate from the beam intensities. The relative change in beam intensity equals the lifetime of the beam

$$\frac{1}{\tau_{tot}} = -\frac{1}{I}\frac{dI}{dt}. \tag{7.3}$$

The beam lifetime can be calculated for the entire beam using the DC current monitor, or per bunch using the fast beam current transformers. The latter case is particularly interesting when you want to look at instabilities due to e.g. filling pattern or collision pattern [99].

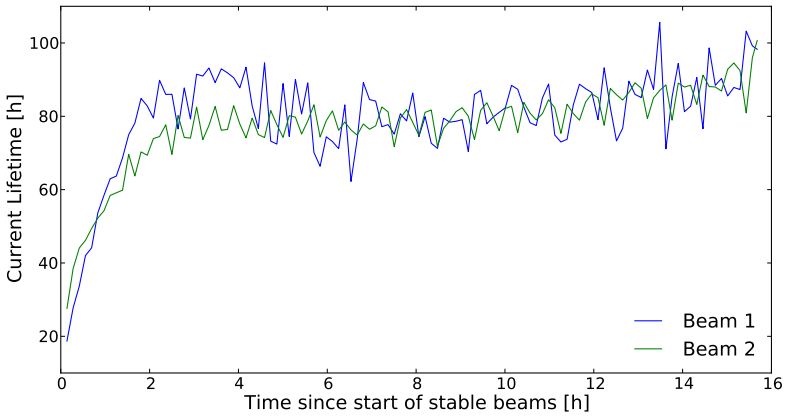

Figure 7.7: The beam intensity lifetime during fill 2219. Beam 1 in blue and beam 2 in green.

The beam intensity lifetime directly gives the amount of lost particles, and is perhaps the most relevant lifetime measurement for background considerations. Since this includes e.g. collision losses, it cannot be directly translated to background.

7.5.4 Luminosity Lifetime

What in the end matters in terms of performance is the luminosity lifetime. If the beam lifetime is good, but the emittance lifetime is low, that still affects the luminosity. The luminosity lifetime is simply the inverse of the luminosity derivative

$$\frac{1}{\tau_{\text{lumi}}} = -\frac{1}{\mathscr{L}} \frac{\mathrm{d}\mathscr{L}}{\mathrm{dt}}. \tag{7.4}$$

If we then assume that only the emittance and the beam intensities change, and round beams, we get

$$\frac{1}{\tau_{\text{lumi}}} = -\frac{\varepsilon}{I_1\, I_2}\frac{d\frac{I_1\, I_2}{\varepsilon}}{dt} = 2\frac{1}{\tau_{\text{tot}}} + \frac{1}{\varepsilon}\frac{d\varepsilon}{dt}. \tag{7.5}$$

The last part in Eq. (7.5) is the inverse of the emittance lifetime. In Figure 7.8 we show the luminosity lifetime for ATLAS and CMS. Since the luminosity in ALICE and LHCb was levelled by means of transverse separation, the luminosity lifetime does not make much sense for these experiments.

At the beginning of the fill we have an estimated beam lifetime of about $20-30$ h, and a luminosity lifetime of around 10 h. At the end of the fill we have a beam lifetime of about $80-90$ h, and a luminosity lifetime of around $20-25$ h, indicating a shorter emittance lifetime at the end of the fill. The beam lifetime is increasing faster in the beginning of the fill, which indicate a minimum emittance lifetime around $2-3$ h after stable beams was declared.

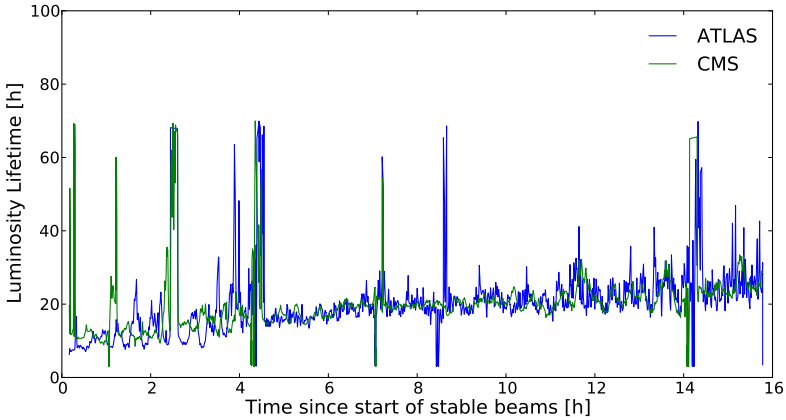

Figure 7.8: The luminosity lifetime during stable beams for fill 2219. We here show ATLAS in blue and CMS in green. Integrated for 10 minutes per point to reduce noise.

7.5.5 Specific Luminosity

In Figures 7.6, 7.7, 7.8 we showed the lifetime directly, which involves time derivatives of measured data. With noisy signals, this can be problematic to do in an automated fashion, because you easily get fluctuations as seen in Figure 7.8. The luminosity is proportional to the product of the beam intensity of the two beams. If we divide the luminosity by the beam intensity, we are left with something that should be constant if the luminosity is dominated by particle losses rather than emittance growth. We call this the specific luminosity

$$\mathscr{L}_{\text{specific}} = \frac{\mathscr{L}}{\mathrm{I}_1\,\mathrm{I}_2} \propto \frac{1}{\sqrt{\sigma_x\,\sigma_y}}. \tag{7.6}$$

In Figure 7.9 we show the specific luminosity for each colliding bunch pair for ATLAS and CMS for fill 2219. We see a similar shape for both experiment, which is expected since the colliding bunch pairs in ATLAS and CMS are the same. Specific luminosity is easier to deal with in automated scripts, and we publish the specific luminosity for each fill on the web page [35]

7.6 Outlook

Up until the end of this thesis work, the beam energy and intensity has been rather low, with the following low background rates in absolute terms. This makes measurements of observables more difficult. Comparing our published results in Appendix D.2 to the LHCb publications from one year later [43], this becomes obvious. The main difference between the two studies is the higher rates available in the latter, and the agreement between simulations and observations increases dramatically.

Still, a lot can be learned indirectly of machine induced background by continuously monitoring essential beam parameters. One of our largest error margins for the background simulations are the estimates for pressure distributions. The best one can typically hope for is about a factor two, and it does not take a lot of wrong assumptions or bad gauges before one is off by an order of magnitude. Having data available as shown in Figure 7.5 available for every fill, will help to at least be more aware of relative changes in the pressure distribution. Further, monitoring the different lifetimes continuously will help to quicker understand the origin of a potential background increase. If you know which processes are dominating the overall beam lifetime, you know which processes could produce background to the experiments as well.

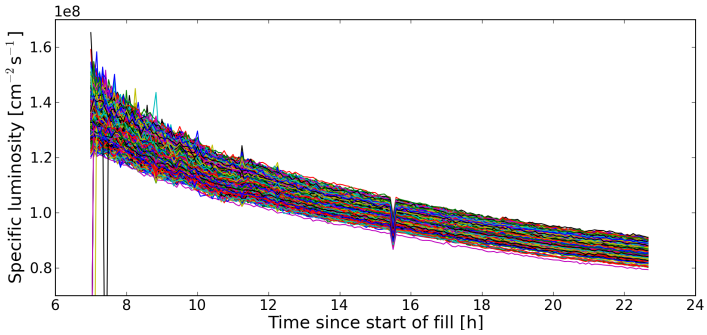

(a) ATLAS

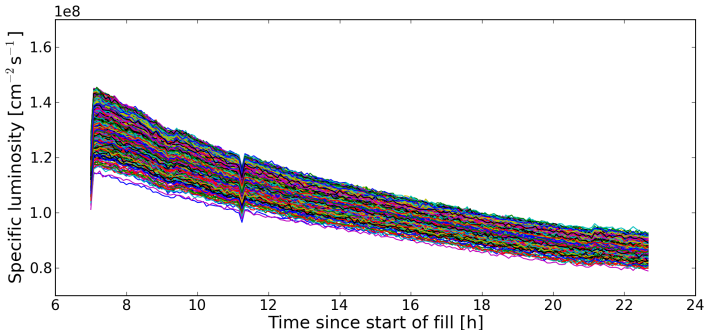

(b) CMS

Figure 7.9: Specific luminosity during stable beams for fill 2219, separately for each colliding bunch pair.

Chapter 8

Summary and Outlook

In this work a detailed assessment of all machine induced background sources has been made for all experiments in the LHC for the first time. We have had a special focus on beam-gas background, which is expected to be the most significant background source in the LHC. Interaction region cross talk has also been studied, and comparisons to tertiary halo background studies have been made. We have presented in detail how the simulations are set up, and gone through the expected rates for the nominal machine parameters for all contributions. We have discussed how the various input parameters affect the results, how the background might affect the experiments and how the different experiments measure the background.

In Appendix D.2 and D.3 similar studies for 3.5 TeV beam energy and lower beam intensities have been presented. The estimated rates from these studies are low, and hard to verify experimentally. The measured background rates by the experiments in the same period were similarly low [59]. There were no indications thus far that the order of magnitude of our estimates is wrong, something which would indicate that an important background source is forgotten.

As a second part of the work, an analysis tool was developed which is used for regular analysis of the machine conditions and performance. The project already has many users, and provide a fundament which can easily be extended for more advanced analysis in the future. In order to understand the background in the experiments, it is important to have a good handle on central machine parameters such as lifetimes and vacuum distributions.

Throughout this work it has become clear that beam-gas background is and will continue to be of particular importance. Allthough the initial rates of halo background is comparable, the amount of background arriving at the experimental cavern is found

to be far less for halo background. In general the expected background rates during nominal machine running conditions are on the order of 1 MHz.

For an optimal understanding of background, it is important to continuously monitor the vacuum pressure conditions in the long straight sections surrounding each experiment. We have already seen several examples where observed changes in background levels in an experiment have been closely correlated to changes on one or several vacuum gauges nearby. Dynamic effects in the LSS from e.g. multipacting, heating by higher-order modes or local deformities, can in unfavourable situations completely dominate the machine induced background. We have in our work demonstrated how the fill analysis tool can be used to effectively obtain such information on a regular basis.

Interaction region cross-talk was expected to be of lesser importance, though it could potentially become important for the low luminosity experiments LHCb and ALICE. We have looked at this source of background in detail both in simulations and during the luminosity calibration scans. The simulations show that the rate of this background component is expected to stay at least 4 orders of magnitude below the collision rate in ATLAS/CMS. We have thus far not seen measurable levels of IR cross-talk background, which is in agreement with our simulations. It is unlikely that IR cross-talk will become a problem for LHCb. IR cross-talk can become a measureable background for ALICE at nominal running conditions, but it is unlikely that it will be the dominant background source.

During the initial commissioning and first year of running, the dynamic effects to the vacuum pressure stayed low, and the estimated machine induced background rate typically stayed below 1% of maximum luminosity during proton physics, and somewhat higher during ion physics running. As the beam intensity increased and dynamic effects started to appear, the picture started to change. The main changes in the observed halo background can be categorised by two parameters, the filling pattern and onset of dynamic vacuum pressure [59].

The full simulation chain is presented in Appendix D.4. It would be beneficial to improve the simulation and analysis suite to go faster through the various simulation stages. One would then be able to compare expected simulated rates to the more current running conditions. At the moment the simulations are at a fairly advanced level, but are done in several steps that must be set up individually. As a result, once the final simulations of the expected detector response is available, the machine parameters have usually changed significantly. The machine parameters will change less frequently as we move from a commissioning phase towards stable physics production, and this will then become less of a problem. In order to keep the simulations relevant for the discussions and more useful for the understanding of current running conditions, the author sees a clear advantage in a faster simulation chain.

In Appendix D.2 we have made a first attempt at comparing the full simulation chain to measured rates, and underestimate the final rate by about one order of magnitude. In [43], LHCb found that simulated and measured background agreed within a fact of 1.6, using a dedicated fill without collisions and with higher rates. Based on these findings, we feel we are now in a position where we can estimate the background to within a factor 5 under normal circumstaces.

When background levels differ significantly from expectations, and/or unexpected asymmetries in the background levels are observed, it can often be a first warning that there are problems in the machine. By analysing our simulations at nominal machine settings, as have been extensively presented in the thesis, we do not currently see any alarming background contributions relative to the nominal luminosity. It is our understanding that beam-gas background will be the most significant background source at nominal machine energy and intensity. It should be kept in mind that in particular dynamic pressure can be hard to predict, and deviations from the simulated vacuum pressure can occur.

Bibliography

[1] L. Evans. The Large Hadron Collider. *Phil.Trans.Roy.Soc.Lond.*, A370:831–858, 2012.

[2] CERN. *LHC Workshop on Experimental Conditions and Beam-Induced Detectors Backgrounds*, Geneva, 2009. CERN.

[3] R Tesarek. Beam-Induced Backgrounds: CDF Experience. In *LHC Workshop on Experimental Conditions and Beam-Induced Detectors Backgrounds*, 2009.

[4] J M Butler, D S Denisov, H T Diehl, A I Drozhdin, N V Mokhov, and D R Wood. Reduction of Tevatron and main ring induced backgrounds in the D0 detector. Technical Report FERMILAB-FN-629, FERMILAB, Batavia, IL, May 1995.

[5] OE Krivosheev and NV Mokhov. CDF forward shielding for Run II. *Fermilab-TM-2045*, 1998.

[6] M Church, A I Drozhdin, A Legan, N V Mokhov, and R Reilly. Tevatron Run-II Beam Collimation System. In *Particle Accelerator Conference*, number FERMILAB-CONF-99-059, 1999.

[7] C. Niebuhr. Background at HERA: Perspective of the Experiments. In *LHC Workshop on Experimental Conditions and Beam-Induced Detectors Backgrounds*, 2009.

[8] G. Barbagli et al. Study of beam-induced backgrounds in the ZEUS detector from 2002 HERA running . http://www-zeus.desy.de/ kuze/zeus-bg/zeusbg020926.pdf, 2002.

[9] Stephen Holmes, Ronald S. Moore, and Vladimir Shiltsev. Overview of the Tevatron Collider Complex: Goals, Operations and Performance, July 2011.

[10] The ATLAS Collaboration. The ATLAS Experiment at the CERN Large Hadron Collider. *J. Instrum.*, 3:S08003. 437 p, 2008. Also published by CERN Geneva in 2010.

[11] The ATLAS Collaboration. *ATLAS detector and physics performance: Technical Design Report*, volume 1 of *Technical Design Report ATLAS*. CERN, Geneva, 1999. technical design.

[12] The ALICE Collaboration. The ALICE experiment at the CERN LHC. *J. Instrum.*, 3:S08002, 2008. Also published by CERN Geneva in 2010.

[13] The CMS Collaboration. The CMS experiment at the CERN LHC. *J. Instrum.*, 0803(S08004):S08004, 2008. Also published by CERN Geneva in 2010.

[14] A. Augusto Alves et al. The LHCb Detector at the LHC. *J. Instrum.*, 3:S08005, 2008.

[15] Chiara Bracco. *Commissioning Scenarios and Tests for the LHC Collimation system*. PhD thesis, EPFL, 2009.

[16] A. Rossi and N. Hilleret. Residual Gas Density Estimations in the LHC Experimental Interaction Regions. Technical Report LHC-Project-Report-674. CERN-LHC-Project-Report-674, CERN, Geneva, Sep 2003.

[17] R. B. Appleby, H. Burkhardt, G. Corti, Y. Inntjore Levinsen, M. H. Lieng, and V. V. Talanov. Simulation of Machine Induced Background in the LHCb Experiment: Methodology and Implementation. In *IEEE Nuclear Science Symposium, Medical Imaging Conference, and Room Temperature Semiconductor Detectors Workshop*, Dec 2010.

[18] Y. Inntjore Levinsen and H. Burkhardt. Fast simulation of loss maps from dust particles, LBS #17. `http://indico.cern.ch/conferenceDisplay.py?confId=103813`, Aug 2010.

[19] Y. Inntjore Levinsen and H. Burkhardt. Worst Case Scenario Simulation for TOTEM Runs. `http://lhc-mpwg.web.cern.ch/lhc-mpwg/`, Apr 2011.

[20] K. Wille. *The Physics of Particle Accelerators - an introduction*. Oxford University Press, 2005.

[21] S. Y. Lee. *Accelerator Physics*. World Scientific Publishing, 2. edition, 2004.

[22] A. W. Chao. *Handbook of Accelerator Physics and Engineering*. World Scientific Publishing Company, 1999.

[23] H. Wiedemann. *Particle Accelerator Physics*. Springer, 3. edition, 2007.

[24] E. D. Courant and H. S. Snyder. Theory of the alternating-gradient synchrotron. *Annals of Physics*, 3(1):1–48, 1958.

[25] Christina Yin Vallgren, Thomas Nilsson, and Mauro Taborelli. *Low Secondary Electron Yield Carbon Coatings for Electron Cloud Mitigation in Modern Particle Accelerators*. PhD thesis, Goteborg, Chalmers U. Tech., Goteborg, 2011.

[26] R. Bruce, J. M. Jowett, S. Gilardoni, and E. Wallen. *Beam loss mechanisms in relativistic heavy-ion colliders*. PhD thesis, Lund University, Lund, 2009.

[27] R. Bruce, J. M. Jowett, M. Blaskiewicz, and W. Fischer. Time evolution of the luminosity of colliding heavy-ion beams in BNL Relativistic Heavy Ion Collider and CERN Large Hadron Collider. *Phys. Rev. ST Accel. Beams*, 2010.

[28] O. S. Brüning, Paul Collier, P Lebrun, Stephen Myers, Ranko Ostojic, J. Poole, Paul Proudlock, et al. *LHC Design Report*, volume 1. CERN, Geneva, 2004.

[29] T. Pieloni, W. Herr, A. Bay, and L. Rivkin. *A Study of Beam-Beam Effects in Hadron Colliders with a Large Number of Bunches.* PhD thesis, EPFL, Lausanne -CH-, 2008. Presented Aug 2008.

[30] G. Robert-Démolaize. *Design and Performance Optimization of the LHC Collimation System.* PhD thesis, Grenoble 1, Grenoble, 2006. Presented on 20 Nov 2006.

[31] J. B. Jeanneret and T. Risselada. Geometrical Aperture in LHC at Injection. Technical Report LHC-Project-Note-66, CERN, Geneva, Sep 1996.

[32] J. B. Jeanneret and R. Ostokic. Geometrical Acceptance in LHC Version 5.0. Technical Report LHC-PROJECT-NOTE-111, CERN, 1997.

[33] Yi-Peng Sun, Ralph Assmann, Javier Barranco, Rogelio Tomás, Thomas Weiler, Frank Zimmermann, Rama Calaga, and Akio Morita. Beam dynamics aspects of crab cavities in the CERN Large Hadron Collider. *Phys. Rev. ST Accel. Beams*, 12(10):101002, Oct 2009.

[34] Simon Mathieu White, H. Burkhardt, and P. Puzo. *Determination of the Absolute Luminosity at the LHC.* PhD thesis, Orsay, Université Paris-Sud 11, Orsay, 2010. Presented on 11 Oct 2010.

[35] CERN LHC Statistics Pages. http://cern.ch/LHC-Statistics.

[36] LHC Web Site. http://cern.ch/lhc.

[37] J Jowett, P Baudrenghien, R Bruce, C Carli, D Manglunki, T Mertens, and D Wollmann. Heavy Ions in 2011 and beyond. In *LHC Chamonix Workshop*, pages 254–263, 2011.

[38] E. Cuautle and G. Paic. Rejection of beam gas interaction in pp collisions and timing requirements. Technical Report ALICE-INT-2004-021, CERN, 2004.

[39] ALICE Background, LBS #29. http://indico.cern.ch/conferenceDisplay.py?confId=135223, Oct 2011.

[40] G. Corti. Beam Gas Studies in LHCb, LBS #24. http://indico.cern.ch/conferenceDisplay.py?confId=109986, Oct 2010.

[41] Ch. Ilgner, M. Domke M. Lieng, M. Nedos, J. Sauerbrey, S. Schleich, B. Spaan, K. Warda, and J. Wishahi. The Beam Conditions Monitor of the LHCb Experiment, January 2010.

[42] V. Talanov, R. Dzhelyadin, A. Bobrov, A. Bondar, F. Alessio, G. Corti, R. Jacobsson, and M. H. Lieng. A Beam Loss Scintillator System for Background Monitoring at the LHCb Experiment. In *Proceedings of RuPAC*, 2010.

[43] D R Brett, R B Appleby, G Corti, F Alessio, R Jacobsson, V Talanov, and M H Lieng. Near beam-gas background for LHCb at 3.5 TeV. In *IPAC'11 San Sebastien, Spain*, Sep 2011. Poster-2011-195.

[44] CERN Press Photos. http://cdsweb.cern.ch/collection/Press Office Photo Selection.

[45] R Bruce, RW Assmann, W Herr, and D Wollmann. Calculation method for safe β^* in the LHC. Technical Report CERN-ATS-2011-140, CERN, Geneva, Sep 2011.

[46] O. Gröbner. Overview of the LHC vacuum system. *Vacuum*, 60(1-2):25–34, 2001.

[47] R. B. Appleby, Y. Inntjore Levinsen, and H. Burkhardt. Beam-Gas Simulations for 2009 LHC Running and First Comparisons with Data. Technical Report LHC-Project-Note-429, CERN, Geneva, Feb 2010.

[48] R. B. Appleby and Y. Inntjore Levinsen. Composition of ALICE machine induced background at nominal beam energy. Technical report, CERN, Jul 2010.

[49] A. Rossi. Estimates of Residual Gas Density in the LHC. In *LHC Workshop on Experimental Conditions and Beam-Induced Detectors Backgrounds*, 2009.

[50] A. Rossi. Private Communication.

[51] D. Griffiths. *Introduction to Elementary Particles*. Wiley, 2. edition, 2009.

[52] S. Navin. Diffraction in Pythia, May 2010.

[53] A. Capella, U. Sukhatme, C. I. Tan, and J. Tran Thanh Van. Dual Parton Model. *Physics Reports*, 236(4-5):225–329, 1994.

[54] M. Deile and The TOTEM Collaboration. Diffraction and Total Cross-Section at the Tevatron and the LHC, February 2006.

[55] V. A. Petrov, E. Predazzi, and A. Prokudin. Coulomb interference in high-energy pp and pbar-p scattering. *The European Physical Journal C - Particles and Fields*, 28:525–533, 2003. 10.1140/epjc/s2003-01191-7.

[56] A. I. Drozhdin and N. V. Mokhov. Modeling of Beam Loss in Tevatron and Backgrounds in the BTeV Detector. In *EPAC'04*, page 3 p, 2004.

[57] M Lamont. Estimates of Annual Proton Doses in the LHC. Technical Report LHC-Project-Note-375, CERN, Geneva, Jun 2005.

[58] E Bravin et al. Collision Rate Monitors for LHC. (LHC-PROJECT-Report-1024):4 p, 2007.

[59] The ATLAS Collaboration. Non-collision backgrounds as measured by the ATLAS detector during the 2010 proton-proton run. Technical Report ATLAS-CONF-2011-137, CERN, Geneva, Sep 2011.

[60] R. W. Assmann. Beam Cleaning and Collimation: Too Bad or Too Good? In *Chamonix Workshop on LHC Performance*, 2011.

[61] G. Corti, M. H. Lieng, and V. V. Talanov. Summary of pre-2008 Machine Induced Background Estimates for the LHCb Experiment. Technical Report LHCb-PUB-2010-001. CERN-LHCb-PUB-2010-001, CERN, Geneva, Mar 2010.

[62] N. V. Mokhov and T. Weiler. Machine-Inudced Backgrounds: Their Origin and Loads on ATLAS/CMS. In *FERMILAB-CONF-08-147-APC*, 2008.

[63] A. Rossi. Residual Gas Density Estimations in the LHC Insertion Regions IR1 and IR5 and the Experimental Regions of ATLAS and CMS for Different Beam Operations. Technical Report LHC-Project-Report-783, CERN, Geneva, Sep 2004.

[64] G. Bregliozzi. Private Communication.

[65] Plamen Hopchev. LHCb beam-gas imaging results. In *LHC Workshop on LHC Luminosity Calibration*, 2011.

[66] FLUKA. `http://www.fluka.org`.

[67] N. V. Mokhov. *The MARS Code System User's Guide, Version 13 (95)*, 1995.

[68] BDSIM. `https://www.pp.rhul.ac.uk/twiki/bin/view/JAI/BdSim`.

[69] R. Bruce et al. Machine-induced showers entering the ATLAS and CMS detectors in the LHC. In *IPAC'11 San Sebastien, Spain*, 2011.

[70] G Ripken and F Schmidt. A symplectic six-dimensional thin-lens formalism for tracking. Technical Report CERN-SL-95-12. CERN-SL-95-12-AP. DESY-95-063, CERN, Geneva, Apr 1995.

[71] G. Robert-Démolaize, R. W. Assmann, S. Redaelli, and F. Schmidt. A New Version of Sixtrack with Collimation and Aperture Interface. In *Particle Accelerator Conference, 2005*, pages 4084–4086, May 2005.

[72] T Trenkler and J. B. Jeanneret. K2, A software package evaluating collimation systems in circular colliders (manual). Technical Report SL-Note-94-105-AP, CERN, Geneva, Dec 1994.

[73] H Grote, F. Schmidt, and L. H. A. Leunissen. LHC Dynamic Aperture at Collision. Technical Report LHC-PROJECT-NOTE-197, CERN, Geneva, Aug 1999.

[74] Y Luo and F Schmidt. Dynamic Aperture Studies for LHC Optics Version 6.2 at Collision. Technical Report LHC-PROJECT-NOTE-310, CERN, Geneva, Jan 2003.

[75] O. Sim Brüning, S. D. Fartoukh, M. Giovannozzi, and T. Risselada. Dynamic Aperture Studies for the LHC Separation Dipoles. Technical Report LHC-Project-Note-349, CERN, Geneva, Jun 2004.

[76] N. V. Mokhov, A. I. Drozhdin, and S. I. Striganov. Beam Losses and Background Loads on Collider Detectors Due to Beam-Gas Interactions in the LHC. In *PAC Vancouver*, number WE6PFP027, 2009. Presented at Particle Accelerator Conference (PAC 09), Vancouver, BC, Canada, 4-8 May 2009.

[77] Y. Inntjore Levinsen, H. Burkhardt, and V. V. Talanov. Simulation of Beam-Gas Scattering in the LHC. In *PAC Vancouver*, May 2009.

[78] F. Cerutti, B. Dehning, A. Ferrari, C. Hoa, M. Mauri, A. Mereghetti, M. Sapinski, and E. Wildner. Estimation of Threshold for the Signals of the BLMs around the LHC Final Focus Triplet Magnets. Jan 2012.

[79] D. Wollmann et al. First cleaning with LHC collimators. In *IPAC'10 Kyoto*, number CERN-ATS-2010-097, Jun 2010.

[80] R. W. Assmann et al. Paper in preparation. 2013.

[81] Y. Inntjore Levinsen, S. M. White, and H. Burkhardt. Dependence of Background Rates on Beam Separation in the LHC. In *IPAC10 Kyoto*, 2010.

[82] S. M. White, R. Alemany-Fernandez, H. Burkhardt, and M. Lamont. First Luminosity Scans in the LHC. In *IPAC Kyoto*, 2010.

[83] M. Sapinski. Private Communication.

[84] S. H. Strogatz. *Nonlinear Dynamics and Chaos*. Westview, 1994.

[85] T. Weiler et al. Beam Loss Response Measurements with a LHC Prototype Collimator in the SPS. Technical Report CERN-AB-2007-040, CERN, Geneva, Aug 2007.

[86] *The final collimation system for the LHC.*, number LHC-PROJECT-Report-919., Jul 2006. revised version submitted on 2006-09-15.

[87] N. V. Mokhov and S. I. Striganov. MARS15 Overview. Technical Report Fermilab-Conf-08-147-APC, Fermilab, 2007.

[88] R. B. Appleby and A Mereghetti. The FLUKA Model of IR8. Technical Report LHC-Project-Note-427, CERN, Geneva, Feb 2010.

[89] C Roderick and R Billen. The LSA Database to Drive the Accelerator Settings. Technical Report CERN-ATS-2009-100, CERN, Geneva, Nov 2009.

[90] HDF5 File Format. `http://www.hdfgroup.org/HDF5/`.

[91] ROOT Analysis Framework. http://cern.ch/ROOT/.

[92] T. B. Bolshakov et al. SDA-Based Diagnostic and Analysis Tools for Collider Run II. In *PAC'05*, pages 1099–1101, May 2005.

[93] Y. Inntjore Levinsen, H. Burkhardt, A. Macpherson, M. Terro Pinheiro, and S. Roe. Fill Analysis and Experimental Background Observations in the LHC. In *IPAC'11 San Sebastien, Spain*, Sep 2011.

[94] G. Rumolo et al. Electron Cloud Observation in the LHC. In *IPAC'11 San Sebastien, Spain*, Geneva, Sep 2011.

[95] Background Observations in Operation by ALICE, LBS #24. http://indico.cern.ch/conferenceDisplay.py?confId=135218, May 2011.

[96] LBS #28. http://indico.cern.ch/conferenceDisplay.py?confId=135222, Sep 2011.

[97] Pressure maps in the LSS, LBS #23. http://indico.cern.ch/conferenceDisplay.py?confId=135217, Apr 2011.

[98] The TOTEM Collaboration. First measurement of the total proton-proton cross section at the LHC energy of $\sqrt{s}$ = 7 TeV. *EPL (Europhysics Letters)*, 96(2), Oct 2011. Comments: 11 pages 5 figures CERN PH Preprint.

[99] W Herr, R Calaga, E Laface, G Papotti, and T Pieloni. Observations of beam-beam effects at high intensities in the LHC. In *IPAC'11 San Sebastien, Spain*, Geneva, Sep 2011.

[100] CollTrack User Manual. http://cern.ch/lhc-collimation-project/code-tracking-2009.htm.

[101] F. Schmidt. SixTrack User's Reference Manual. http://cern.ch/SixTrack/Documentation/doc.html, Apr 2011.

[102] BeamLossPattern and CleanInelastic Documentation. http://cern.ch/lhc-collimation-project/BeamLossPattern.htm.

[103] Y. Inntjore Levinsen, R. B. Appleby, and H. Burkhardt. Beam-gas Loss Rates in the LHC. In *IPAC10 Kyoto*, 2010.

[104] F. Schmidt. Mad-X PTC Integration. pages 1272–1274, May 2005.

Appendix A

Linear Equations of Motion

The linear equations of motions form the basis of accelerator optics, and are derived from the Lorentz equation (3.1) which we can write as

$$m\ddot{\mathbf{r}} = e\dot{\mathbf{r}} \times \mathbf{B}. \tag{A.1}$$

We define the position of the particle as

$$\mathbf{r} = \mathbf{r}_0 + \mathbf{x} + \mathbf{y},$$

where the dot is the Newton notation for time derivative.

Hence we need to find the single and double derivative of $\mathbf{r}$ with respect to time. If we denote unit vector like $\hat{\mathbf{x}}$, then we have the time derivative of a vector as

$$\dot{\mathbf{x}} \;=\; \dot{x}\hat{\mathbf{x}} \;+\; x\frac{\mathrm{d}\hat{\mathbf{x}}}{\mathrm{d}t}.$$

Because the unit vectors in the Frenet–Serret coordinate system changes with time, we need to find the derivative of the unit vectors as well. We have a horizontal rotation only for simplicity, so the time derivative of $\hat{\mathbf{y}}$ is zero. Let us consider a small movement along the orbit from position $\mathbf{r^1}$ to position $\mathbf{r^2}$ for a constant vector (x,z) as demonstrated in Figure A.1.

From a geometrical consideration, we have the new coordinates x,z is given from the relation

$$\begin{pmatrix} x_2 \\ z_2 \end{pmatrix} = \begin{bmatrix} \cos\varphi & \sin\varphi \\ -\sin\varphi & \cos\varphi \end{bmatrix} \times \begin{pmatrix} x_1 \\ z_1 \end{pmatrix}. \tag{A.2}$$

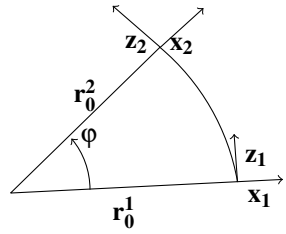

Figure A.1: A delta movement of a particle along an orbit between two points for a rotation with a radius of curvature r_0.

The path length s that the particle has travelled is given by

$$s = \varphi r_0,$$

and since movement is along the radius of curvature, we have the time derivative

$$\dot{s} = \dot{\varphi} \cdot r_0. \tag{A.3}$$

We then get the time derivative for x and z

$$\begin{aligned} \frac{\mathrm{d}}{\mathrm{d}t}\begin{pmatrix} x \\ z \end{pmatrix} &= \dot{\varphi} \times \frac{\mathrm{d}}{\mathrm{d}\varphi}\begin{bmatrix} \cos\varphi & \sin\varphi \\ -\sin\varphi & \cos\varphi \end{bmatrix}\begin{pmatrix} x \\ z \end{pmatrix} \\ &= \frac{1}{r_0}\dot{s}\begin{bmatrix} -\sin\varphi & \cos\varphi \\ -\cos\varphi & -\sin\varphi \end{bmatrix}\begin{pmatrix} x \\ z \end{pmatrix} \\ &= \frac{1}{r_0}\dot{s}\begin{pmatrix} z \\ -x \end{pmatrix}. \end{aligned} \tag{A.4}$$

Doing the same procedure again we get the double derivative

$$\frac{\mathrm{d}^2}{\mathrm{d}t^2}\begin{pmatrix} x \\ z \end{pmatrix} = \frac{1}{r_0}\left[\ddot{s}\begin{pmatrix} z \\ -x \end{pmatrix} - \frac{\dot{s}^2}{r_0}\begin{pmatrix} x \\ z \end{pmatrix}\right] \approx -\frac{\dot{s}^2}{r_0^2}\begin{pmatrix} x \\ z \end{pmatrix}. \tag{A.5}$$

We now have a function for the time derivative of a constant vector in the rotating frame which depends on the position and velocity $\dot{s}$ of the movement. The last approximation in Eq. (A.5) is that the acceleration of the beam $\ddot{s}$ is slow compared to the movement of the particle.

If we expand the derivatives of $\mathbf{r}$ then we get

$$\begin{aligned}\dot{\mathbf{r}} &= \dot{x}\hat{\mathbf{x}} + x\dot{\hat{x}} + \dot{y}\hat{\mathbf{y}} + \dot{r}_0 \\ \ddot{\mathbf{r}} &= \ddot{x}\hat{\mathbf{x}} + 2\dot{x}\dot{\hat{x}} + x\ddot{\hat{x}} + \ddot{y}\hat{\mathbf{y}} + \ddot{r}_0\end{aligned} \tag{A.6}$$

As mentioned, the unit vector in the vertical direction, $\hat{\mathbf{y}}$, is zero as long as we have a pure horizontal rotation. We then insert from Eq. (A.4) and Eq. (A.5) the derivatives of $\hat{\mathbf{x}}$, which are

$$\begin{aligned}\dot{\hat{x}} &= \frac{\dot{s}}{r_0} \\ \ddot{\hat{x}} &= -\frac{\dot{s}^2}{r_0^2}\hat{\mathbf{x}}\end{aligned} \tag{A.7}$$

Inserting Eq. (A.6) and Eq. (A.7) into the Lorentz equation, we obtain

$$\ddot{x}\hat{\mathbf{x}} + 2\frac{\dot{x}\dot{s}}{r_0} - \frac{x\dot{s}^2}{r_0} + \ddot{y}\hat{\mathbf{y}} + \ddot{\mathbf{r}}_{\mathbf{0}} = \frac{e}{m}(\dot{x}\hat{\mathbf{x}} + \frac{x\dot{s}}{r_0}\hat{\mathbf{z}} + \dot{y}\hat{\mathbf{y}} + \dot{\mathbf{r}}_{\mathbf{0}}) \times \mathbf{B}. \tag{A.8}$$

Looking at Figure A.1, we note that the differential vector $\mathrm{d}\mathbf{r}_0$ is equal to the orbit distance $\mathrm{d}s$ multiplied by the vector $\hat{\mathbf{z}}$. Hence

$$\begin{aligned}\dot{\mathbf{r}}_{\mathbf{0}} &= \dot{s}\hat{\mathbf{z}} \\ \ddot{\mathbf{r}}_{\mathbf{0}} &= \dot{s}\dot{\hat{z}} + \ddot{s}\hat{\mathbf{z}} \approx \dot{s}\dot{\hat{z}} = -\dot{s}\frac{\dot{s}}{r_0}\hat{\mathbf{x}}.\end{aligned} \tag{A.9}$$

The approximation made for the double derivative is again that the beam acceleration is slow. Inserting these results into Eq. (A.8) and reorganising in matrix form, we obtain

$$\begin{pmatrix} \ddot{x} - \dot{s}^2(\frac{x}{r_0^2} - \frac{1}{r_0}) \\ \ddot{y} \\ 2\frac{\dot{x}\dot{s}}{r_0} \end{pmatrix} = \frac{e}{m}\begin{pmatrix} \dot{x} \\ \dot{y} \\ (\frac{x}{r_0} + 1)\dot{s} \end{pmatrix} \times \begin{pmatrix} b_x \\ b_y \\ b_z \end{pmatrix} \tag{A.10}$$

The normal accelerator magnets have a field which is transverse to the particle trajectory, in order to deflect and focus the particles. Hence, we can assume that

$$\dot{s}b_y >> \dot{y}b_z, \dot{s}b_x >> \dot{x}b_z. \tag{A.11}$$

While it is always true that the transverse velocity is always much smaller than the longitudinal, it is not automatically true that the longitudinal magnetic field is smaller

than (or equal to) the transverse field. Hence one could have situations where the longitudinal field is much larger than the transverse field (e.g. a solenoid), and this approximation breaks down.

If we consider the velocity of a particle with a position x along the unit vector $\hat{\mathbf{x}}$, we note that its' velocity is not simply $\dot{s}$, but instead $\frac{x+r_0}{r_0}\dot{s}$, since the radius of curvature of its trajectory is $x+r_0$. We now end up with three equations by inserting the approximation into Eq. (A.10), namely

$$\begin{aligned} \ddot{x} - \frac{\dot{s}^2}{r_0}(1+\frac{x}{r_0}) &= -\frac{e}{m}vb_y \\ \ddot{y} &= -\frac{e}{m}vb_x \\ 2\frac{\dot{x}\dot{s}}{r_0} &= \frac{e}{m}(\dot{x}b_y - \dot{y}b_x). \end{aligned} \tag{A.12}$$

We can rewrite the time derivative of x (and y)

$$\frac{\mathrm{d}x}{\mathrm{d}t} = \frac{\mathrm{d}x}{\mathrm{d}s}\frac{\mathrm{d}s}{\mathrm{d}t} \equiv x'\dot{s} \tag{A.13}$$

$$\frac{\mathrm{d}^2x}{\mathrm{d}t^2} = \frac{\mathrm{d}x'\dot{s}}{\mathrm{d}t} = \dot{x}'\dot{s} + x'\ddot{s} \approx \dot{x}'\dot{s} = x''\dot{s}^2, \tag{A.14}$$

where we again for the double derivative used the assumption that the acceleration is slow. The first equation of Eq. (A.12) can then be rewritten as

$$(x'' - (1+\frac{x}{r_0}))\dot{s}^2 = -\frac{e}{m}vb_y \tag{A.15}$$

$$x'' - (1+\frac{x}{r_0} = -\frac{e}{m}\frac{v}{\dot{s}^2}b_y = \frac{e}{mv}(1+\frac{x}{r_0})^2 b_y, \tag{A.16}$$

and for the second equation we get

$$y'' = -\frac{e}{m}\frac{v}{\dot{s}^2}b_x = -\frac{e}{mv}(1+\frac{x}{r_0})^2 b_x. \tag{A.17}$$

mv we recognise as the momentum of the particle, which we can write as $p = p_0 + \Delta p$, where p_0 is the reference momentum of a particle perfectly on orbit. The fractional

$$\frac{1}{1+x}$$

can be expanded as

$$\frac{1}{1+x} = 1 - x + x^2 - x^3 + \ldots,$$

which means we can write

$$\frac{1}{p} = \frac{1}{p_0 + \Delta p} = \frac{1}{p_0}\frac{1}{1+\frac{\Delta p}{p_0}} = \frac{1}{p_0}(1 - \frac{\Delta p}{p_0} + (\frac{\Delta p}{p_0})^2 - \dots) \approx \frac{1}{p_0}(1 - \frac{\Delta p}{p_0}) \quad \text{(A.18)}$$

In the last approximation we assume that the difference in momentum inside the beam is small compared to the reference/nominal momentum, so that we can ignore higher order terms in $\frac{\Delta p}{p_0}$. The final approximation we make is that also $x \ll 1$ and $y \ll 1$, so that we can ignore any terms which is a multiplication of x,y, and/or $\frac{\Delta p}{p_0}$. Inserting this into Eq. (A.16) and Eq. (A.17), expanding the parentheses and reorganising, we end up with

$$\begin{aligned} x'' + (\frac{1}{r_0^2} - k)x &= \frac{1}{r_0}\frac{\Delta p}{p_0} \\ y'' + ky &= 0 \end{aligned} \quad \text{(A.19)}$$

Here we have inserted the magnetic field in the horizontal direction as a pure quadrupolar field,

$$\frac{eb_x}{p_0} = -ky,$$

and the vertical field as a sum of dipolar and quadrupolar field,

$$\frac{eb_y}{p_0} = \frac{1}{r_0} - kx.$$

We have used the optical functions $\frac{1}{r_0}$ and k for the strengths, as defined in Eq. (3.5). The sign convention chosen for k is that $k > 0$ means that the field is focusing, and $k < 0$ means the field is defocusing. Equation Eq. (A.19) is called the "Linear Equations of Motion", and forms the basis for accelerator beam optics.

Appendix B

Courant–Snyder Parametrization

The motion of a particle through an accelerator follows an oscillatory function about the closed orbit. This we see from the solution of the Hill's equation in Eq. (A.19), which has the general solution

$$y(s) = A(s) \cdot \cos(\mu(s)) \tag{B.1}$$

The amplitude A and phase μ are functions of the location s along the accelerator. Inserting Eq. (B.1) into Eq. (A.19), we get

$$\begin{aligned} A'' \cos(\mu(s)) - 2\,A'\,\mu' \sin(\mu(s)) - A\,\mu'' \sin(\mu(s)) \\ + A\,(\mu')^2 \cos(\mu(s)) - k\,A \cos(\mu(s)) = 0. \end{aligned} \tag{B.2}$$

Since μ varies along s, everything in front of sine and cosine must separately be equal to zero. We get the two equalities

$$\begin{aligned} A'' + A\mu'' - kA = 0 \\ 2A'\mu' + A\mu'' = 0. \end{aligned} \tag{B.3}$$

The second equality in Eq. (B.3) can be solved in the following way. First we reorganise

$$-2\frac{A'}{A} = \frac{\mu''}{\mu'} \tag{B.4}$$

We can now integrate on both sides, by using

$$\int \frac{f'(x)}{f(x)} = \ln(f(x)).$$

We get

$$-2\ln(A) + \ln(C) = \ln(\mu') \tag{B.5}$$

$$\frac{C}{A^2} = \mu', \tag{B.6}$$

where C is an integration factor. Integrating again we obtain

$$\mu(s) - \mu_0 = \int_{\sigma=s_0}^{s} \frac{C}{A^2} d\sigma \tag{B.7}$$

μ is denoted the phase, or phase advance between two points s_0 and s. We define $\sqrt{\varepsilon} \equiv C$, and β as the part of the amplitude that is varying along the orbit, such that $A(s) = \sqrt{\varepsilon \cdot \beta(s)}$. This gives us the following definition for the phase μ:

$$\mu(s) - \mu_0 = \int_{\sigma=s_0}^{s} \frac{1}{\beta(\sigma)} d\sigma \tag{B.8}$$

Inserting into Eq. (B.1) and deriving with respect to s, we get for the divergence

$$\begin{aligned} y'(s) &= \sqrt{\varepsilon}\left[\frac{\beta'(s)}{2\sqrt{\beta(s)}}\cos(\mu(s)) - \sqrt{\beta(s)}\mu'(s)\sin(\mu(s))\right] \\ &= -\sqrt{\varepsilon/\beta(s)}\left[\frac{\beta'(s)}{2}\cos(\mu(s)) + \sin(\mu(s))\right] \\ &\equiv -\sqrt{\varepsilon/\beta(s)}\left[\alpha(s)\cos(\mu(s)) + \sin(\mu(s))\right]. \end{aligned} \tag{B.9}$$

In the last equality we have defined

$$\alpha = -\frac{\beta'}{2}. \tag{B.10}$$

We now have the linear equations of motion defined as

$$y(s) = \sqrt{\varepsilon\beta(s)}\cos(\mu(s)) \tag{B.11}$$

$$y'(s) = -\sqrt{\varepsilon/\beta(s)}\left[\alpha(s)\cos(\mu(s)) + \sin(\mu(s))\right]. \tag{B.12}$$

ε is known as the emittance of the beam, and is an invariant. This can be sown by removing the dependency on the phase μ from Eqs. B.11, B.12. We start by getting $\cos(\mu(s))$ from Eq. (B.11). Inserting into Eq. (B.12) we get

$$y'(s) = -\sqrt{\varepsilon/\beta(s)}\left[\alpha(s)\frac{y(s)}{\sqrt{\varepsilon\beta(s)}} + \sin(\mu(s))\right]. \tag{B.13}$$

$$\sin(\mu(s)) = -\left[y'(s)\sqrt{\beta(s)/\varepsilon} + \alpha(s)\frac{y(s)}{\sqrt{\varepsilon\beta(s)}}\right]. \tag{B.14}$$

By using

$$\sin^2(x) + \cos^2(x) = 1,$$

we now have

$$\left[y'\sqrt{\beta/\varepsilon} + \alpha\frac{y}{\sqrt{\varepsilon\beta}}\right]^2 + \left[\frac{y}{\sqrt{\varepsilon\beta}}\right]^2 = 1, \tag{B.15}$$

$$\beta y'^2 + 2\alpha y' y + \frac{(1+\alpha^2)}{\beta}y^2 = \varepsilon. \tag{B.16}$$

Finally, we define

$$\gamma \equiv \frac{(1+\alpha^2)}{\beta},$$

and get

$$\gamma y^2 + 2\alpha y' y + \beta y'^2 = \varepsilon. \tag{B.17}$$

Eq. (B.17) is an elliptic function in y-y' space. This is known as Liouville's theorem, which states that a particle undergoing canonical transformations will not increase it's action. In other words, that the emittance is constant as the beam move through the accelerator. The emittance can change due to e.g. synchrotron radiation and the interaction between the particles in the beam, but Liouville's theorem is still a very important fundamental principle for accelerators. α, β, and γ are called the TWISS parameters, with their interpretation shown in Figure 3.4.

Appendix C

BeamGas Module in Sixtrack

In this appendix we will describe how the BeamGas module in SixTrack can be used, and the basics of how it is implemented.

C.1 Compiling SixTrack with BeamGas Module

BeamGas is written as an optional module in SixTrack. That means that you will have to get a binary version with BeamGas included, or write your own. The BeamGas module requires that the collimation module "collimat" is activated as well. The latest source can be obtained from `http://svnweb.cern.ch/world/wsvn/SixTrack/trunk/SixTrack`. In the source, there is a configuration script which is called "make_six". With this script you can compile SixTrack on Unix systems. Flags can be turned on by giving the names as input arguments, or turned off by doing the same, but with an additional minus sign in front.

After downloaded and extracted, run

```
./make_six collimat beamgas -crlibm gfortran
```

The two first options are needed. As of this writing, "crlibm" has not been confirmed working properly together with "collimat", so it is recommended to currently turn it off. The default compiler for SixTrack is the Lahey (lf95). If you do not have that compiler available, the author recommends to first try using "gfortran" as shown in the example. Another option is to use "ifort", which can potentially give you a faster binary. "ifort" support in SixTrack is still under development at the moment of writing.

A second module called “hdf5” has also been developed for this thesis work. The collimation module produce a file called “track2.dat” which contains all particle trajectories from the simulation, from the point the particles have become secondary particles. Secondary particles are particles that have undergone a collision with a primary collimator, or for the BeamGas module, when they have undergone a collision with rest-gas. The “hdf5” module writes these trajectories in a binary HDF5 [90] file format instead, which reduce the file size by about one order of magnitude, and the simulation speed by up to a factor two in some occasions. “make_six” currently links to the static libraries on afs when you select the hdf5 module to be used.

C.2 Running Beam-Gas Simulations

The BeamGas module works by triggering a subroutine when an element which name starts with “press” is found in the sequence. The subroutine will then look for a corresponding normalised pressure at this location, and distribute the total number of events at disposal accordingly.

You will need to start by editing a thin-lens Mad-X sequence and add these markers at the locations where you want a collision. We recommend that you use “rcollimator”, which is a marker that SixTrack does not ignore (most markers are ignored for speed improvements). After that you produce the SixTrack files with the “sixtrack” command inside Mad-X. In between, you need to have a sufficient amount of twiss and use commands to make sure you get the right optics and drifts. In Listing C.1 we show an example where we place one marker at IP1 and one in IP5.

Listing C.1: Mad-X Sequence Edit Example

```
use, period=lhcb1;
seqedit,sequence=lhcb1;
press.00001: rcollimator;
install, element=press.00001, at=0.0, from=ip1;
install, element=press.00001, at=0.0, from=ip5;
endedit;
...
sixtrack, MULT_AUTO_OFF;
```

A successful Mad-X run will give you the file “fort.2” which holds the sequence information for SixTrack. You will also need other input files that are also needed for a collimation studies, see the Collimation web page [100], and the SixTrack User Manual [101]. We will not describe these input files further here.

C.2.1 Input Files

Some special input files are needed for the BeamGas module as well. The first is the file containing the relative pressure distribution. This is a simple file holding two columns, one which should be the longitudinal position from the start of the sequence, and the second should be the relative pressure at that location. The sum of the second column should hence be less than or equal to one. If the sum is higher, the simulation will only be carried out starting from zero until the sum has reached one. If less than one, some fraction of the protons will be left untouched. In Listing C.2 we show an example which corresponds to the two markers we installed in Listing C.1.

Listing C.2: pressure_profile.txt

```
0.0 0.5
13329.289 0.5
```

The second file you need holds the special configuration for the BeamGas simulation. The BeamGas module is constructed to split the pressure profile in many jobs. In order to do so, each job needs to know how many jobs there are in total, and which job number the particular job has. If you only want one job, set njobs and thisjob to 0. In Listing C.3 we show an example of this input file. As you can see, you can write additional comment lines to keep track of what the parameters are. The "dpmjetev" value is the number of generated collision events available for this job. The total number of collisions simulated will be this value multiplied by the number of jobs.

SixTrack uses an expanded Hamiltonian, which does not accurately track heavily off-momentum particles. However, these particles are quickly lost, so the accuracy is less relevant. You can set the "ecutoff" value if you want to specify The minimum energy required in order to track a proton after the collision (here set to 80 % of the beam energy). Protons with energy below this value are considered lost immediately.

Listing C.3: beamgas_config.txt

```
# Any line not starting with
# njobs, thisjob, ecutoff or dpmjetev are ignored

# The total number of jobs in this simulation
njobs 10

# The job number of this particular job
# This together with njobs are used for paralellising
thisjob 1

# The number of dpmjet events that have been
# produced for this job.
```

```
# The events are read from dpmjet.eve
dpmjetev 1000

# Energy cutoff value, between 0 and 1.
ecutoff 0.8
```

The final input needed is the file "dpmjet.eve". An example of how this file should look is shown in Listing C.4. The columns are event ID, particle ID as defined by the Particle Data Group, forward cosine horizontal and vertical, and finally the energy in GeV. The Monte Carlo simulation producing these events should be simulating collision of a proton beam colliding head-on with the rest gas particle. The Lorentz boost is applied inside SixTrack if needed.

Only protons are tracked in SixTrack, but it can be useful to include other particles in this event list. That way, it will be possible to produce output which will give the full shower information to other simulation tools like FLUKA, Geant4, or BDSIM. It is important that this list is ordered by event ID.

Listing C.4: DPMJET Collision Events

```
1   2212  -0.275633038467E-04   0.105659113572E-03   0.229610029278E+04
1   -211   0.199676150495E-03  -0.186593246012E-03   0.231711296681E+04
2   2212   0.306961678030E-03   0.234290260213E-03   0.155623491554E+04
2   -211   0.181805826338E-03   0.533377947837E-03   0.160979138592E+04
2    130   0.306151624382E-03  -0.208566993864E-03   0.609571738099E+03
```

C.3 Output

As for the collimation studies, the main information is given in form of FLUKA input files and summary files showing the number of hits on the collimators. Since the aperture is not available in SixTrack, the particle trajectories and the FLUKA input file must be post processed using e.g. the BeamLossPattern/CleanInelastic binaries provided by the Collimation team [102].

In addition, a file named "scatterLOC.txt" is produced. This file gives all information about the location where the particles were scattered. Together with "dpmjet.eve" and the FLUKA impacts list you can then generate the full output including the untracked particles (give the location and direction/energy at the location of scattering)

C.4 Implementation Details

The collisions between the beam particles and the rest gas (or more generally, collisions with an obstacle as simulated by the external Monte Carlo code) are distributed in the first turn of the simulation. The code has been written with a minimal amount of inserts into the main SixTrack code. At one point in the start of the program, an initialisation subroutine must be called which reads the necessary information from the input files. Then, when looping over the elements, the beamGas() subroutine must be called whenever the correct element is found in the sequence.

Since SixTrack is written in Fortran 77, there is no dynamic memory allocation. As a result, we needed to increase the arrays which sets the number of elements and blocks in the code, in order to be able to simulate gas scattering at sufficiently many locations. In Listing C.5 we show all insertions into the original SixTrack code that was needed.

Listing C.5: Inserts in main SixTrack code

```
 ...
 ! For large amount of pressure markers, we need to increase
 ! nele, nblo and nblz:
 parameter(nele=50000,nblo=10000,nper=16,nelb=140,nblz=200000,
&nzfz = 300000,mmul = 11)
 ...
 ! Initialize BeamGas module
 call beamGasInit(myenom)
 ...
 ! during the loop over elements,
 ! call beamGas subroutine
 ! when press elements are found
 if( iturn.eq.1 ) then
   if (bez(myix)(1:5).eq.'PRESS' .or.
&    bez(myix)(1:5).eq.'press' ) then
         call beamGas(myix, secondary,totals,myenom,ipart)
    endif
 endif
```

Fortran 77 is a pure subset of Fortran 90, so it was decided to write the BeamGas module in Fortran 90. That means one can take advantage of modules, as exemplified in Listing C.6.

Listing C.6: BeamGas common module

```
  module beamgascommon
    integer, parameter :: bgmaxx=40000,bamount=1000
    integer bgmax,bgid,bgiddb(bgmaxx),ibgloc,pressID, &
     njobs,njobthis, dpmjetevents
    real pressARRAY(2,bgmaxx)
```

```
  double precision bgParameters(3)
  double precision minenergy
  real bgxpdb(bgmaxx),bgypdb(bgmaxx),bgEdb(bgmaxx),pSCATT(
      bamount)
end module beamgascommon

...

subroutine beamGas(...)
use beamgascommon
implicit none
...
end subroutine
```

The main subroutine is first calculating the number of collisions that should be produced at current location. It then iterates over the particles currently tracked, 64 at the time in SixTrack. Each particle is associated to one event. If there are no protons with sufficiently high energy for a given event, the corresponding particle is tagged lost at the location of the scattering. The angles introduced by the Monte Carlo event generator are added on top of the beam divergence as illustrated in Figure C.1. This can be of high importance as the mean scattering angle typically can be around the same order of magnitude as the beam divergence.

For small angles, a simple addition should be sufficient under the approximation

$$\sin x \approx x.$$

Since beam-gas collisions does not necessarily deal with exclusively small angles, the rotation matrix is calculated and a proper rotation is performed.

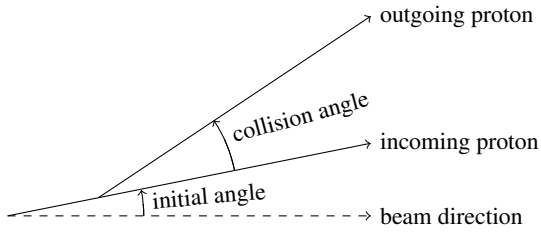

Figure C.1: The event read into SixTrack is assumed to be from a head-on collision. The collision angle is then added on top of the initial angle that the proton has before the collision.

Afterwards, all needed information about the collision is written to “scatterLOC.txt”, and the proton is tagged “secondary”, which means that the collimation routine will write the particle trajectory at every element to file.

Appendix D

Articles

This appendix includes a copy of publications the author has contributed to as a part of this thesis work. Before each article, the information about title, abstract, authors, kind of publication and detailed information about what the author has contributed is included. The articles are added in a chronological order, with the original formatting as it was published.

D.1 Simulation of Beam-Gas Scattering in the LHC

- Title: Simulation of Beam-Gas Scattering in the LHC
- Abstract: We report on background studies for the LHC with detailed simulations. The simulations now include generation of beam-gas scattering in combination with multiturn tracking of protons. Low beta optics and available aperture files for this configuration make it possible to generate loss maps according to the pressure distribution in the LHC.
- Where: PAC09, Vancouver, Canada
- When: May, 2009
- Contribution: Yngve was the main author of this paper, and the presenting author at the conference. The particle tracking including the implementation of new code in SixTrack was performed by him, and the analysis of the results were done by him. Yngve made the poster for the presentation.
- Co-authors: Helmut Burkhardt, Vadim Talanov
- Bibliography entry: [77]

Simulation of Beam-Gas Scattering in the LHC

Yngve Inntjore Levinsen *,
Helmut Burkhardt †,
Vadim Talanov ‡

Abstract

We report on background studies for the LHC with detailed simulations. The simulations now include generation of beam-gas scattering in combination with multiturn tracking of protons. Low beta optics and available aperture files for this configuration make it possible to generate loss maps according to the pressure distribution in the LHC.

INTRODUCTION

The study we describe is part of a more general study to understand and optimize the experimental conditions in the LHC [1]. The LHC will soon start to run and produce proton-proton collisions which will be observed by four large experiments, installed at the four interaction regions IP1 (ATLAS), IP2 (ALICE), IP5 (CMS) and IP8 (LHCb) of the LHC. The LHC is designed for a high nominal luminosity of $10^{34}\,\mathrm{cm}^{-2}\mathrm{s}^{-1}$. This is a rather ambitious goal and will likely require several years of stepwise commissioning. In particular, it is planned to increase the single bunch intensity from a few 10^{10} protons per bunch to the nominal 1.15×10^{11} protons per bunch, to increase the collision energy from initially about 5 TeV to the nominal 7 TeV per beam, to decrease the transverse beam sizes at the interaction by decreasing β^*, and to increase the number of bunches circulating and colliding in the LHC. It is planned to start initial operation with $43 - 156$ bunches, which would allow sufficiently large bunch spacing to eliminate any parasitic beam encounters in the ± 58 m common beam pipe around each interaction region. At every stage, we will try to understand and minimize the machine induced backgrounds to be able to predict conditions for the next steps.

The LHC is equipped with a three stage collimation system [2], which is primarily designed to keep the flux of particle losses on the cold parts of the LHC machine below the quench level. The performance of the collimation system is simulated by following up secondary particles which first hit the primary collimators at small impact parameters. These primary halo losses are further reduced by secondary and tertiary collimators. A small fraction of these losses will impact on the tertiary collimators placed in the straight sections around the experiments and result in a small fraction of secondary particles which can reach the experimental detectors.

* Univ. of Oslo and CERN, Yngve.Inntjore.Levinsen@cern.ch
† CERN, Geneva, Switzerland
‡ IHEP Protvino, Protvino, Moscow Region

To allow to predict the total flux of beam induced machine backgrounds into the experiments, we have to consider any direct losses of the circulating protons as a result of the scattering of the protons with particles of the rest-gas in the beam pipe.

EVENT GENERATION

The collisions between the high energy protons and the residual gas are not implemented directly into the tracking tool. An interface is developed so that the collision events can be simulated prior to the tracking using DPMJET [3] as the event generator. The output format from DPMJET is simple and flexible, including a particle ID, energy and angles with respect to the angle of the incoming proton. It will be a straight forward task to replace or compare DPMJET with other event generators if that would be a request or a necessity at any point in time.

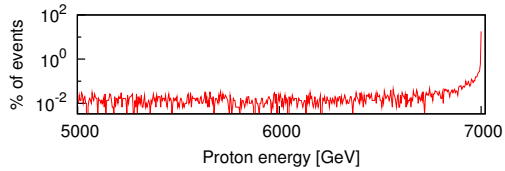

Figure 1: Percentage of events generating a proton with a given energy, from the scattering of 7 TeV protons with H atoms at rest. The elastic peak is observed for proton energy close to 7 TeV.

So far, we simulate proton collisions with a H atom, and the H_2 equivalent pressure distribution (normalized by cross section ratios) is used in the simulations. A histogram of the energy distribution can be seen in Fig. 1. Recent discussions have emphasized that one in the future should simulate the collisions with all types of residual gas due to the different ratios of energy distribution and ratios of residuals. This inclusion is part of the future plans for this project.

PROTON TRACKING

The event generation is followed by tracking of protons around the LHC ring using SixTrack [4]. This kick-code tracking tool provides a fast tracking including collimation, providing multiturn tracking and the ability to study

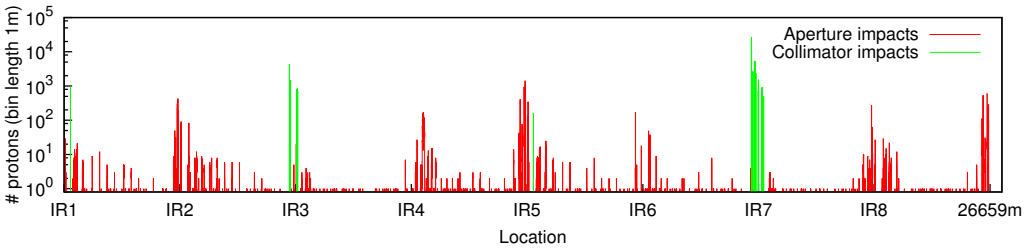

Figure 2: In about 22% of the scattering events, a proton with more than 90% of initial beam energy is generated. The loss locations of those protons are shown here. In addition, 78% of the events are generating locally lost particles only, and are not a part of this plot.

halo generation from beam-gas. The proton tracks are subsequently used in an aperture code, determining aperture losses. In order to track protons after the beam-gas event, it is required they are not very much off-momentum due to a reduced Hamiltonian. The exact limitations regarding off-momentum particles are under investigation, and results so far indicates that at least a few percent off momentum will not be a problem. In other words, since the dispersion limitation in the arcs is expected to be less than one percent, the code seems to be fitting for our purpose. What remains is the tracking of all residues in the long straight sections (LSS) and to compare tracking of protons with different tracking tools for the highly off-momentum particles over shorter terms.

Beam-gas scattering is normalized so that all particles in the simulation is scattered once during the first turn of tracking, according to given pressure distributions around the ring. Multiple beam-gas scattering is not considered since the probability of this to happen should be insignificant. For each type of parent atom, a separate tracking simulation will be ran. The output is then afterwards normalized according to

$$P(z) = \text{lossMap}(z) \cdot \sigma_{\text{tot}} \cdot \frac{n_{\text{p in ring}}}{n_{\text{p in sim}}} \cdot \frac{c}{r_{\text{LHC}}} \cdot \oint p(z)dz.$$

In this equation, lossMap(z) is the losses at position z around the ring (according to the given pressure map), σ_{tot} is the total cross section for a beam-gas interaction (elastic and inelastic), $n_{\text{p in ring}}$ is the total number of protons stored in the LHC ring, $n_{\text{p in sim}}$ is the number of simulated events, $\frac{c}{r_{\text{LHC}}}$ is the speed of light divided by the circumference of LHC which mounts to about 11 200 turns per second. Finally, $p(z)$ is the partial pressure distribution for the given parent atom.

The pressure distribution has been simulated by the vacuum group at CERN [5], and seems to correspond well with measurements (static pressure only as we have not had a high energy beam inside LHC yet). The plan is to include a full simulation with the partial pressure for at least four different gas residuals (H_2, CH_4, CO and CO_2). In the example shown below the simulated pressure distribution is not implemented. The implementation of a pressure distribution is ready, and will be included in future simulations.

Summarizing $P(z)$ for all residual gases that are included in the simulation, one then has the losses per second at location z. The output includes all particles generated, but only protons within a given off-momentum limit is tracked after the beam-gas event. The other particles are still part of the output, directly written to file from their position inside the beampipe. The same is true for particles coming out from a given event other than the high energy proton. They will be written to file at the location where the scattering event took place. The principle is that all particles are tracked as far as possible with our tool, but not further.

OUTPUT AND SIMULATION EXAMPLE

The output from the tracking includes particle type, 6D coordinates and current condition. This can be that the particle is still inside the beampipe or that it hit some aperture or a collimator. The output also includes the type of the parent atom in the scattering process and the event id so that one can keep track of what came out of a given event.

The output can be used as input for loss studies in the LSS. Similar studies has been performed in the past [6]. What is new here is the halo generation from the elastic scattering with the realistic residual gas pressure map, followed by multiturn tracking with the full LHC ring considered. The simulation does not give priority to any of the IRs, but is instead developed as a general tool where the losses in a given region can be extracted for detailed studies afterwards.

As an example run, 500 000 protons underwent a beam-gas scattering on a H atom and were subsequently tracked for 300 turns. For this example, the pressure were set constant around the entire ring. The off-momentum acceptance in the code is not yet well known, but was here set to 10%, which includes a proton from about 22% of the scattering events. 10% is at least an order of magnitude larger than the momentum acceptance in the arcs. The result can be seen in Fig. 2 and Fig. 3. The losses on aperture drops to zero within the first few turns, and the losses on the col-

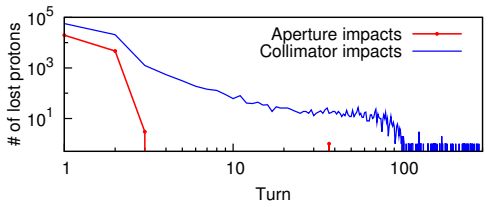

Figure 3: The spread of lost protons as a function of number of turns since the beam-gas event. After about 100 turns, there seems to be little to no losses anymore. Losses on aperture drops much faster, within the first few turns.

limators drops by about three orders of magnitude in the same amount of turns.

If one wants to combine these data with data from the collimation studies [7], one should remember that there could a double count when considering the losses on the collimators. This is probably more present for protons surviving many turns before impact with the collimators. The losses on the collimators fall off more slowly after the first few turns before they more or less disappear after about 100 turns. Only one beam is simulated (clockwise rotation around the ring). Independent studies [8] have shown that for the clockwise beam the background is worse for CMS (IR5), whilst for the other beam the background is worse for ATLAS (IR1). This lossmap seems to be in agreement with such a statement, as we see more losses around IR5. The code is parallelized (hardcoded), so the simulation may run in a few hours on a large server.

The idea is that the simulation can be ran more or less automatically on a server when one has a new pressure profile to study (e.g. a pressure bump). Another possibility would be to run a very large simulation with a constant pressure map and map on the pressure profile to this simulation afterwards.

SUMMARY

The project presented is a work in progress. The output data are expected to be ready well in time before the LHC startup this fall. Amongst the first users of this code are probably LHCb and ALICE where the output provided from these beam halo simulations will then be used to estimate the background flux towards the detectors. ATLAS and CMS in collaboration with Fermilab use different tools for similar studies and from what has been seen until now the simulations seems to be consistent.

REFERENCES

[1] Proc. of Workshop on Exp. Conditions, April 2008, http://indico.cern.ch/conferenceDisplay.py?confId=25768, CERN-2009-0nn.

[2] R. W. Assmann et al. The final collimation system for the lhc. LHC-PROJECT-Report-919., Jul 2006.

[3] S. Roesler, R. Engel, and Johannes Ranft. The monte carlo event generator dpmjet-iii. Proc. of the Monte Carlo 2000 Conf., Lisbon, October 2000.

[4] G. Robert-Demolaize et al. A new version of sixtrack with collimation and aperture interface. Proc. of PAC, May 2005.

[5] A. Rossi and N. Hilleret. Residual gas density estimations in the lhc experimental interaction regions. LHC-Project-Report-674, Sep 2003.

[6] R W Assmann, et al. Tertiary halo and tertiary background in the low luminosity experimental insertion ir8 of the lhc. LHC-PROJECT-Report-953, Aug 2006.

[7] C. Bracco. Commissioning scenarios and tests for the lhc collimation system. PhD thesis, EPFL, 2009.

[8] N. Mokhov. Presentation of current status of simulations *ATLAS/CMS beam-induced background WG*, Feb 2009.

D.2 Beam-Gas Loss rates in the LHC

- Title: Beam-Gas Loss Rates in the LHC
- Abstract: We report on detailed simulations and first observations of beam-gas rates in the LHC. For the simulations, a set of comprehensive tools has been set up, which incorporate pressure maps, collimator settings, and beam optics. The simulations include both elastic and inelastic beam-gas events in the arcs and long straight sections of the LHC. This provides, amongst other things, realistic collimator loss distributions, fluxes of secondary particles into the experiments and multi-turn tracking of elastic event residues.
- Where: IPAC10, Kyoto, Japan
- When: May, 2010
- Contribution: Yngve was the main author of this paper. Yngve obtained pressure distributions and did the simulations of long-distance beam-gas background. All parts of the paper excluding the section on LSS beam-gas was written by Yngve, with iterations and corrections by the co-authors. Yngve was the presenting author at the conference.
- Co-authors: Robert Barrie Appleby, Helmut Burkhardt
- Bibliography entry: [103]

BEAM-GAS LOSS RATES IN THE LHC

Yngve Inntjore Levinsen, Univ. of Oslo, Norway and CERN, Geneva, Switzerland
Robert B. Appleby, CERN, Geneva, Switzerland and Univ. of Manchester, United Kingdom
Helmut Burkhardt, CERN, Geneva, Switzerland

Abstract

We report on detailed simulations and first observations of beam-gas rates in the LHC. For the simulations, a set of comprehensive tools has been set up, which incorporate pressure maps, collimator settings, and beam optics. The simulations include both elastic and inelastic beam-gas events in the arcs and long straight sections of the LHC. This provides, amongst other things, realistic collimator loss distributions, fluxes of secondary particles into the experiments and multi-turn tracking of elastic event residues.

INTRODUCTION

LHC had its first collisions in November 2009, with a quickly following world record in collision energy at the end of the month. These days we are getting an instantaneous luminosity of about $10^{27}\,\mathrm{cm^2 s^{-1}}$ without squeezed optics, at a collision energy of 7 TeV. From the initial pilot beam intensity of 5×10^9 protons/bunch and 1 bunch/beam, we eventually want to end up with the nominal intensity of 1.15×10^{11} protons/bunch and 2808 bunches/beam. The beams should eventually be strongly focused at the interaction points, further increasing the luminosity. These changes will not only change the luminosity, but the background as well. In order to get a good prediction of the signal to noise ratio and the protection of the machine, it is important to know how the different background sources scales with these changing parameters.

In this paper we will present the current status of our knowledge of the beam-gas background, i.e. background arising from protons in the beam colliding with the residual gas left in the beam pipe. This is a part of a larger effort to obtain the full picture of and scaling laws for background sources. We presented our simulation framework for distant beam-gas at PAC 09 together with V. Talanov [1]. In this paper we will present predictions for background rates from this simulation package, together with shower simulations for the long straight sections around ALICE and LHCb using Fluka. The predictions from the simulations are then compared to the early data that has currently become available from the LHC running. A more detailed presentation of these simulations for the LHC injection energy can be found in [2].

SIMULATIONS AND EXPECTATIONS

Input parameters

For the simulations, the nominal settings for 3.5 TeV is used. That includes a β^* of 10 m in ALICE, 3 m in LHCb, and 2 m in ATLAS and CMS. The external crossing angle is turned off, limiting the maximum number of bunches in the machine to 156 bunches/beam. The experimental magnets are set at full power, with inversed polarity in LHCb. The RF voltage is at nominal 16 MV.

Beam-gas by its nature depends linearly on the pressure, hence the pressure assumed is important. At 3.5 TeV, synchrotron stimulated desorption is assumed to be insignificant in the straight sections. In the arc, there is a slight increase in pressure from the purely static pressure maps. The H_2 equivalent pressure map can be seen in Figure 1.

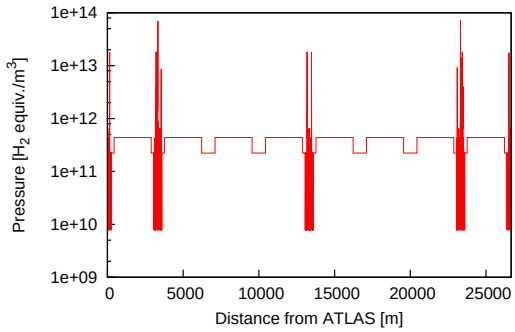

Figure 1: The H_2 equivalent pressure map used for the simulations. We see the four experimental regions, where a detailed simulated pressure map is available. The map starts at IP1, which is ATLAS.

LSS beam-gas

Beam-gas interactions in the long straight sections (LSS) of the experiments give a direct background source to the experiments. The elastic interactions contribute to the beam emittance growth, while the inelastic interactions generally produce forward hadrons and locally lost products at large angles. The forward hadrons (generally pions), and the resulting decay to muons, give the LSS beam-gas experimental background contribution.

The LSS beam-gas background to the LHC experiments was calculated using the simulated pressure map shown in Figure 1. A FLUKA geometrical model [3, 4] was constructed of the LSSs of the LHC, with a model of the magnetic elements, tunnel, shielding, collimators and all relevant mass distributions. The magnetic fields were included either through explicit field maps or ideal fields. Full details of the model for IR8 (LHCb) can be found

in [3, 4]. The proton-gas molecule interactions are simulated using DPMJET and distributed in the LSS according to the pressure profile. Note the calculation is done in terms of hydrogen-equivalent pressure profiles. The resulting hadronic and EM showers give the background flux contribution into the experimental caverns. The particle showers are cut off at a kinetic energy of 20 MeV for all particles except neutrons, which are followed down to thermal energies.

The total rate of beam-gas interactions is obtained from the integral of the gas pressure profile in the LSS (up to the experimental interface plane) and the proton-hydrogen/proton-carbon nuclear cross section. Table 1 gives the total rates of LSS beam-gas inelastic interactions in the LSSs of LHCb and ALICE, assuming 2×10^{10} protons in the LHC and a pH inelastic cross section of 36 mb. The interface plane locations of LHCb are 2.1 m for beam 1 and 19.9 for beam 2, and 19.5 m on both sides for ALICE.

Table 1: LSS inelastic beam-gas interaction rates, assuming 2×10^{10} protons in the LHC.

LSS	rate [protons/s]
LHCb left	1.45
LHCb right	1.45
ALICE	1.25

The resulting LHCb MIB fluxes from beam-gas interactions in the LSS at 3.5 TeV beam energy are 3.3 charged hadrons/s and 0.2 muons/s for beam 1, and 5.9 charged hadrons/s and 0.5 muons/s for beam 2. Note the longitudinal location of these results differ due to the different location of the beam 1 and beam 2 interface plane for LHCb. The resulting MIB flux for ALICE beam 1 and beam 2 are 3.0 charged hadrons/s and 0.3 muons/s. These results are obtained for a proton fill of 2×10^{10} protons.

Distant beam-gas

Distant beam-gas provides additional background signal in form of protons hitting the tertiary collimators (TCTs) upstream of the final triplets in the insertion regions. As such, this background component does not have a clear signature that we see from the local beam-gas background. It will look more or less identical to the normal halo component, and will add on top of that signal. This will make distant beam-gas harder to disentangle than LSS beam-gas.

At the current beam energy we do not have dynamical contributions to the pressure. Hence, the beam-gas background is orders of magnitude below what we expect at nominal machine parameters. For nominal machine conditions, we have estimated based on simulations that the proton rate on the TCTs are on the order of MHz, and the simulated pressure maps gives a lifetime for the beam-gas component of about 1000 h. Calculations of beam-gas lifetime are further explained in [2]. This means that the distant beam-gas component can be expected to reach the same order of magnitude as the normal halo component.

Figure 2 shows a simulated loss map for 3.5 TeV. In this simulation we have used a β^* of 2 m in ATLAS and CMS, 3 m in LHCb and 10 m in ALICE. For the normalization to a rate, a bunch intensity of 9×10^{10} protons and 156 bunches per beam. The beam-gas lifetime is estimated to be on the order of 10^5 h, using the simulated pressure map for 3.5 TeV.

Table 2 gives the proton fluxes on the different TCTs, assuming the same parameters. The rates scale linearly with the total stored current for a given beam, so they can be rescaled to the actual intensity in the machine. The purpose of the TCTs is to protect the final triplets. As one decreases the β^*, the transversal beam size in the final triplets increases. Hence, the TCTs must be placed closer to the beam (in units of transversal beam size). That means that these rates would be higher for a β^* of 2 m in ALICE and LHCb, instead of 10 m and 3 m, respectively.

The proton rates in Table 2 must be transported to the experiments interface plane. This is done with the same FLUKA code that is used for the shower simulations of the inelastic beam-gas. From this one obtains a conversion factor in e.g. number of muons at the interface plane per proton at the different tertiary collimators. An example of such conversion factors for LHCb beam 1 can be found in [5].

EARLY DATA FROM LHC

As we see from Figure 2, the proton flux on the collimators is too low to be observed with the beam loss monitors at the moment. The experiments can still measure even single beam-gas events. This is done by measuring the trigger rate for bunches which are not colliding with a bunch in the other beam, what is defined as beam-empty trigger rates. The showers to the interface plane are then transported through the experimental cavern, and the expected trigger rate efficiency for the activated trigger scheme is calculated for the different background sources. This procedure is covered in [5] for the case of LHCb.

In the data following below we had a fill of three bunches in each beam, where there were two centred bunch col-

Table 2: Simulated rates in protons per second hitting the horizontal (H) and vertical (V) tertiary collimators for the 3.5 TeV parameters.

Experiment	Orientation	Rate [protons/s]	
		Beam One	Beam Two
ATLAS	H	40.4	46.2
	V	22.1	42.8
ALICE	H	2.54	2.87
	V	4.37	2.77
CMS	H	49.0	37.6
	V	54.1	30.3
LHCb	H	18.0	19.5
	V	14.4	46.0

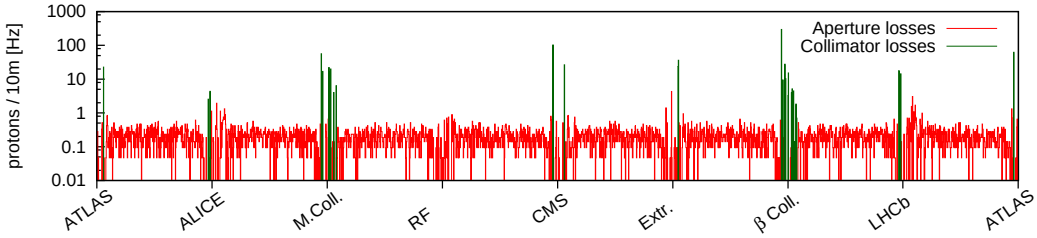

Figure 2: Simulated loss rates from beam 1 at 3.5 TeV. About 71 % of the events are lost locally, in addition to the losses shown here. The y-axis shows the number of protons hitting the aperture at the given location. Elastic hits on the collimators are not counted, the protons are then subsequently tracked until inelastic impact takes place.

lisions in each interaction point (IP). LHCb had for this fill an average trigger rate of 0.65 per second for beam-empty collisions for beam 1. With the trigger algorithm used, LHCb simulations show that this corresponds to a inelastic beam-gas rate of about 8 protons per second, to be compared with Table 1.

The bunch intensity for the non-colliding bunch was measured with the fast beam current transformer (BCT) and found to be about 9×10^9 over the course of the fill. Hence, the estimated rate of protons from inelastic beam-gas from our simulations is 0.65, one order of magnitude lower than measured. Betatron halo and elastic beam-gas do bring up the trigger rate slightly, but it is found that for the 3.5 TeV beam energy, inelastic beam-gas is the dominating background component in LHCb. Ignoring these components cannot explain the discrepancy, but they will result in a smaller difference between simulations and measurements. Background components can be significantly larger than expected, due to e.g. optics imperfections and misalignments that are not included in simulations.

We published an estimate for the beam-gas rates at 450 GeV in a note earlier this year [2], where we used a simplified pressure map based on measurements instead of simulations. Measured pressure levels should always be considered an overestimate, due to gauge outgassing, location of gauges etc.

The average pressure in the pressure profile we generated is close to one order of magnitude higher than the simulated pressure. If the average pressure is closer to our estimates pressure than the simulated pressure, that could explain some of the discrepancy between the simulated and measured trigger rate for this fill. It has always been stressed that the simulated pressure maps are order of magnitude studies, and that safety margins must be applied. The same pressure map simulations give a beam lifetime of about 1000 h for the nominal machine, whereas the lower limit requirement defined in the LHC design report is 100 h [6, 7].

SUMMARY

We have here presented an extensive framework for beam-gas background simulations in LHC. From this framework, we have estimated expected rate of background particles showering towards the experiments ALICE and LHCb for 3.5 TeV beam energy, in addition to providing a loss map for the rest of the LHC. The showers are compared to measured trigger rates for LHCb, and the simulations predict the trigger rates to be one order of magnitude lower than measured. This is not alarming for a first approach. We are pleased to see that we can already compare data with simulations at this early stage.

ACKNOWLEDGEMENTS

The authors would like to acknowledge the help from the LHCb collaboration in obtaining experimental trigger rates to compare with the simulated data, and for fruitful discussions. A particular thanks goes to M. Lieng, F. Alessio, and G. Corti.

REFERENCES

[1] Y. Inntjore Levinsen, H. Burkhardt, and V. V. Talanov. Simulation of beam-gas scattering in the LHC. In *PAC Vancouver*, May 2009.

[2] R. B. Appleby, Y. Inntjore Levinsen, and H. Burkhardt. LHC-Project-Note-429, CERN, Geneva, Feb 2010.

[3] R. B. Appleby and A Mereghetti. LHC-Project-Note-427, CERN, Geneva, Feb 2010.

[4] R. B. Appleby, G. Corti, M. Lieng, D Macina, and V. V. Talanov. LHC-PROJECT-Report-1180, CERN, Geneva, Jan 2010.

[5] M. Lieng, R. B. Appleby, G. Corti, and V. V. Talanov. In *IPAC Kyoto*, number MOPEC001, 2010.

[6] A. Rossi and N. Hilleret. LHC-Project-Report-674, CERN, Geneva, Sep 2003.

[7] O. S. Brüning, Paul Collier, P Lebrun, Stephen Myers, Ranko Ostojic, John Poole, and Paul Proudlock. *LHC Design Report*, volume 1. CERN, Geneva, 2004.

D.3 IR Crosstalk in the LHC

- Title: Dependence of Background Rates on Beam Separation in the LHC.
- Abstract: To some extent, background and loss rates vary when beams are brought into collision in the LHC and when the beam separation is varied during luminosity scans. We have searched for these effects in the early LHC operation. The data are analysed and compared with models and simulations.
- Where: IPAC10, Kyoto, Japan
- When: May, 2010
- Contribution: Yngve was the main author for this paper, and the presenting author at the conference. He wrote all sections of the paper, with co-authors providing suggestions and corrections. Yngve did the analysis which is presented in this paper. The simulations presented in the paper were done by Yngve. Yngve produced all figures but figure 3.
- Co-authors: Helmut Burkhardt, Simon Mathieu White
- Bibliography entry: [81]
- Note: Eq. (1) is inaccurate, see correct formula in Section 6.1. In the figure label for Fig. 2, it should have been protons per collision, not Hz.

DEPENDENCE OF BACKGROUND RATES ON BEAM SEPARATION IN THE LHC

Yngve Inntjore Levinsen *, Helmut Burkhardt †, R.B. Appleby ‡, Simon Mathieu White §

Abstract

To some extent, background and loss rates vary when beams are brought into collision in the LHC and when the beam separation is varied during luminosity scans. We have searched for these effects in the early LHC operation. The data are analysed and compared with models and simulations.

INTRODUCTION

The LHC includes four experimental regions. The collisions in each interaction region will result in scattered particles, some of which may be lost in another interaction region resulting in cross talk between the experiments. Proton colliding in one experiment with a small energy loss could survive in the beam for a short while, being lost around another experiment. Depending on optics, phase advance, aperture and so forth, the level of background arising from this cross talk can change significantly. As part of a larger effort to map out and understand the different background sources in LHC, we have been simulating and studying the cross talk as a function of the interaction rates in the different experiments.

Interaction region cross talk as potential source of background has been known for a while. Earlier studies on loss maps from collisions in the CMS interaction region already showed evidence for this effect [1], and motivated for a more dedicated study as presented here. The design luminosity of the LHC is $10^{-34}\,\mathrm{cm}^{-2}\,\mathrm{s}^{-1}$, for the two high luminosity experiments ATLAS and CMS. The two other experiments, LHCb and ALICE were designed for luminosities which are several orders of magnitude below the LHC design luminosity. ALICE in particular will run at a nominal luminosity of about $10^{-29}\,\mathrm{cm}^{-2}\,\mathrm{s}^{-1}$ up to a maximum of $3\times10^{-30}\,\mathrm{cm}^{-2}\,\mathrm{s}^{-1}$, and will therefore be rather sensitive to cross talk from the high luminosity interaction regions [2]. The background is dependent on the specific machine parameters. A simulation tool is required to predict the background levels in a given setting. Of importance is the luminosity in each experiment, the positions of the tertiary collimators, and the phase advance between different elements (experiment to experiment, or experiment to a given aperture bottleneck upstream of other insertions).

Small angle elastic proton collisions in one experiment give an angular kick to the protons, acting as a transversal diffusion process. Since collisions are more probable in the centre of the beam, this will typically increase the betatron action of the colliding proton. As a result, one would expect a peak in losses from one experiment at locations which are at a phase advance

$$90 + \mathrm{atan}(\alpha/\beta) + 180\cdot n \qquad (1)$$

degrees downstream of the collision point, where n is an integer and where the twiss parameters are taken at the point the potential loss points.

In addition, we also expect losses from proton collisions which result in a small energy loss. A proton will be lost from the stable rf-bucket for an energy loss of $\Delta E/E > 3.5\times10^{-3}$ but may still travel through one or several of the LHC arcs up to $\Delta E/E \approx 7\times10^{-3}$. This is included in our simulations. The dispersion around the experiments is small so that most of the off-momentum protons will be lost far from the experiments and not contribute much to the observed backgrounds.

We searched for signs of cross talk during luminosity scans. These scans are done for only one of the four interaction regions at a time. The duration of these scans is less than 30 min, which is short compared to the beam and luminosity lifetime (>10 h), so that any changes in the observed background rates at the other interaction regions would be evidence for cross talk.

SIMULATIONS

A simulation has been set up, in similar manner to the beam-gas simulations [3, 4]. A detailed optics and aperture model is available. Sixtrack is used for tracking, providing the availability of high speed multiturn tracking of protons. Other residues from the collisions are not able to survive from one experiment to the next without getting lost.

DPMJET III is used to generate collision events. DPMJET can use internally PYTHIA and PHOJET. The framework developed for these background studies is highly modular, which means that other event generators can be tested.

In Figure 1, a simulated loss map from IP cross talk is shown for beam one (moving clockwise when seen from above). A detailed view around the IPs is shown in Figure 2. The beam energy is 3.5 TeV. For the simulations we assumed a β^* of 2 m in ATLAS and CMS, 3 m in LHCb, and 10 m in ALICE. This differs somewhat from the current machine, which has 2 m β^* commissioned in all four IPs.

* Univ. of Oslo, Norway and CERN
† CERN, Geneva, Switzerland
‡ CERN and Univ. of Manchester, United Kingdom
§ Univ. de Paris-Sud 11, France and CERN

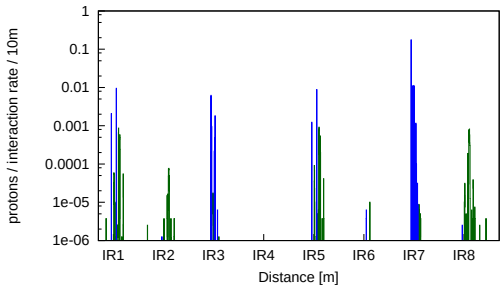

Figure 1: The loss map from beam one. Rates coming from different experiments are normalized to the squeeze optics at those experiments. The blue line show losses on collimators, whereas the green line shows losses on other aperture restrictions.

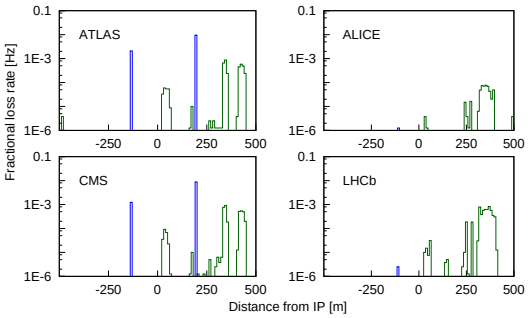

Figure 2: Detailed loss maps around the experiments. Losses downstream of the IP are for the most part coming from the IP itself. What is interesting are losses upstream of the IP, which can cause particle showers into the caverns.

Elastic and quasi-elastic collisions make up for a large fraction of the collisions in the insertion regions. For 3.5 TeV, about 28 % of the protons are found to be within an energy range which makes it possible to survive through one arc without being lost. About 10 % of the protons are found to survive for more than 100 turns after the collision. These numbers vary slightly for different machine settings. We are left with slightly less than 1/5 of the protons which are potentially contributing to the cross talk between the experiments.

LUMINOSITY CALIBRATION SCANS IN LHC

An application has been developed [5] to separate the beams locally in the insertions and obtaining the luminosity as a function of the separation of the two beams. This application has two purposes. First, it is used to optimize the luminosity. This is a quick procedure performed regularly during operation. The second purpose is to do calibration scan in order to obtain an estimate on the luminous region and then an estimate on the absolute luminosity. These scans are slower (in order to obtain sufficient statistics) and more points are required for a proper fit. An example of the resulting interaction rate on one of the collision rate monitors (BRANs) can be seen in Figure 3. The duration of a full scan depends on the available intensity. With an interaction rate on the BRANs of around 100 Hz that we had during this scan, a full scan took about 20 min.

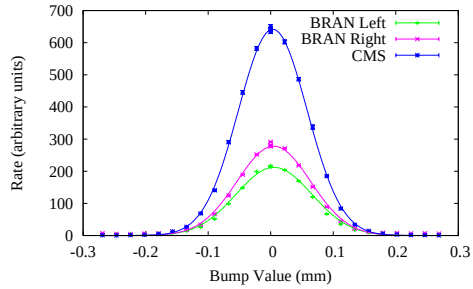

Figure 3: The interaction rate during a luminosity scan in CMS [6]. This full scan took about 20 min to finish.

Because the luminosity scans give a particular signal to the luminosity as a function of time, it was considered worthwhile to search for correlations between this signal and background signals at other places in the machine.

In LHC there are many different detectors that could be used to search for cross talk. To study all signals in detail for all luminosity scans would be very time consuming. Hence one has developed an analytical tool that calculates the correlation between a specified signal (e.g. the signal from a BRAN) to all other signals selected. The correlation should then give a quick indication if there is something worth looking at. An example is given in Figure 4.

In the figure we observe that only the luminosity signals in the insertion itself show a clear correlation. Even the physics debris collimators (TCL R/L 5) do not see any signal variation. We expect that higher intensity would be required in order to study the IR cross talk in detail.

DISCUSSIONS AND OUTLOOK

In the simulations, it is observed that a high fraction of the collisions in ALICE result in a proton hitting the TCTs in CMS and ATLAS for beam one and beam two respectively. This can be understood from the fact that the β^* is larger in ALICE than the other experiments, which means that γ^* is lower. Hence a given angular kick (which is dependent on neither β^* nor γ^*) will result in a larger betatron action for the proton collisions in ALICE than the other experiments. In addition, the TCTs are more relaxed when β^* is larger in a given IP, decreasing the fraction of the beam they are scraping.

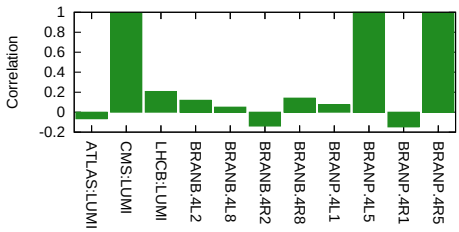

(a) Luminosity monitors

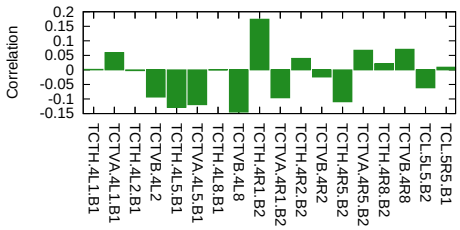

(b) Tertiary collimators and physics debris collimators in IR5 (TCLs)

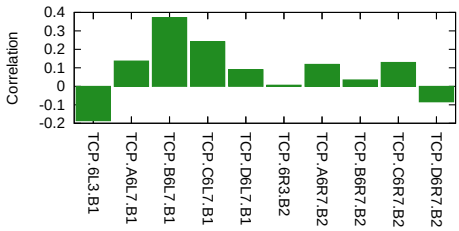

(c) Primary collimators

Figure 4: Table of correlation values from a horizontal scan in CMS. All signals are correlated to the BRAN left of CMS (downstream for beam 2). Of particular interest are the signals in Figure (a). For the collimators in Figure (b) and (c), the gas ionisation BLMs are used.

If it is correct that β^* is the dominating factor together with the phase advance, then this is good news. It means that the cross talk produced in an experiment will be reduced when we increase the squeeze in the originating experiment, counteracting the increased interaction rate. As we unsqueeze the low luminosity insertions, we will further reduce the incoming background at those experiments, because the TCTs are at a more relaxed position.

It is observed that the vertical phase advance in the simulation from ALICE to the vertical tertiary collimator in front of ATLAS is 78 degrees, and the maximum amplitude would be expected at 86 degrees. Hence, we are close to the maximum amplitude in addition to the fact that this is the first major aperture restriction beam two meet after the collisions in ALICE.

We are not observing significant cross talk in the LHC at the moment — which is good and as expected. We did a short simulation of the nominal 7 TeV machine, where we learned that one could expect a hit rate on the TCTs originating from cross talk up to about one order of magnitude less than that of the normal halo component. We are fairly confident that we now have the tools ready to both simulate IR cross talk and analyse the data that becomes available from the LHC.

REFERENCES

[1] R. W. Assmann and T. Weiler. IR cross talk simulations. Work in progress.

[2] V. V. Talanov. Simulation of machine backgrounds. *Workshop on Experimental Conditions and Beam Induced Detector Backgrounds*, 2008.

[3] Y. Inntjore Levinsen, H. Burkhardt, and V. V. Talanov. Simulation of beam-gas scattering in the LHC. In *PAC Vancouver*, May 2009.

[4] Y. Inntjore Levinsen, R. B. Appleby, and H. Burkhardt. Beam-gas loss rates in the LHC. In *IPAC Kyoto*, number TUPEB072, 2010.

[5] M Lamont, R Alemany-Fernandez, H. Burkhardt, and S. M. White. Luminosity optimization and calibration in the LHC. CERN-ATS-2009-071.

[6] S. M. White, R. Alemany-Fernandez, H. Burkhardt, and M. Lamont. First luminosity scans in the LHC. In *IPAC Kyoto*, 2010.

D.4 Methodology of MIB Simulations

- Title: Simulation of Machine Background in the LHCb Experiment: Methodology and Implementation
- Abstract: Numerical analyses of machine induced background at the LHC are needed to evaluate the complete running environment of an experiment. In order to have a comprehensive view of the machine background in an experiment all of its sources, ranging from collimators' cleaning inefficiency to distant and local beam-gas interactions need to be estimated; particles showering from the losses are then to be transported all the way to the experimental setup and the response of the detector evaluated. In this paper we describe a novel methodology implemented in LHCb to achieve this. Each step in the chain is simulated with software specific to the task and provides input to the subsequent step through a well-defined and clear interface. We will describe the methodology used for the studies and give some examples of the results obtained. Further, we will discuss in detail the various steps in the chain together with the advantages such a modular method allows in evaluating operational conditions where scaling of the initial sources can be applied.
- Where: IEEE Nuclear Science Symposium Workshop, Knoxville, Tennessee, USA
- When: November, 2010
- Contribution: Yngve was the main responsible for the part on long-range beam-gas including estimates of rates on the TCT's in IR8. Yngve helped organising the reviews from the different authors. Figure 3 was made by Yngve. Yngve wrote the introduction to the section on distant MIB sources together with R. Appleby.
- Co-authors: Robert Barrie Appleby, Helmut Burkhardt, Gloria Corti, Magnus H. Lieng, Vadim Talanov
- Bibliography entry: [17]
- Note: Revised version approved for publication in Transactions of Nuclear Science (TNS)

Simulation of Machine Induced Background in the LHCb Experiment: Methodology and Implementation

R. B. Appleby, H. Burkhardt, G. Corti, Y. I. Levinsen, M. H. Lieng and V. Talanov

***Abstract*—Numerical analyses of machine induced background at the LHC are needed to evaluate the complete running environment of an experiment. In order to have a comprehensive view of the machine background in an experiment all of its sources, ranging from collimators' cleaning inefficiency to distant and local beam-gas interactions need to be estimated; particles showering from the losses are then to be transported all the way to the experimental setup and the response of the detector evaluated. In this paper we describe a novel methodology implemented in LHCb to achieve this. Each step in the chain is simulated with software specific to the task and provides input to the subsequent step through a well-defined and clear interface. We will describe the methodology used for the studies and give some examples of the results obtained. Further, we will discuss in detail the various steps in the chain together with the advantages such a modular method allows in evaluating operational conditions where scaling of the initial sources can be applied.**

I. Introduction

An accelerator environment always contains particles not originating from beam collisions at the interaction point (IP). These background particles can reach the detector and give rise to a certain level of background in the LHC experiments. It is important to evaluate the amount and characteristics of this background, not only in the design of an experiment but also during operation in order to minimize its potential impact.

Particles originating from proton beam interactions with the gas residue in the vacuum chamber or with the aperture material of the accelerator on either side of the interaction points and reaching the experimental areas from the machine tunnel constitute what we call the *Machine Induced Background* (MIB). The rate of this type of background is generally proportional to the machine beam current and depends on a given operating condition; depending on the luminosity of an experiment the MIB may contribute to its radiation environment, influence its trigger and physics measurements.

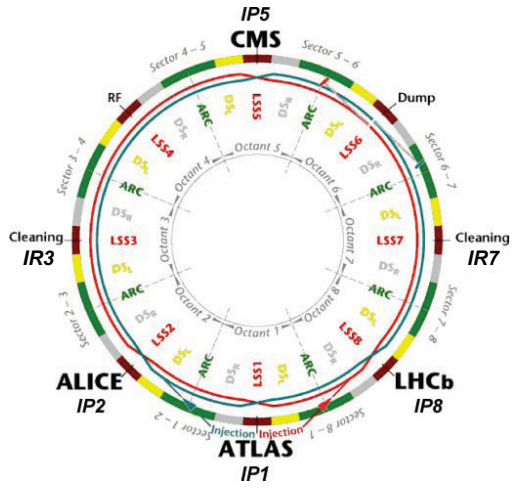

Fig. 1. Layout of the LHC ring. The interaction points are indicated with LHCb being in IP8.

The Large Hadron Collider (LHC) [1] at CERN started operation at the end of 2009 and, after a short period at 450 GeV/beam, has been operating at an energy of 3.5 TeV/beam. A planned upgrade will bring LHC to the nominal 7 TeV/beam within the next years. The layout of the machine is shown in Fig. 1. The ring is divided in eight sectors each comprising a long straight section (LSS) of about 600 m length where the beam trajectory (apart from separation dipoles) is straight. These straight sections are surrounded by dispersion suppression regions (DS) and arcs where the beams are bent in their circular paths around the machine by the main dipole magnets. The interaction points where the experiments are located are in the middle of four LSS with the LHCb detector installed at IP8. Insertion regions for betatron and momentum halo cleaning are found in two of the remaining sectors, IR7 and IR3 respectively.

The LHCb experiment [2] is designed to investigate the

The work was supported in part by the Russian Foundation for Basic Research grant (No. 10-07-00435)

R. B. Appleby is with the School of Physics and Astronomy and the Cockcroft Institute, University of Manchester, Manchester, M13 9PL, United Kingdom (telephone: +44-161-275-4223, e-mail: robert.appleby@manchester.ac.uk). He was formally with CERN, CH-1211 Genève 23, Switzerland until September 2010.

H. Burkhardt is with CERN, CH-1211 Genève, Switzerland (telephone: +41-22-767-5464, e-mail: Helmut.Burkhardt@cern.ch).

G. Corti is with CERN, CH-1211 Genève, Switzerland (telephone: +41-22-767-2376, e-mail: Gloria.Corti@cern.ch).

Y. I. Levinsen is with University of Oslo, Norway and CERN, CH-1211 Genève, Switzerland (telephone: +41-22-767-0989, e-mail: Yngve.Inntjore.Levinsen@cern.ch).

M. H. Lieng is with Experimental Physics 5, Technische Universität Dortmund, Dortmund, Germany (telephone: +49-231-755-4526, e-mail:Magnus.Lieng@cern.ch).

V. Talanov is with Institute for High Energy Physics (IHEP), RU-142 281 Protvino, Moscow Region, Russia (telephone: +7-4967-713-420, e-mail:Vadim.Talanov@ihep.ru).

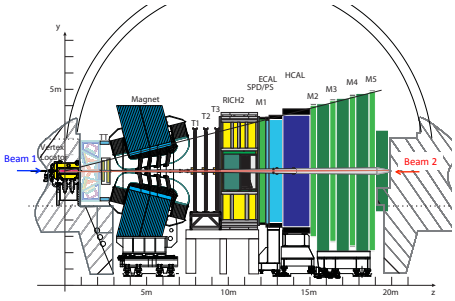

Fig. 2. The LHCb detector. The directions of the clockwise and counter-clockwise beams, respectively beam 1 and beam 2, are indicated.

possibility of new physics beyond the standard model by performing precision measurements in the beauty and charm sectors. In order to perform such measurements LHCb intends to operate at an average rate of a few proton-proton interactions per bunch crossing; once the experimental optimal instantaneous luminosity is reached, the pile-up from multiple collisions in single bunch crossings will be optimised by levelling the luminosity profile during the fill. This will result in an increase of the relative MIB to collisions ratio.

The detector, shown in Fig. 2 is a single arm spectrometer in the direction of the clockwise beam (beam 1), and as a result is more sensitive to MIB coming from this beam than the beam going in the counterclockwise direction (beam 2).

II. Simulation Overview

A complete chain of simulations has been put in place in order to obtain a comprehensive view of machine induced background in the LHCb experiment. Dedicated software is used for each aspect of the problem:

- The evaluation of the rates of the different sources of background.
- The simulation of the proton beam interactions with gas or machine aperture restrictions (known as beam losses).
- The transport of the shower to the LHCb cavern.
- The transport of the surviving particles in the detector itself.

Each step in the chain provides the input for the next, allowing to fully evaluate the effect of each background component on the detector, the trigger, reconstruction and physics measurement in the experiment. The modular method adopted allows to combine the different sources to provide the overall view of the MIB in a given operation condition and to evaluate a variety of operational conditions when scaling of the initial sources is applicable as is the case for MIB contributions directly proportional to local gas pressures.

In the following sections the various steps in the simulation chain are discussed in detail and examples of the results obtained are provided.

III. Sources of Machine Induced Background

The total rate of the machine induced background depends on the contribution to the particle flux from secondary cascades originating from the different sources. Secondary particles, produced in any of the sources, have different probability to reach LHCb depending on where they originate with respect to the interaction point (IP8). This can be inferred from Fig. 1 where LHCb is indicated in the LHC layout.

The following MIB sources are relevant for the LHCb experiment:

1 Inelastic and elastic interactions of the beams with residual gas nuclei in the LSSs close to LHCb.
2 Elastic and diffractive beam-gas interactions in the whole LHC.
3 Betatron cleaning inefficiency at IR7 which results in beam halo protons scattered and not absorbed in the collimation system in this region.
4 Momentum cleaning inefficiency at IR3, where an off-momentum beam halo is produced.
5 Collisions in the higher luminosity experiments, where a fraction of elastic and diffractive interactions may reach LHCb.

The first source is local to LHCb and gives a *direct* background to the experiment. All other sources result in halo buildup where beam protons, due to various processes, are spread in transverse and longitudinal phase space and will impact the aperture restrictions they will encounter around the machine. As a result some of the MIB sources depend heavily on the LHC machine optics. In the LSS on both sides of LHCb the smallest apertures are given by tertiary collimators (TCTs) designed to protect the quadrupoles triplets and, as a result, the experiment itself. Showers originating from any of these sources hitting the TCTs will give an *indirect* background to the experiment. Note that we do not consider all of these sources in this paper, for example momentum halo backgrounds, but the methodology presented is directly applicable to all sources

Estimation of proton beam losses are performed individually for the various sources listed above. The first step in the simulation chain for all but the *local* beam gas source is to evaluate the distribution of the beam losses in the aperture restrictions along the ring and in particular for LHCb losses in the nearby TCT collimators. We consider different machine energies to study the evolution of MIB sources for the possible range of LHC operating parameters.

IV. Distant MIB sources

Distant machine induced background sources are defined as background components which originate further away than the LSSs where the interaction point is located. Therefore the distant MIB sources include the tertiary halo, the elastic or long range beam-gas interactions and the cross talk between the experiments.

The accelerator beam will have a limited lifetime, which will generally depend on the beam size (and so emittance), the number of transversal oscillations it performs per turn (tune), alignment and stability of magnet positions, impedance and so

forth. The particles in the beam will as a result drift slowly outwards to higher transversal amplitudes, known as halo growth. This halo is removed with a collimation system [3] designed with a three level collimator hierarchy.

The third level of collimators, the tertiary collimators, are placed about 70-120 metres away from each interaction point. The protons which hit these collimators will produce a certain amount of background flux to each experiment. The proton loss rate on the tertiary collimators is estimated by the collimation group [3], [4].

From the interactions between the beam and the residual gas in the beam pipe one can have elastic or diffractive interactions where the proton gets a small angular kick but emerges essentially with no energy loss. The proton can then stay in the beam for many turns, causing a contribution to the slow halo growth.

The LHC consists of four interaction points, where the beams collide. A fraction of the residues from these collisions will travel with the beam and part of them can impinge on some aperture restriction of another interaction point, producing background to the experiment that is located there. The amount of this depend on the number of collisions in the originating interaction point, the machine optics between the source and the experiment and will never exceed the collision rate. As a result, this background component will become a concern for LHCb once it reaches its optimal luminosity while that in the high luminosity interaction points (ATLAS and CMS) will continue to increase. It is expected that the cross-talk from ATLAS will be most relevant for LHCb as it is in the neighbouring interaction point while CMS is located three octants away.

There are two main computational issues which are important when studying these long range interactions. The first is the precision in the particle trajectory and aperture model, and the second is the speed of the simulation. Whereas localised shower simulations run over a region of a few hundred metres, these tracking simulations are computing particle dynamics over a few hundred turns of 27 kilometres each. The symplectic six-dimensional tracking code called SixTrack, developed for long term tracking studies at CERN and elsewhere [5], [6] has been used for this work. An extra module was added to SixTrack which allows reading information on the collimators positions and material [7], [8], and to include elastic physics for protons in matter [9]. An alternative approach to the use of SixTrack for the calculation of the LHC halo can be used and is being investigated for future calculations. They are described in [10].

A. Tertiary Halo

The rate of proton losses on a given collimator has been calculated for nominal optics, collimator layout and settings and a beam energy of 7 TeV. The machine parameters used can be found in the LHC design report [11]. An initial transverse halo distribution, either in the vertical or horizontal plane, is tracked for several hundred turns with a complete model of the beam pipe aperture and collimator positions. Re-scattering of protons occurs on the collimator jaws, with elastically interacting protons allowed to continue tracking until they interact inelastically with a collimator jaw or intersect the beam pipe.

The resulting distribution of lost protons around the ring is localized on the primary and secondary collimators in LSS7 but losses are also seen on all tertiary collimators, with a different loss pattern for beam 1 and beam 2 determined by the proximity and the phase advance to the betatron cleaning, and (to a lesser extent, due to less halo build-up) the momentum cleaning section [11] in LSS3. In this paper we only consider the larger losses from betatron beam cleaning. The fraction of total lost protons at a given collimator is termed the cleaning inefficiency, η. Table I shows the cleaning fractions for the LHC collimation SixTrack calculation of 5×10^6 protons with nominal optics at 7 TeV/beam described in [4] and a LHCb β^* of 10 m. The tertiary collimators are set to 8.3 σ, which is equivalent to 1.35 mm half-gap for the vertical collimator close to LHCb.

TABLE I
THE PROTON LOSS RATE ON THE TERTIARY COLLIMATORS OF LHCB FOR BEAM 1 FOR A BEAM LIFETIME OF 30 HOURS. THE RATES ARE COMPUTED FOR NOMINAL OPTICS AT 7 TEV BEAM ENERGY AND β^* OF 10 M

Halo type	TCTVB	TCTH
Vertical	2.57×10^6 p/s	0.10×10^6 p/s
Horizontal	7.23×10^3 p/s	0.51×10^6 p/s

An asymmetry between beam 1 and beam 2 of the losses arises because the tertiary halo is dominantly produced in the betatron cleaning section in LSS7, which is adjacent to IP8 for beam 1 and very far around the LHC ring for beam 2. For this reason we first concentrate on the analysis for beam 1. As discussed in the previous section, the halo type refers to the initial halo distribution in the SixTrack calculation, with a pure vertical or horizontal halo referring to the possible extremes of the true halo distribution. The cleaning fractions can be normalized to a proton loss rate through the total beam lifetime. The rate of proton loss on a tertiary collimator is related to the beam lifetime τ by

$$\dot{\mathrm{p}} = \frac{\eta}{\tau} \cdot \mathrm{p_{beam}}, \tag{1}$$

where $\mathrm{p_{beam}}$ is the number of protons in the beam. In this work the betatron halo beam lifetime is assumed to be 30 hours and the total number of protons in the LHC is assumed to be 3×10^{14} per beam, giving an initial total loss rate (integrated around the machine) of 2.78×10^9 protons per second. This can be combined to give the proton loss rate at a given collimator, which is shown in Table II for the LHCb tertiary collimators for the cleaning fractions in Table I for beam 1.

TABLE II
THE BEAM 1 LHCB BACKGROUND FLUXES FOR THE TCTS, EXPRESSED IN TERMS OF PER PROTON LOST. THE RATES (PER SECOND) CAN BE OBTAINED USING TABLE I. THE RATES ARE COMPUTED FOR NOMINAL OPTICS AT 7 TEV BEAM ENERGY AND β^* OF 10 M.

Collimator	muon rate [/p]	charged hadron rate[/p]
TCTVB	0.16	0.06
TCTH	0.15	0.15

B. Long Range Beam-Gas

For the studies of the beam-gas component that survives for longer distances, an addition to SixTrack has been developed which reads an ASCII formatted list of proton-gas collision events and distribute them around the ring according to the gas pressure distribution [12], [13]. The beam gas interaction is simulated using the DPMJET-III event generator [14]. The direction and energy of the incoming proton is taken into account and the gas particle taken at rest.

The tracking simulation is usually done over a maximum of 100 turns, with the most significant losses within the first three turns after an interaction took place. The tracking of a proton stops as soon as it has hit the beam pipe or when it has made an inelastic collision with a collimator jaw.

The simulation of long range beam-gas is done with parameters very close to the machine configuration in 2010 (which are not those of the nominal LHC). These parameters are a beam energy of 3.5 TeV, no external crossing angle, and a simulated static pressure map for an early unscrubbed machine, with a rescaled dynamic contribution to the pressure in the arcs coming from synchrotron radiation. An average H_2 molecule density around the ring of 3.49×10^{11} H_2/m^3 was used in the simulation [16]. The focussing in LHCb is set to a β^* of 3 m instead of 3.5 m, which means that the tertiary collimators are set slightly closer in the simulation compared to how they are set in the machine. In the later part of 2010 the LHC was run with external crossing angle, something that is not considered in the simulation. The difference is not expected to be of large significance to beam-gas studies. The simulated loss maps has to be scaled to a given beam current. With the assumption of 368 bunches/beam and 1.1×10^{11} protons/bunch the results obtained are given in Table III.

TABLE III
SIMULATED RATES IN PROTONS PER SECOND HITTING THE HORIZONTAL (H) AND VERTICAL (V) TERTIARY COLLIMATORS AROUND LHCB FOR THE 3.5 TEV/BEAM PARAMETERS.

Orientation	Rate [protons/s]	
	Beam One	Beam Two
H	51.9	56.2
V	41.5	132.6

C. Output

All information about the particles are then written to an ASCII file to be used in the shower simulations in the LSSs. This information includes position, energy, and direction of each particle, in addition to information of where in the ring the interaction took place and what species of gas participated in the beam-gas collision the particle came from. The latter makes it possible to rescale for pressure changes.

These simulations are simultaneously providing input to all experiments around the ring, in form of loss maps on aperture and collimator hits. It would also be usable for e.g. machine protection studies at other locations. An example of the loss distribution from collisions on hydrogen can be seen in Fig. 3.

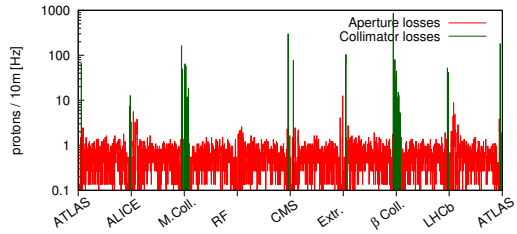

Fig. 3. The loss map produced from both inelastic and elastic collisions between protons in the beam and hydrogen atom at rest. This example shows the result of a simulation of 3.5 TeV beam energy for beam 1, with a simulated pressure map. This is further explained in [13].

V. SHOWER FORMATION IN THE LONG STRAIGHT SECTIONS OF THE LHC

The interaction of protons in the LHC beam with elements of the machine, collimators or residual gas molecules in the vacuum chamber results in a variety of processes and distribution of final state particles. The proton interactions in collimators generally result in inelastic processes and the formation of secondary particle showers composed of particles like pions and muons. For the case of showers induced in collimators around LHCb, the relevant collimators for normal operation are tungsten tertiary collimators (TCTs) located 74 m and 118 m from the experimental interaction point. The interaction of a proton with a gas nucleus can be elastic or inelastic, producing quasi-elastic intact protons or initiating a secondary electromagnetic (EM) and hadronic particle shower. The collision of a high energy proton with a stationery atomic nucleus is a collision system strongly boosted in the forward direction and results in secondary particle showers peaked in the beam direction.

For the case of collimation-induced backgrounds, the EM and hadronic showers themselves are initiated in the tungsten insert block of the tertiary collimators. The LHC tracking calculation gives the distribution of inelastic proton-nucleus events in the tungsten block, and so the cascade was initiated with a proton-Tungsten nuclear interaction at the relevant location. This interaction itself can be calculated with an explicit DPMJET-III [14] calculation and an appropriate boost to the frame of the collimator, or implicitly in the FLUKA source routine. Both methods give the same results. For the case of beam-gas interactions, the vacuum pressure map measured by the LHC vacuum gauges in the straight region around the LHCb experiment [15] is sampled to distribute inelastic proton-H_2 collision products. Each proton-nuclear event is simulated using DPMJET-III. The boosted reaction products are then showered towards the IP. Note that the proton-nucleus interactions produce many high energy forward pions, with the shower transverse size growing transversely as the particles move towards the experiment. An important topological difference between collimator-induced showers and beam-gas collision induced showers is produced when the dense collimator material moderates the shower development and reduces the energy of the forward pions. This results in a

higher energy and more forward peaked shower from beam-gas interactions than collimator interactions as can be observed in Fig. 4

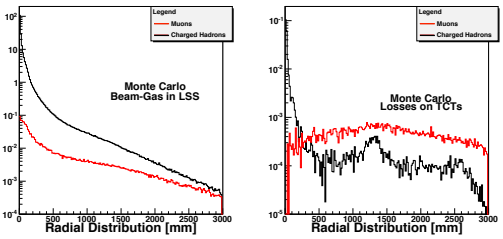

(a) (b)

Fig. 4. Radial charged hadrons and muons distributions arriving at the LHCb cavern for beam 1 at 3.5 TeV, for beam gas in LSS on the left and halo on TCTs on the right.

The measurement of the residual gas pressure profiles in the LHC by vacuum gauges is an essential input to beam-gas calculations. The residual gas composition is a mix of species, dominated by H_2 in cold regions of the machine and by CH_4 in warm regions of the machine but including other species such as CO_2 and CO, and a full pressure profile by species is needed for complete MIB calculations. However, the measurements are often formulated by terms of H_2-equivalent species, where the pressure of non-H_2 species is replaced by an equivalent number of H_2 molecules according to the ratio of the proton-nucleus interaction cross section. This equivalent H_2 profile can give a feeling for total MIB rates but, due to differing interaction kinematics, does not fully describe the MIB produced from separated-species pressure profiles. In this work, H_2-equivalent profiles are used, because they relate directly to static pressure measurements in the LHC. The potential impact of true species or equivalent H_2 pressure profiles on MIB rates and distributions is under study. However, to allow re-weighting of secondary particle distortions, the location and parent atom atomic number of proton-nucleus collisions is recorded and passed down the secondary particle showers and stored in the secondary particle data arrays.

A. The simulation model of the long straight sections close to LHCb

The hadronic and EM showers initiated by the proton-nucleus inelastic interactions are calculated using the shower Monte Carlo FLUKA [17], [18]. A geometrical model of the LHC straight section around LHCb was constructed, comprising of tunnel, beam pipe, all accelerator elements and the tunnel shielding. This model is described in detail in [19] and summarised here.

The model is divided into separate pieces for the left side and the right side of the machine around the IP as viewed from the middle of the ring (LSS8-left and LSS8-right respectively) for computational simplicity and because of the presence of the LHCb detector at the IP. The model consists of the LSSs from $\pm$ 280 m from the IP to the interface plane between the machine and experiment at -2.1 m for beam 1 (LSS8-left) and +19.9 m for beam 2 (LSS8-right). Taken together, the two halves of the model provide a complete picture of LSS8, with a gap in the middle for the detector. The LHC layout database [20] and optics web-page [21] was used to produce the layout, and engineering drawings were taken from the CERN drawing database [22].

The description of the final triplet magnets were adapted from the existing final triplet model for LSS1 [23]. The magnetic field in the final triplet is modelled with an explicit field map in the quadrupoles in the final focusing triplet (known as Q1, Q2 and Q3). The model for the normal conducting separating dipole (D1) was adapted from the superconducting separating dipole (D2) in the LSS1 FLUKA model [23] already mentioned, and the remaining quadrupoles are models of the standard LHC components [23]. In the separation dipoles and the remaining quadrupoles the fields are ideal and localized to the vacuum chamber. For LSS8, new models were made of the corrector magnets around the experiment, which are part of the LHCb inner crossing angle bump. The fields for these elements are ideal. The reference orbit for an incoming and outgoing nominal proton was checked against the LHC reference optics and agreement achieved.

The collimators in the LSS of IR8 are the tertiary halo collimators (TCTs) for the circulating beam. These are designed to intercept the tertiary beam halo before it hits the superconducting final triplet magnets and also provide protection in the event of anomalous beam dump events. They are located on the incoming beams, with one collimator with vertical jaws and one with horizontal jaws, with a tungsten jaw inset for proton collimation. The horizontally collimating TCTH is derived from a standard LHC one-beam collimator [23], [24] and is located around 118 m from the IP. The TCTVB is a two-beam vertical collimator located around 74 m from the LHCb interaction point on the incoming beam. The close proximity of the two beams at the TCTVB location means the collimator is a two-beam type, consisting of a large aperture to accommodate both beams and a shaped collimator block with a tungsten insert, designed to ensure only the incoming beam impacts the tungsten. The model of the TCTVB is a specific two-beam collimator model, adapted from the one-beam standard LHC collimator. The collimators are aligned with the incoming beams, and the jaw position set by the optics and beam energy.

The interaction region of LHCb is the injection region for beam 2, and there are injection-related elements in the model of the LSS around LHCb.

Beam 2 is injected in the right-side of the IP from the outside of the accelerator ring, as shown in Fig. 1. Septum magnets (MSI) deflect the beam in the horizontal plane by 12 mrad onto the horizontal orbit. The MSI also has an aperture for the circulating beam 1, and a new model of the elements was introduced. The beam orbit is kicked horizontally by the four kicker modules of the MKI, the injection kicker. The kicker is currently described in a simple way. The LSS8-right model also contains injection-related collimators for injection protection. For further details on the description of these elements see [19].

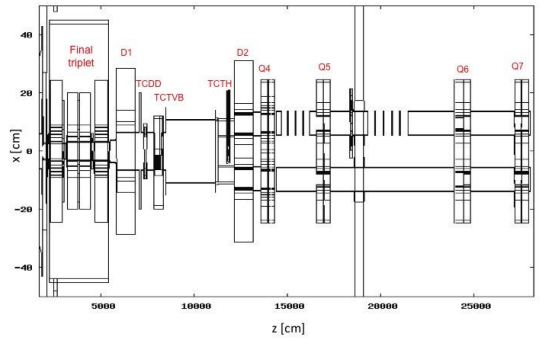

Fig. 5. Layout of the long straight section left of LHCb as used in the simulation. The IP is at $z = 0$.

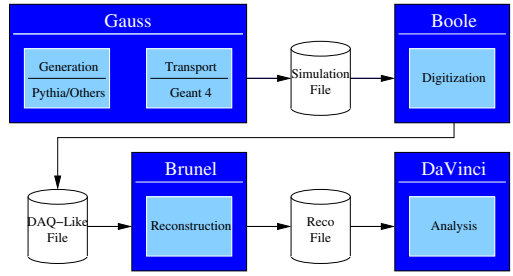

Fig. 6. The LHCb data simulation chain. Particle generation and interactions with the detector are simulated in Gauss. Boole translates the particle hits on the sensors into a DAQ-equivalent format. Brunel reconstructs tracks and particles from the DAQ information while analysis is performed using DaVinci.

The tunnel shielding of LHCb is modelled in terms of blocks of iron and concrete in the model of the LHC tunnels. The role of the shielding is to screen the LHCb detector from the MIB particle fluxes, and is expected to be most effective for the charged hadron contribution. For example, on the left-hand side of the IP (RB84), the shielding is grouped in three regions, 80 cm of concrete closest to the IP, 80 cm of iron and 120 cm of concrete in the tunnel, and then 80 cm of iron and 120 cm of concrete forming a tunnel chicane.

An overview of the FLUKA geometrical model as it is has been implemented of LSS-left is shown in Fig. 5. In this paper, z is defined as the direction along the beam.

The EM and hadronic showers were propagated with a 20 MeV cut on kinetic energy of all charged hadrons, electromagnetic particles and muons, whilst allowing neutrons down to thermal energies. The multiplicity of the EM cascade was controlled with a leading particle bias on the cascade below 1 GeV. The choice of cut or bias was checked not to impact the LHCb background fluxes scored above 20 MeV. The secondary particle products from the showers are scored at -2.1 m from the IP for beam 1 and 19.9 m from the IP for beam 2 [25]. An exchange file format has been defined which contains all the information needed in order to import the particles into the next step of the simulation, that of the LHCb detector. All particle species are recorded, with energy, weight (to account for the use of biasing in the cascades), phase space coordinates, arrival time (with t=0 corresponding to the original beam proton interaction and with respect to the reference particle), the longitudinal position of the original loss location and the species of the parent interaction atom.

VI. Simulation of Machine Induced Background Particles in the LHCb detector

In order to ascertain the impact of various MIB sources on LHCb, these particles must be imported and simulated in the standard software of the LHCb experiment.

The simulation application Gauss [26], [27] mimics what happens in the detector. Like all LHCb data processing software it is based on a framework named Gaudi [28], [29] and as such Gauss follows its architectural design, with a clear separation between data and algorithms and with well defined component interfaces. The Gauss simulation specific code is encapsulated in specific *Algorithms* and *Tools* (smaller pieces of code) callable and controllable from the framework.

Gauss is divided into two phases, generation of the initial particles and simulation of their transport through the LHCb detector making use of the Geant4 toolkit [30]. For the generation phase various generator algorithms exist, each dedicated to represent a specific particle source. Most notably various type of events, for example specific physics signals or soft-QCD events produced in proton-proton collisions at the IP, are generated using libraries developed in the HEP community (e.g. PYTHIA [31]). Following this scheme a dedicated MIB algorithm has been implemented, able to import and sample the MIB estimates.

As indicated in Fig. 6, after the simulated data has been generated and transported through the LHCb detector description by Gauss, the data is processed by Boole. This application calculates the expected detector response and transforms the data into a DAQ equivalent format. This, as well as real data, is reconstructed into standard track and particle candidates in Brunel. Finally data analysis is predominantly performed using the DaVinci application.

A. File exchange format

In order to simplify the task of importing MIB estimates into the LHCb simulation system it is essential that the data is presented in a consistent way. A text based file format has been created in order to provide a well defined interface for the exchange of particle information. In addition to assuring consistency between the various background sources it simplifies the analysis process as standardised tools can be created.

Whenever possible a file represents only one background type. For example in the case of beam-gas interactions, having one file for each type of gas atom simplifies the task of re-scaling the sources with different gas densities. Furthermore, this allows them to be studied separately as well as to combine them with appropriate scaling factors in the simulation stage.

The particle information of the estimate files is given at a vertical interface plane at a certain distance from the LHCb

TABLE IV
MIB ESTIMATE FILE FORMAT. EACH PARTICLES IS REPRESENTED THROUGH A LINE CONTAINING ALL THE VARIABLES

Element	Description
LossID	Proton loss identifier
LossT0	LHC clock offset of proton loss (ns)
LossZ	Proton loss z coordinate (mm)
LossA	Type of atom involved in proton loss
LossW	Proton loss "weight" (likelihood)
PartPdgId	PDG particle ID number
PartX	Particle x coordinate at interface plane (mm)
PartY	Particle y coordinate at interface plane (mm)
PartZ	Particle z coordinate origin at creation (mm)
PartDx	Particle x direction cosine at interface plane
PartDy	Particle y direction cosine at interface plane
PartEk	Particle kinetic energy (GeV)
PartDt	LHC clock offset for particle arrival at interface plane (ns)
PartW	Particle "weight" (likelihood)

IP. In order to make sure all relevant detector components are inside the simulated area, the preferred interface planes are at $z = -2.1$ m for beam 1 and at $z = 19.9$ m for beam 2, where $z = 0$ is the IP location.

The estimate files are flat text files where the particle entries are separated by line-breaks. Each line represents a particle where the various values are space-separated, representing the variables listed in Table IV.

As can be seen from the Table, there are two main type of properties, those related to secondary particles and those related to the original proton loss. The loss information is related to the proton interaction from which the particle has originated. Thus several particles can contain the same loss information. In effect the MIB event originates from a proton loss and contains the particles associated to this loss through the LossID element. The reason for this system is to keep the correlations between the individual particles, so that particles that are members of the same shower can be re-generated as such.

The variable LossW is a special weighting parameter requiring further explanation. The value of this variable is a relative likelihood of the associated MIB event with respect to the sum of the weights of all N events in the estimate file. The probability P of choosing a certain event from the estimate is given by equation (2).

$$P = \frac{\mathrm{LossW}}{\sum_0^N \mathrm{LossW}} \tag{2}$$

Similarly the PartW parameter is the probability that the particle will be generated when the associated event is selected and is related to the probability of the particle reaching or not the interface plane due to interactions with the material traversed while being transported from the initial loss.

The rest of the elements are used either for scaling purposes or, in the case of the particles kinematic variables, for continued propagation of the particles.

As the estimate files are potentially very large, it is not possible to contain all information in memory. However, fast and easy access to the data is needed as random sampling procedures are utilized in the generation algorithms. For this purpose the reading and parsing of flat text files is too time consuming and a binary file format is needed. For this purpose

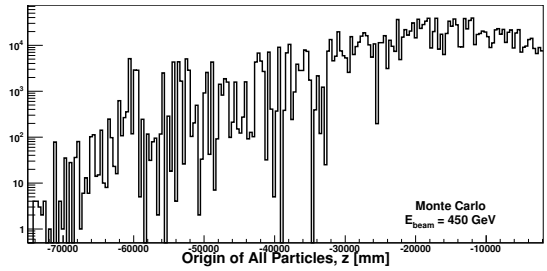

Fig. 7. Distance to IP of primary proton loss for beam-gas in the LSS at 450 GeV for beam 1. Vertical axis indicate particle flux from this position.

the ROOT [32] software is used. This is convenient as the LHCb software suite is already ROOT-compatible and the resulting data format is both platform and architecture independent. The event and particle data are saved in two separate tuples (or specifically *TTrees*). The association between the two is preserved through the use of reference indices.

The translation from the flat estimate files to the ROOT file format is done through a python script. The script also allows for the addition of header information. This header contains global information relevant for the re-generation of the particles, ranging from estimate scaling to beam direction and interface plane position.

The ROOT file can be analyzed directly, which already allows for an in-depth understanding of the MIB sources. As an example Fig. 7 shows the distance from the IP of the primary proton loss for beam-gas in the LSS at 450 GeV. Fig. 4(a) and 4(b) have also been produced by analyzing the file.

B. MIB generator algorithm

The MIB algorithm is designed to produce MIB events in the generator phase of the Gauss application and pass them to the subsequent processing simulation phase. This algorithm can run stand-alone or in conjunction with other particle generators to create a mixed sample. In order to enable several MIB sources to be evaluated in the same event, the actual particle sampling is not performed in the algorithm itself, but rather delegated to a set of generator tools. Each tool instance is set up to represent a given MIB source defined by its settings and the ROOT file to which it has access. The software can be controlled through user-configurable options, giving information about, amongst others, which source, rate and production location should be used.

Whenever Gauss calls the MIB generator algorithm, the call is passed on to the MIB tools instances. In each of them the number of MIB events created are randomly determined in a way consistent with the related MIB source. These events are randomly selected from the associated estimate ROOT file. In order to take the weight, and thus the probability, of the events into account one can not simply randomly select the events. For this the LossW parameter must be used.

Each event i gets a parameter s_i assigned which is equal to the sum of the LossW parameter for the current event and

all events listed before it ($s_i = \sum_0^i \mathrm{LossW}$). For the event selection, a uniformly distributed random number in the range $[0, \sum_0^N \mathrm{LossW}]$ is attained. The event where s_i is larger than or equal to the random number and that of the preceding event was smaller is the event to be selected.

In order to reduce the amount of file access requests required during the event search, every Jth event (where J is a user-settable parameter) is stored in memory. The search is first conducted on these *envelopes* in order to find the approximate location of the event in the file. The search directly in the file is thus limited to a subset of J events, saving computing time.

When the events have been selected, the associated particles are generated with a probability equal to the parameter PartW. The particles are created using the particle ID and kinematic parameters. The MIB algorithm combines the particles and events (if any) arriving from the MIB tools, and passes them over to the simulation step of Gauss in order to ascertain their impact on the LHCb experiment. Particles from other generators can also be added at this point. In particular MIB events can be generated together with standard proton-proton interactions, providing a complete view of the environment in which the LHCb detector collects data.

VII. Example Simulation Results

By utilizing the applications and algorithms described in the previous sections, MIB simulation files are produced. These can be compared to the simulations of proton-proton interactions as well as real data in order to ascertain the viability of our estimates and ultimately to explain various features of the data. When a populated bunch from one beam crosses an empty bunch from the other, no proton-proton interaction is possible, thus the resulting signal only contains MIB and beam-gas from within the experiment. This is referred to as a beam-empty (BE) event as opposed to a beam-beam (BB) event, where both bunches are filled. Strictly, one should note that BE events can contain a small amount of actual proton-proton collisions, from debunched beam or mismatch with the injectors, which to some extent will fill the empty bunch locations. This is particularly true for empty bunch locations close to filled ones. This contribution is neglected in this paper as BE events can be selected with a small contamination.

A good understanding of the MIB signal characteristics is needed to discriminate and understand its contributions. This section shows a few examples of MIB characteristics as obtained with the simulation chain described and indicating what criteria can be used in order to separate the various components.

Machine induced background typically arrives on time with the originating proton bunch, making it hard to distinguish between the MIB particles and the products of the proton-proton interactions at the IP. However this is only true for particles traveling away from the IP. As the bunch travels towards the IP it is only accompanied by MIB.

The LHC has a nominal bunch separation of 25 ns, corresponding to about 7.5 m. This means that the bunches meet each other at every 3.75 m as can be seen from figure 8. When MIB from the two beams arrive at these locations they are

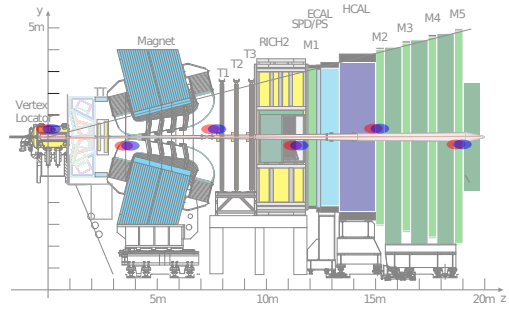

Fig. 8. Bunch crossing locations within the LHCb. The red and blue dots represent the proton bunches. Two time slots are shown; during crossing at IP (upper dots) and offset by 12.5 ns (lower dots).

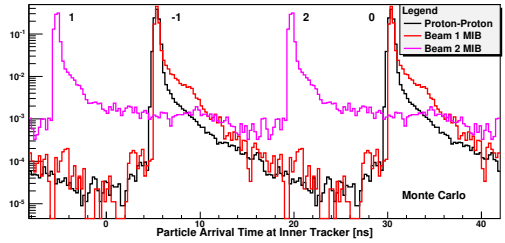

Fig. 9. Time of arrival of particles at the LHCb inner tracker originating from MIB from beam 1 and 2 as well as proton-proton interactions. The scaling is arbitrary. Bunch crossing ID is indicated at each peak.

undistinguishable from each other. In other regions between these locations the timing of the detectors signals can allow the discrimination of the MIB originating from the two beams.

An example of such a region is shown in Fig. 9 for one of the trackers located at about 9.5 m from the IP. One can clearly see that the signal from beam 1 MIB is on-time with the proton-proton signal, while beam 2 MIB is separated by about 10 ns. Due to the single arm design of LHCb the visibility of beam 2 MIB by the spectrometer is highly reduced. This is a result of both the geometry of the detector and the read out of the electronics. The data acquisition has been designed to record particles as they travel through the detector, originating from the region of the IP. In order to allocate the various sub-detector hits to the same interaction event, timing information is used. MIB from beam 2 arrives at the detector elements in the wrong order and would thus be assigned to different events, making the signal in the sub-detectors appear as uncorrelated.

MIB analysis using single sub-detectors is possible for both beam directions when appropriate read out timing is used. The addition of special background sensors called the Beam Loss Scintillators allows analysis of MIB independent of the data acquisition. This device is located upstream of the experiment, allowing for the detection of un-diluted beam 1 MIB.

Another feature of MIB events that may allow their discrimination from other type of events is particle multiplicity, that is reflected in the number of signal channels per event

in the different sub-detectors. An example of this can be seen in Fig. 10(a), at 450 GeV where the MIB events in general have a different distribution than proton-proton collision in the Vertex Detector where higher cluster multiplicities be clearly seen allowing for a clear separation between this two different categories of events. It can be argued that the higher multiplicity component is due to the fact that the MIB particle showers have had a longer distance to develop compared to the collisions. However, at higher energies (Fig. 10(b)) this effect is much less pronounced. In addition the rate of MIB events in BB events is so low with respect to proton-proton collisions in normal operating conditions that it is more efficient to investigate discriminating variables with respect to local beam gas in the Vertex Detector in BE events.

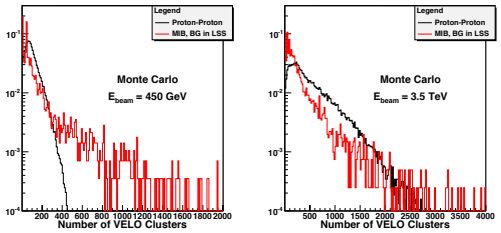

(a) (b)

Fig. 10. Total cluster multiplicity in the vertex detector due to proton-proton collisions and MIB from beam-gas in the LSS at 450 GeV (on the left) and 3.5 TeV beam energy (on the right). The curves have each been normalized to 1.

Charged particle traversing the detector can be reconstructed as tracks by the Brunel application. As the MIB events arrive from outside of the experiment one can expect the related tracks to have a comparatively flat slope. This parameter is defined as the distance traveled in the plane perpendicular to the beam axis per unit length along the same axis. Figure 11 shows the slope of charged MIB particles as they are given at the interface plane upstream of the experiment. This is reflected in slope of the tracks as reconstructed from MIB events that can be seen together with those from beam gas occurring locally in the Vertex Detector in Fig. 12(a)

Another discriminating criteria is the radial distance from the track to the nominal interaction point (IP). Particle originating in the area of the Vertex Detector should have a small radial distance to the IP while MIB events typically have a higher value for this variable. This criteria, together with the track slope, enables the distinction between MIB and beam-gas interactions in the experiment itself, as can be seen from Fig. 12.

By comparing a linear combination of these two distributions to the signal recorded from BE events, the fraction between the two can be approximated. Furthermore, cuts on these variables can be used to increase the purity of MIB events either at the trigger level for dedicated background studies or during analysis. At 450 GeV, the loose machine settings limits the number of MIB sources to the beam-gas in LSS. At higher energies the tighter collimator settings mean background sources from the TCT collimators become larger

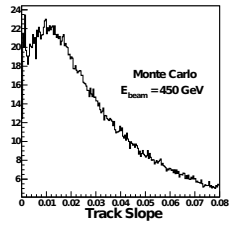

Fig. 11. Slope of charged particles for beam-gas in the LSS at 450 GeV as given at the interface plane 2.1 m upstream from the IP.

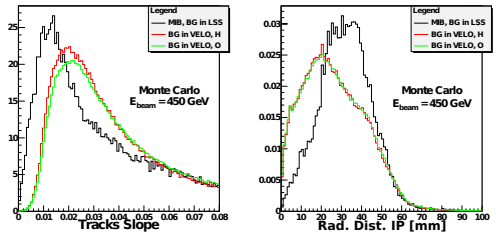

(a) (b)

Fig. 12. Track slope (left) and radial distance to the IP (right) for beam-gas in the LSS and in the vertex locator at 450 GeV.

and need to be folded into the analysis, making their analysis more complex.

VIII. Conclusions

Machine induced background at the LHC arises from proton interactions with elements of the machine and gives a flux of background particles into the LHCb experiment. It is important to evaluate the amount and characteristics of this background, not only for the design of an experiment but also during operation in order to understand what is happening in case of degradation of the conditions and be able to take corrective measures. The backgrounds arise in the machine from proton interactions with beam gas molecules, either close to or far away from the experiment, interactions of protons with the beam collimation system and from fluxes produced by beam-beam collisions in the other LHC experiments. Any calculation scheme for these background sources needs to simulate both the machine and detector response, and would be a valuable tool for understanding and mitigating the impact on the experiment and possibly providing information for future experimental upgrades.

In this paper a full and novel chain of simulations has been described, and a coherent data flow designed, for the LHCb experiment. A modular architecture allows to study all sources independently from each other, as well as combine them for a complete and comprehensive understanding of the background and operation conditions of the experiment in different modes of the machine. Furthermore, steps in the simulation chain can be modified without impacting the overall data flow and analysis. The resulting simulation chain and data flow uniquely models the LHC machine and detector components, allowing

cradle-to-grave analysis, with well-defined interfaces between the simulation steps. The comprehensive simulation chain begins with models of the LHC machine, covering the beam-gas interactions and the collimation system and continues with a model of the LHCb detector. MIB simulated data can then proceed through event reconstruction and selection. Validation of the methodology and data flow has been performed and the system has allowed to quickly compare measured data at 450 GeV showing qualitative agreement of particle flux distributions in the LHCb detector. While not all of the MIB sources have been considered in this paper, for example the background arising from momentum halo formation, the methodology is applicable to any MIB source in the LHC.

The scope of this paper was a full presentation and validation of the complex simulation chain and data flow. Studies are in progress for a beam energy of 3.5 TeV, exploiting the simulation chain, to analyse the data and compare them to the various sources at the different energies collected. Once good quantitative agreement has been proved, an in depth analysis of expected background conditions for the nominal machine will be carried out.

ACKNOWLEDGMENT

The authors would like to acknowledge the LHC collimator group for providing the loss rates for the cleaning and the Vacuum group for the residual pressure simulations and measurements.

REFERENCES

[1] L. Evans *et al*, "LHC Machine," *2008 JINST 3 S08001*, Aug. 2008
[2] The LHCb Collaboration, "The LHCb Detector at the LHC," *2008 JINST 3 S08005*, Aug. 2008
[3] R. W. Assmann *et al*, "The final collimation system for the LHC," *LHC-PROJECT-Report-919*, Jul. 2006
[4] Chiara Bracco, "Commissioning Scenarios and Tests for the LHC Collimation system," *Ph. D. Thesis*
[5] G. Ripken and F. Schmidt, "A symplectic six-dimensional thin-lens formalism for tracking," *CERN-SL-95-12. CERN-SL-95-12-AP. DESY-95-063*, Apr 1995. http://cdsweb.cern.ch/record/281283
[6] K. Heinemann, G. Ripken and F. Schmidt, "Construction of Nonlinear Symplectic Six-Dimensional Thin-Lens Maps by Exponentiation," *DESY-95-189*, 1995. http://arxiv.org/pdf/acc-phys/9510005
[7] G. Robert-Démolaize, "Design and Performance Optimization of the LHC Collimation System," http://cdsweb.cern.ch/record/1004869
[8] G. Robert-Démolaize, R. W. Assmann, S. Redaelli and F. Schmidt, "A New Version of SixTrack with Collimation and Aperture Interface," *Proceedings of the Particle Accelerator Conference, 2005. PAC 2005.* pp. 4084–4086, May 2005. http://cdsweb.cern.ch/record/851591
[9] T. Trenkler and J. B, Jeanneret, "K2, A software package evaluating collimation systems in circular colliders (manual)," *SL-Note-94-105-AP*, Dec. 1994. http://cdsweb.cern.ch/record/703539
[10] R.B. Appleby *et al*, "Simulations of the LHC Collimation System," The proceedings of IPAC10, Kyoto, Japan, May 23-28 2010
[11] O. S. Brüning, *et al*, "LHC Design Report," CERN, 2004, http://cdsweb.cern.ch/record/782076
[12] Y. Inntjore Levinsen, H. Burkhardt and V. Talanov, "Simulation of Beam-Gas Scattering in the LHC," PAC Vancouver, May 2009, submitted for publication.
[13] Y. Inntjore Levinsen, R. B. Appleby and H. Burkhardt, "Beam-gas Loss Rates in the LHC," IPAC Kyoto, Jun. 2009, http://cdsweb.cern.ch/record/1269890
[14] S. Roesler, R. Engel and J. Ranft, "The Monte Carlo event generator DPMJET-III," *arXiv: hep-ph/0012252, HEP-PH/0012252*. http://cdsweb.cern.ch/record/481840
[15] The LHC vacuum group, private communication.
[16] A. Rossi, "Estimations for beam-gas scattering calculations for the first year run," Presented at LHC Background Study Group. http://indico.cern.ch/conferenceDisplay.py?confId=54698
[17] A. Fasso, A. Ferrari, J. Ranft and P. R. Sala, "FLUKA: A multi-particle transport code," *CERN-2005-10 (2005), INFN/TC_05/11, SLAC-R-773*
[18] G. Battistoni, *et al.*, "The FLUKA code: Description and benchmarking," *Proceedings of the Hadronic Shower Simulation Workshop 2006, Fermilab 6-8 Sep 2006, M.Albrow, R.Raja eds., AIP Conference Proceeding 896, 31-49, (2007)*
[19] R. B. Appleby and A. Mereghetti, "The FLUKA Model of IR8," CERN-LHC-Project-Note-427, http://cdsweb.cern.ch/record/1238789
[20] "LHC Layout Database," https://cern.ch/ts-dep-ic/LI/
[21] "LHC optics web page," http://cern.ch/lhcoptics
[22] "CERN Drawing Database," http://cern.ch/edms-service/CDD/
[23] C. Hoa, F. Cerutti, E. Wildne, "Energy Deposition in the LHC Insertion Regions IR1 and IR5," *LHC Project Report 1167*
[24] M. Magistris, M. Santana Leitner, K. Tsoulou, M. Brugger, F. Cerutti, A. Ferrari and V. Vlachoudis, "Technical Description of the implementation of IR7 section at LHC with the FLUKA transport code," *CERN-AB-Note-031-ATB*
[25] G. Corti, M. Lieng and R. Jacobsson, "Requirement for Machine Induced Backgrounds Studies in LHCb," *LHCb-INT-2009-017*
[26] The LHCb Collaboration, R. Antunes Nobrega *et al.*, "LHCb Computing Technical Design Report, *CERN-LHCC-2005-019 (2005).*
[27] S. Miglioranzi *et al*, "The LHCb Simulation Application, Gauss: Design, Evolution and Experience" *Submitted to Proceedings of Conference on Computing in High-Energy and Nuclear Physics 2010, Taipei, Taiwan, 18-22 Oct 2010, CERN-LHCb-PROC-2011-006.*
[28] G. Barrand *et al.*, "GAUDI - A software architecture and framework for building HEP data processing applications, Comput. Phys. Commun. 140 (2001) 45.
[29] M. Clemencic, H. Degaudenzi, P. Mato, S. Binet, W. Lavrijsen, C. Leggett and I. Belyaev, "Recent Developments In The LHCb Software Framework GAUDI, J. Phys. Conf. Ser. 219 (2010) 042006.
[30] J. Allison *et al*, "Geant4 developments and applications," IEEE Transactions on Nuclear Science. v. 53, n. 1, p. 270-278, Feb. 2006.
[31] T. Sjostrand, S. Mrenna and P. Z. Skands, "PYTHIA 6.4 Physics and Manual", JHEP 0605, 026 (2006).
[32] R. Brun and F. Rademakers, "ROOT - An Object Oriented Data Analysis Framework", *Proceedings AIHENP96 Workshop, Lausanne, Sep. 1996, Nucl. Inst. and Meth. in Phys. Res. A 389 (1997) 81-86. See also http://root.cern.ch/*

D.5 Fill Analysis and Background Observations

- Title: Fill Analysis and Experimental Background Observations in the LHC
- Abstract: We have developed a fill analysis tool which automatically extracts data and analyses each fill in the Large Hadron Collider. All generated and extracted information is stored in flexible binary formats for outside use. The tool is modular and easily extendable. In this work we make use of the information produced and look at experimental background under different conditions for the 2011 running. We will discuss the observations in the context of the residual gas pressure, beam halo, and cross-talk between experiments, which depend on luminosity at neighbouring experiments.
- Where: IPAC11, San Sebastien, Spain
- When: September, 2011
- Contribution: Yngve was the main author, and presenting author at the conference. For the project, Yngve was responsible for the Python back-end, including extraction, recombination, and storage of data, and calculating additional information. For the paper, Yngve did the background analysis which included figures 2 and 4-6.
- Co-authors: H. Burkhardt, A. Macpherson, M. Terro Pinheiro, S. Roe
- Bibliography entry: [93]

FILL ANALYSIS AND EXPERIMENTAL BACKGROUND OBSERVATIONS IN THE LHC

Yngve Inntjore Levinsen, Helmut Burkhardt, Alick Macpherson, Mario Terro Pinheiro, Shaun Roe,
CERN, Geneva, Switzerland

Abstract

We have developed a fill analysis tool which automatically extracts data and analyses each fill in the Large Hadron Collider. All generated and extracted information is stored in flexible binary formats for outside use. The tool is modular and easily extendable. In this work we make use of the information produced and look at experimental background under different conditions for the 2011 running. We will discuss the observations in the context of the residual gas pressure, beam halo, and cross-talk between experiments, which depend on luminosity at neighbouring experiments.

MOTIVATION

In 2011, the LHC has already produced several fb^{-1} of data, as shown in Figure 1. The peak luminosity has quickly increased, from about $2 \times 10^{32}\,\mathrm{Hz/cm^2}$ at the end of 2010, to more than $2 \times 10^{33}\,\mathrm{Hz/cm^2}$ as of August this year. The increase in performance means that the machine parameters are quickly changing. The increase in beam intensity can increase beam emittance (growth) and reduce lifetime due to collective effects. The dynamic vacuum pressure can increase, which in turn increases the background levels for the experiments. It is important to monitor and understand these changes in order to optimise the beam conditions and make more accurate predictions for the future.

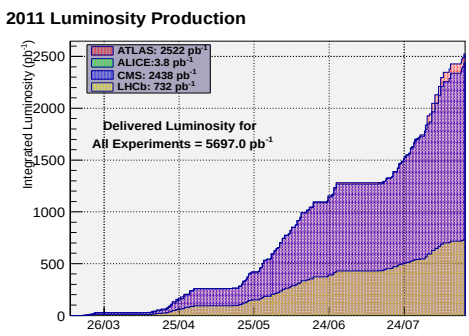

Figure 1: The integrated luminosity delivered for the 2011 running for each experiment in the LHC. This information is continuously updated at [1].

The information available from the LHC monitors can be reached through the TIMBER interface [2], and machine settings can be found in LSA [3]. These databases are highly important for getting the needed information for a proper analysis. There are some limitations however. Due to security, TIMBER can only be used inside CERN, and LSA only on trusted machines in the technical network. Further, manual extraction is time-consuming for large-scale analysis. The amount of information available in TIMBER can be overwhelming to the user, and the knowledge of how trustworthy the data are must be found elsewhere.

We found that a tool which automatically extracts the essential data from the various sources, applies corrections, and/or adds calculated data, would be of value to understand the machine behaviour and to get a better overview. Further, the data should be made available for outside use, in a suitable format for the analysis tools used at CERN.

PROJECT DESIGN

We have written the project mainly in the Python programming language. We have found Python to be simple, efficient, and extendable, suitable for writing the modular code that was needed for this project. Python can be used to work with compiled libraries (e.g. PyROOT), as well as Java libraries through e.g. Py4J. In recent years Python has gained traction as an efficient and flexible scripting language.

Extraction of data from TIMBER is done through the command-line Java interface provided by the Data Management group [5]. Making use of the Online Model [6] is foreseen to retrieve the full TWISS table[1] for the squeezed optics used during stable beams.

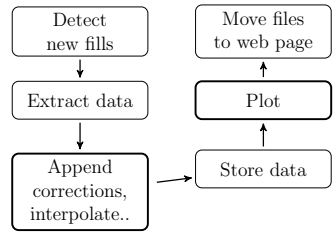

Figure 2: The schematic of the analysis script process. For each fill which goes at least to “injection physics” mode, a selected set of data is extracted, corrections are applied if available (e.g. offline luminosity calculation), and new information is added (e.g. collision pattern). The data are stored and the plotting module is run before all information about the fill is pushed to the web page. Major parts are marked with a thick frame.

In Figure 2 we show the main modules of the project. The project is written so that all new fills are analysed at regular intervals using a ‘cron’ job. The data are read into Python objects that have the needed flexibility for cleaning,

[1] Table of linear beam optics parameters

manipulation and restructuring of data. Empty variables are removed, and all data are time aligned using various interpolation algorithms for different data, making further analysis across all subsystems coherent and flexible. Additional information like collision pattern and time-stamps for various machine state changes is added, and everything is stored to file.

Data that have one value per fill (e.g. delivered luminosity) are written to a JSON formatted ASCII file, an efficient and clean format readable by humans and easily parsable by programming languages. Detailed fill data are provided in a tree structured binary ROOT format. ROOT is an extensive analysis tool package [4], widely used at CERN and elsewhere.

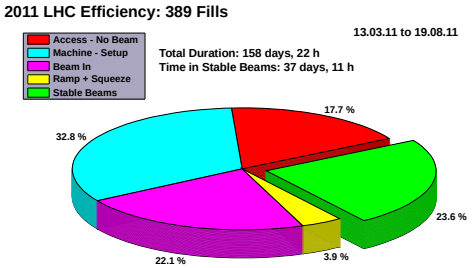

Figure 3: The total machine efficiency so far in 2011. In total, about 25 % of the time has been spent in stable beams. This information is continuously updated at [1].

The second part of the analysis is done in ROOT through the Python interface PyROOT. The ROOT binary file and the JSON file are loaded into memory before the analysis modules are run one by one. This approach allows third parties to contribute with additional analysis modules without the need to know about the internal structure of the project. Templates are provided so that all figures will have a similar look and feel. In Figure 3 we show a good example of useful performance monitoring for the LHC operators, giving a quick overview of the amount of time spent in different beam modes. This information is kept continuously updated on our web page, both for short and long term statistics.

BACKGROUND IN THE LHC

Monitoring background in the LHC is a complex matter. So far the observed background in the LHC has been fairly low, typically below 1 % during proton-proton physics, somewhat higher for ion runs [7]. It is important that we have a good knowledge of what to expect in the future and know what we can do to improve potentially problematic conditions. One should also remember that no matter how low the background is, experiments can always benefit from even better conditions. In LHC we have experiments with vastly different nominal luminosities, which can prove challenging due to background as luminosity further increases for the high luminosity experiments.

The experiments report three main online background parameters back to the machine, which are used as a guideline for online analysis on the machine side. Currently we have an informal guideline as to what these numbers should represent. The first number should be a measure of the total detector background. The second number should be a measure of the beam halo, while the third should measure detector radiation in percentage of dump threshold. Hence, the two first numbers are ideally measurements of background alone, while the third includes collision debris as well in order to measure the total amount of radiation to the experiment.

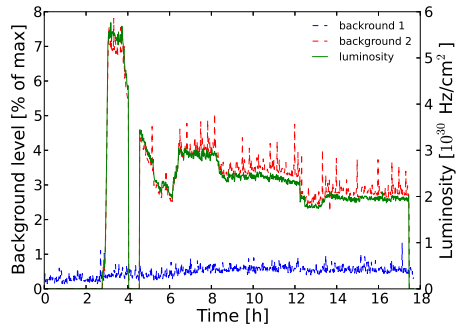

Figure 4: Luminosity and background in ALICE during fill 1901. The luminosity is shown in green, while the background number 1 is in blue and 2 in red. The sudden changes are coming from the automatic luminosity levelling which is applied in ALICE.

The algorithms to calculate the background differ from experiment to experiment, depending on what detectors they have available. It can be difficult to define an algorithm that scales correctly with the background and is independent of the luminosity.

There are some non-colliding bunches for each filling scheme. These bunches are widely used in background algorithms, since they in principle should see no normal collisions, though satellites and debunched beam still can produce some collisions.

In Figure 4, we see an example from ALICE where the algorithm to calculate beam halo background almost exactly follows the luminosity calculation. In this fill ALICE had difficulties because the background was much higher than the luminosity, and the calculation of the luminosity was not successfully excluding the background.

Machine induced background is usually split in three different categories. The beam halo background comes from the halo of the beam interacting with aperture restrictions close to the experiment. The beam-gas background arises from particles in the beam colliding with rest gas molecules in the beam chamber. The final background is interaction region (IR) cross talk, which are residues from collisions in one interaction point (IP) that reach the experimental cavern of another IR. The latter is more relevant when luminosities in different experiments differ by several orders of magnitude.

The aperture restriction which is relevant for the experiments in the LHC are the tertiary collimators, located 70-

140 m upstream of each IP. Their purpose is to protect the final focusing system, which means that they are placed closer to the beam when β^* is reduced. As a result, background originating at the collimators is expected to increase when we go to nominal β^*, which is three times lower than what is used now (1.5 m vs. 0.55 m). This background is lower for ALICE and LHCb, which are operating with higher β^*.

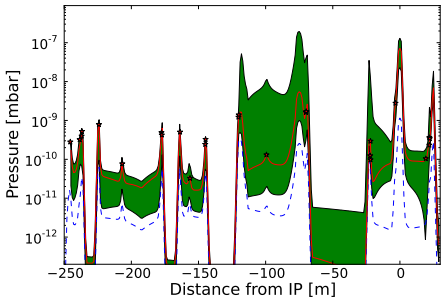

Figure 5: The vacuum distribution for beam 1 in the region around LHCb for fill 2006. In dashed blue we show the simulated static pressure profile provided by the vacuum group [8]. In red the average pressure during the fill is shown, while the green shows the spread during the fill. The relative difference between gauge reading and simulation is assumed to change linearly between pressure gauges. This is a crude assumption since synchrotron radiation will change the profile at top energy. Simulations of dynamic pressure profile will become available later.

The beam-gas component is proportional to the beam current and the vacuum in the beam. However, since the beam current can produce a dynamic vacuum increase, beam-gas can increase faster with beam current if the intensity and energy is above a certain threshold. In Figure 6 we see that the pressure increases due to the energy ramp. In Figure 5 we see the interpolated pressure range during a full fill for LHCb. Here, we have made a linear interpolation of the relative difference between simulated static pressure and measured pressure, which has a dynamic contribution at top energy. The collisions at the IP can also heat the beam-pipe locally, further increasing the local vacuum pressure. We see this in Figure 6, where one gauge is almost exactly following the luminosity level in both ATLAS and CMS.

SUMMARY

We have now made available an extensive suite for making data easily available for analysis of each fill in the LHC. The application runs in an automated mode, and data are provided in efficient formats which make extensive analysis possible. It is easily extendable, and it is foreseen to include other sources at a later point.

We have presented some examples regarding background conditions in the LHC for 2011. Having these data readily available for every fill will make it significantly easier and faster to monitor the background conditions, and more generally the machine performance. The statistics

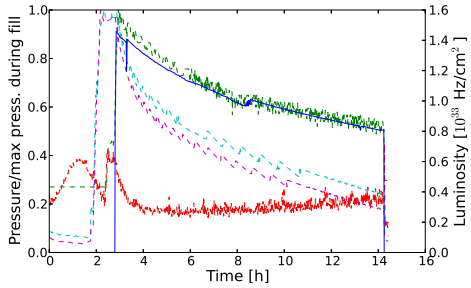

(a) ATLAS

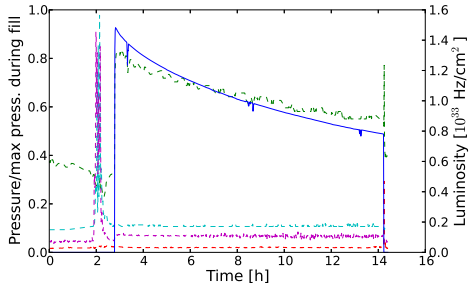

(b) CMS

Figure 6: The luminosity in solid blue, together with a selection of gauges close to the experiment in dashed lines. The pressure is divided by the maximum measured for the gauge during the fill. The gauge presented by the green line is located around 18 m from the IP.

pages already have many users, and we believe it will even prove more useful as the analysis package matures.

ACKNOWLEDGEMENTS

The authors would like to thank all collaborators from the LHC Background Study group for countless fruitful discussions.

REFERENCES

[1] LHC statistics page. `http://cern.ch/LHC-Statistics`.

[2] TIMBER data extraction interface. `http://cern.ch/timber`.

[3] LSA controls project. `http://cern.ch/ab-project-lsa/`.

[4] `http://root.cern.ch/`

[5] TIMBER command line interface. `https://cern.ch/be-dep/CO/DM/CALS/DataExtraction.aspx`.

[6] C Alabau Pons, X Buffat, M Giovannozzi, G Müller, S Redaelli, K Fuchsberger, M Lamont, and F Schmidt. The online model for the large hadron collider. (CERN-ATS-2010-184):4 p, May 2010.

[7] LHC background study group, various meetings. `http://cern.ch/project-LBS/`.

[8] G. Bregliozzi. Pressure maps in the LSS. LBS presentation, 23. of May, 2011.

D.6 Summary of Notes

In this section we will briefly summarise notes where we published work related to this thesis which was not published in a reviewed article. In all papers, the FLUKA simulations were not done by the candidate but instead by Robert Barrie Appleby, while the SixTrack simulations were done by the candidate.

D.6.1 Beam-Gas Simulations for the 2009 run

- Title: Beam-Gas Simulations for 2009 LHC Running and First Comparisons with Data
- Abstract: This note describes the calculations made for the pressure maps, beam-gas events and lifetime for comparison to the first machine running at the end of 2009 at a beam energy of 450 GeV. This includes a full set of pressure maps and equations to calculate beam-gas. The beam-gas loss rates around the machine, and the expected flux of beam-gas induced background particles into the LHCb and ALICE experiments are calculated. Wherever possible at this early state, the consistency of the measured beam-gas rates and the simulations is assessed.
- Co-authors: Robert Barrie Appleby, Helmut Burkhardt
- Bibliography entry: [47]
- Comment: The title is somewhat misleading. There was not an actual comparison to background data, which was not available at the time it was published.

In this paper we published our first simulations of an actual running scenario, the 2009 run at 450 GeV. We simulated beam-gas background only. The LSS beam-gas was simulated and all background sources were transported to the interface plane for LHCb and ALICE, where we had a FLUKA geometrical model available.

For the first time we made an estimate of the pressure in the long straight section of LHCb, with input from Vincent Baglin. The estimates were based on a combination of simulations, pressure gauge readings and knowledge of the vacuum design. Only hydrogen and methane were considered.

In Figure D.1 we show the simulated beam-gas loss rates from the simulation. When compared to Figure 5.10 (blue curve in Figure D.1) or Figure 5.11 (green curve), the losses are several orders of magnitude lower. This is due to two main factors, the much lower beam intensity, and the beam energy which at 450 GeV is not sufficient for

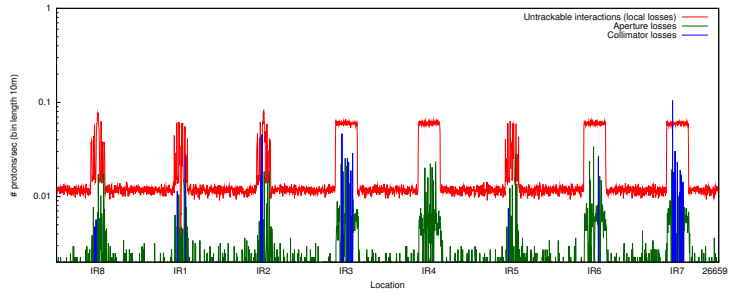

Figure D.1: Simulated losses from beam 1 during 2009 running. Assuming 450 GeV beam energy, and 2×10^{10} protons/beam.

a dynamic pressure contribution. It was found that for these conditions, the LSS beam-gas produces significantly more background to the experiments, due to the higher particle multiplicity per originating event. Even though the background levels were low, the paper still present our first quantitative estimates which allowed for a comparison to actual data.

D.6.2 ALICE MIB at Nominal Energy

- Title: Composition of ALICE machine induced background at nominal beam energy
- Abstract: The understanding of the background to the LHC experiments induced by the machine is important to maximising the performance of the collider. The background environment is complex, with contributions from beam-gas interactions around the ring, the halo collimation system and cross talk from one experiment to another. In this note, the background rates for ALICE beam 1 are calculated for nominal beam energy and 1/3 nominal intensity, including all of the large sources, and the relative background composition discussed.
- Co-author: Robert Barrie Appleby
- Bibliography entry: [48]

Robert B. Appleby was the main author of this paper. In this paper we published the first total assessment of the expected background rates for ALICE at nominal machine settings. This included distant and LSS beam-gas, tertiary beam halo, and IR cross-talk.

We used the simulated vacuum pressure for the "early machine", which assumed a not fully scrubbed beam pipe and 1/3 of nominal beam intensity. The IR cross-talk was simulated using PTC [104] by R. Appleby, and the simulation was afterwards checked using SixTrack with a good agreement. This paper was aimed to provide a baseline for detector response simulations for ALICE.

Table D.1: Summary table of the estimated machine induced background rates from beam 1 towards the ALICE experiment. The total rates are scored at the interface plane, 19.5 m from the interaction point. 1/3 of nominal beam intensity assumed, and vacuum pressure according to "early machine conditions".

Contribution	**Lifetime**	**Total rate**	**On-axis density**
Unit	Hours	MHz	p / cm^2 /s
Betatron halo	30	0.104 / 0.085	2 / 0.02
LSS beam-gas		0.560 / 0.039	400 / 2
Distant beam-gas	1000	0.046 / 0.030	1.2 / 0.02
IR cross-talk		0.018 / 0.012	0.5 / 0.01
Sum		0.73 / 0.17	405 / 2.1

If we compare the results for distant beam-gas simulations in this note to the results presented in Chapter 5, we note that the rates in this paper is lower. The exact reason for this is difficult to assess, but the simulation code has since been polished and in addition some problems with the thin lens sequence used in SixTrack was found. It is believed that the results we published in the thesis should be closer to the truth. We have seen that the simulations and data are closer to an agreement in recent studies. As an example, in Appendix D.2 we found that the estimated rate was a factor ten lower than measured, while in [43] the data and simulations agreed within a factor two.